SANDIA REPORT

SAND2017-9774
Unlimited Release
Printed September 2017
Supersedes SAND2014-17174 dated September 2014

Hydrogen Isotope Exchange in a Metal Hydride Tube

David B. Robinson

Prepared by
Sandia National Laboratories
Albuquerque, New Mexico 87185 and Livermore, California 94550

Sandia National Laboratories is a multi-mission laboratory managed and operated by National Technology and Engineering Solutions of Sandia, LLC., a wholly owned subsidiary of Honeywell International, Inc., for the U.S. Department of Energy's National Nuclear Security Administration under contract DE-NA-0003525.

Issued by Sandia National Laboratories, operated for the United States Department of Energy by National Technology and Engineering Solutions of Sandia, LLC.

Available to DOE and DOE contractors from
U.S. Department of Energy
Office of Scientific and Technical Information
P.O. Box 62
Oak Ridge, TN 37831

Telephone: (865) 576-8401
Facsimile: (865) 576-5728
E-Mail: reports@adonis.osti.gov
Online ordering: http://www.osti.gov/scitech

Available to the public from
U.S. Department of Commerce
National Technical Information Service
5301 Shawnee Rd
Alexandria, VA 22312

Telephone: (800) 553-6847
Facsimile: (703) 605-6900
E-Mail: orders@ntis.fedworld.gov
Online order: http://www.ntis.gov/search

SAND2017-9774
Unlimited Release
Printed September 2017
Supersedes SAND2014-17174 dated September 2014

Hydrogen Isotope Exchange in a Metal Hydride Tube

David B. Robinson
Energy Nanomaterials Department
Sandia National Laboratories
P.O. Box 969
Livermore, California 94551-MS9291

Abstract

This report describes a model of the displacement of one hydrogen isotope within a metal hydride tube by a different isotope in the gas phase that is blown through the tube. The model incorporates only the most basic parameters to make a clear connection to the theory of open-tube gas chromatography, and to provide a simple description of how the behavior of the system scales with controllable parameters such as gas velocity and tube radius. A single tube can be seen as a building block for more complex architectures that provide higher molar flow rates or other advanced design goals.

ACKNOWLEDGMENTS

The author thanks Maher Salloum for his generous assistance with the COMSOL software, and Steve Rice, who helped identify important references. Stewart Griffiths provided early guidance on this topic. Work with Andrew Shugard on Ref. 13 provided insights beneficial to this work. Shugard and Weifang Luo provided helpful technical reviews of this document.

CONTENTS

FIGURES

TABLES

NOMENCLATURE

Acronyms

GC	Gas chromatography
DOE	Department of Energy
PLOT	Porous-layer open tube

Roman Symbols

a	Avogadro's number [$6x10^{23}$ mol^{-1}]
A_c	Packed column cross-sectional area [cm^2]
A_g	Gas phase cross-sectional area within tube [cm^2]
A_g^*	Gas phase cross-sectional area within pore [cm^2]
A_s	Solid phase cross-sectional area within tube [cm^2]
A_g^*	Solid phase cross-sectional area within pore [cm^2]
B	Effective permeability of a porous medium [cm^2]
C_g	Gas phase molar concentration [mol/cm^3]
C_s	Solid phase molar concentration [mol/cm^3]
D	Gas-phase atomic concentration of eluent [mol/cm^3]
D_s	Solid-phase atomic concentration of eluent [mol/cm^3]
D	Gas-phase binary diffusion coefficient [cm^2/s]
D_s	Solid-phase binary diffusion coefficient [cm^2/s]
d_m	Molecular diameter [m]
d_p	Diameter of solid-phase particle [cm]
E	Error signal [dimensionless]
E_a	Activation energy [J/mol]
E_d	Damped error signal [dimensionless]
$[H_2]$	Diatomic eluent concentration [mol/cm^3]
[HD]	Diatomic mixed-isotope concentration [mol/cm^3]
$[D_2]$	Diatomic eluate concentration [mol/cm^3]
H	Gas-phase atomic eluent concentration [mol/cm^3]
H_s	Solid-phase eluent concentration [mol/cm^3]
$\overline{H}_s$	Average solid-phase eluent concentration [mol/cm^3]
ID	Inner diameter of tube [cm]
K	First-order equilibrium constant
K_{HD}	Equilibrium constant for formation of HD
k	Reaction rate constant [mol/cm^2 s]
k'	Ratio of solid-phase to gas-phase capacity
k_{gain}	Feedback loop gain [dimensionless]
k_V	Pressure vessel decay constant [s^{-1}]
L	Axial length of the tube [cm]
M	Gas molecular mass [g/mol]
n	Capacity of diatomic gas molecules that can be eluted from the solid [mol]
$\dot{n}$	Molar flow rate of diatomic species through tube [mol/s]
$\dot{n}_{out,H}$	Molar flow rate of H atoms at outlet [mol/s]

$\dot{n}_{ref,H}$	Reference molar flow rate of H atoms [mol/s]
$\dot{n}_{set,H}$	Feedback loop set point [mol H atoms/s]
N	Number of theoretical plates [dimensionless]
N_{opt}	Number of theoretical plates under optimal conditions
OD	Outer diameter of tube [cm]
P	Total gas pressure [kPa]
P_0	Initial inlet pressure [kPa]
P_{eq}	Equilibrium pressure [kPa]
P_{in}	Inlet pressure [kPa]
P_{out}	Outlet pressure [kPa]
P_{max}	Maximum inlet pressure [kPa]
ΔP	Pressure loss across the tube [kPa]
q	Tortuosity factor [dimensionless]
R	Reaction rate [mol/cm^2 s]
R_g	Universal gas constant [8.314 J/mol K]
r	Radial coordinate [cm]
r_0	Inner radius of tube [cm]
r_p	Radius of pore in stationary phase
s	Laplace-domain parameter [s^{-1}]
S	Phase boundary surface area per unit length of tube [cm^2/cm]
S^*	Phase boundary surface area per unit length of pore [cm^2/cm]
T	Temperature [K]
t	Time [s]
t_{el}	Elution time [s]
$t_{el,lead}$	Leading-edge elution time [s]
$t_{el,trail}$	Trailing-edge elution time [s]
t_{ss}	Time needed to reach steady-state pressure distribution [s]
v_0	Average gas velocity [cm/s]
v_{el}	Outlet gas velocity at elution time [cm/s]
v_k	Reaction rate parameter [cm/s]
v_m	Mean speed of gas molecules [cm/s]
v_{opt}	Optimal gas velocity [cm/s]
x	Axial coordinate in COMSOL output [m]
x_{HH}, x_{DD}, x_{HD}	Mole fractions of H_2, D_2, and HD [dimensionless]
z	Axial coordinate [cm]

Greek Symbols

α	Isotope separation factor (second-order equilibrium constant)
δ	Solid-phase surface layer thickness [cm]
μ	Gas viscosity [Pa s]
ξ	Ratio of outside to inside tube diameter
ρ	Packed column density [g/cm^3]
ρ_{bulk}	Density of nonporous solid hydride [g/cm^3]
σ	Front width parameter [cm]
σ_{HD}	HD peak width [cm]

τ_d	Feedback loop damping time constant [s]
ϕ	Stationary phase void fraction (porosity)
ϕ_c	Packed column void fraction (porosity)

Some symbols appear that are intermediate mathematical parameters that do not have much physical significance. These include j_1, j_2, u_1, u_2, and u_3. Some variations of units are used (such as cm vs. m).

1. INTRODUCTION

In the mid-20th century, many advancements were made to the theory of chromatography. Among the significant milestones, Marcel Golay provided a description of gas chromatography in a tube coated on the inside with a sorbent material.[1] In gas chromatography (GC), a sample is introduced as a narrow plug at one end of the tube, and blown through with an inert carrier gas. One or more sample components bind reversibly to the sorbent material, moving through the tube at a reduced speed that is specific to each component. Several mechanisms cause broadening of the sample plug, including axial diffusion (when that process is fast), and radial diffusion and absorption/desorption (when those processes are slow). These lead to an optimal value for the flow rate of the carrier gas for a given tube geometry. A GC system of this geometry that operates under conditions that minimize broadening can separate sample components with greater speed, shorter columns, and lower pressures than columns made of packed-powder sorbent materials. For scientific studies of the sorption reactions, a well defined geometry can lead to more clearly defined measurements of reaction rates, because measured values are averaged over a narrower range of conditions. Open-tube gas chromatography is now a mature, commercialized chemical separation method that is well established in industry and research, with a market in the billion-dollar range.

Isotopic displacement has been studied in packed-powder columns by various authors. The concept was proposed by Glueckauf and Kitt in the 1950s.[2] Palladium,[3,4,5,6,7,8,9] palladium alloy,[10,11] lanthanum-nickel alloy,[12] and uranium[13] hydrides are among the studied materials. The process is similar to GC, except that instead of pushing a plug of sample through the column, a boundary between the two isotopes is pushed through the column. A carrier gas is often not used. The displacement reaction is a bimolecular (second-order) chemical reaction, meaning that the rate of the reaction is proportional to the concentrations of two different species. GC is treated as first-order by Golay, where the rate of binding is proportional to the concentration of only the gas-phase species (though many nonlinear elaborations have been described[14,15]). Ion-exchange chromatography, essentially the same process as is used in household water softeners, also involves bimolecular or other higher-order chemical reactions.

In packed-powder columns, gas flows through a distribution of channel widths, around a distribution of solid-phase depths, at a distribution of pressures; some of which may be far from the conditions that minimize broadening. It may be possible to construct a column with higher performance by fabricating flow channels with more well defined geometry, given a clearer understanding of what the optimal conditions are. To obtain this, it is necessary to understand how an analysis like Golay's can be extended to the case of a second-order reaction.

This report attempts to chart a rapid path to this. It gradually builds a set of conceptual tools, while seeking simple sets of assumptions that capture the dependence on designable parameters like channel geometry and flow rate. It draws heavily from the work of Vermeulen and others who studied second-order reactions in the context of packed-powder columns for ion-exchange chromatography. Chapter 2 first describes the physical situation and parameterization of the problem for both first-order and second-order reactions, and then Chapter 3 examines the first-order case leading to Golay's results, and the optimal conditions that it predicts. Chapter 4

considers the case of the second-order reaction, along with the difference between the first- and second-order cases.

In these initial treatments, the effect of slow mass transport in the solid phase is unrealistically ignored. That effect is considered in Chapter 5, where a remedy is proposed in which two types of tube are hierarchically arranged. The effect of a finite and possibly time-dependent pressure drop is considered in Chapter 6, along with the effect of the pressure drop on optimization schemes. Further elaborations are briefly discussed in Chapter 7, including a comparison to the case of a packed-powder column.

This report builds on a previous version[16] by considering pressure drop in more detail, and adding clarifications throughout the document.

2. DEFINITION OF MODEL SYSTEM

The scenario considered here is a tube with an open channel through the middle, an impenetrable outer wall, and a layer of metal hydride on the inside of the tube wall. A pure gas-phase hydrogen isotope differing from that in the metal hydride enters the left end of the tube with a defined velocity distribution. As gas flows down the tube, a chemical reaction occurs between the gas and the metal hydride, in which the initial isotope is displaced by the isotope that is flowing in. The gas flowing in is called the eluent, and the gas that is displaced from the solid and flows out is the eluate.

2.1. Tube Geometry

Figure 1 illustrates the geometry of the tube. It has an inside diameter *ID* that defines the width of the open channel through which gas flows, and an outside diameter *OD* that is equal to *ID* plus twice the wall thickness. The tube length is *L*. Typical values used in analytical gas chromatography columns from vendors such as Phenomenex, Supelco, or Restek are 0.1 to 0.5 mm *ID*, 5 to 30 m *L*, and wall thickness 0.1 to 10 micrometers. Thicker walls are desirable for a preparative-scale isotope separation system. Palladium is a hydride-forming metal that can be obtained in tube geometries. Palladium tubing 0.8 mm *ID*, 0.2 m *L*, and 0.1 mm wall thickness is a catalog item sold by Goodfellow. Methods exist to chemically deposit palladium on the inside of tubes.[17]

Figure 1. Geometry of open tube with inner surface of tube coated with metal hydride. Tube is typically much longer vs. its diameter than illustrated here.

A distance along the length of the tube is denoted by *z*, and along the radius of the tube by *r*. In some cases, it is convenient to refer to the inside radius $r_o = ID/2$. Other important values are the surface area of the wall per unit length *S*, which is the same as the circumference of the cross section of the gas channel; and the volumes of the gas and solid phases per unit length, A_g and A_s, which are the same as the corresponding areas of the cross section.

$$S = \pi \cdot ID = 2\pi r_0 \tag{1}$$

$$A_g = \frac{\pi}{4} ID^2 = \pi r_0^2 \tag{2}$$

$$A_s = \frac{\pi}{4}\left(OD^2 - ID^2\right) \tag{3}$$

2.2. Properties of gas and solid phases

2.2.1. Gas molecules

The hydrogen isotope ^{1}H is simply called "H" in this report, and ^{2}H is called "D". In this work, it is helpful to avoid the complications associated with the fact that gas-phase hydrogen is diatomic. However, it is valuable to predict the concentrations of the diatomic species, including mixed-isotope species such as HD. The differential equations presented in this report will account for gas-phase hydrogen by atoms. The concentrations of the diatomic species can be calculated in a post-processing step once the atom concentrations are known, with the assumption that the diatomic species are always at chemical equilibrium with each other.

This work builds on the assumptions that the temperature T is constant, and the pressure drop across the tube is small, so the pressure P and concentration C_g of the gas atoms can be taken as constant, according to the ideal gas law, $C_g = 2P/R_gT$, R_g being the ideal gas constant. C_g is about 82 mM at room temperature and pressure. In later chapters, larger pressure drops are considered. It is also assumed that no gas properties such as viscosity, diffusivity, or molecular speed are isotope- or composition-dependent.

When determining the concentrations of diatomic species, the enthalpy of formation of the mixed-isotope species is assumed to be zero. In that case, the atoms combine as if they were drawn out of a hat in pairs. If the hat contains equal numbers of H and D atoms, two combinations form the single mixed-isotope species that can be denoted DH or HD, and one each form H_2 and D_2, so their ratio will be 2:1:1. More generally, the diatomic gases will obey the equilibrium relationship

$$K_{\mathrm{HD}} = \frac{[\mathrm{HD}]^2}{[\mathrm{H_2}][\mathrm{D_2}]} = 4 \tag{4}$$

where the brackets indicate the concentration of each species, and K_{HD} is the equilibrium constant. This corresponds to the chemical reaction

$$\mathrm{H_2} + \mathrm{D_2} \Leftrightarrow 2\mathrm{HD} \tag{5}$$

If H is the concentration of gas-phase hydrogen atoms, with the number of deuterium atoms being the difference between this and C_g, the diatomic species can be calculated by summing the number of each type of atom in each diatomic species, and incorporating the equilibrium expression. The summation results in the intermediate expressions in Equations 6 through 8. Substituting these in the equilibrium expression yields the rightmost expressions in these equations.

$$[\mathrm{H_2}] = \frac{H - [\mathrm{HD}]}{2} = \frac{H^2}{2C_g} \tag{6}$$

$$[\mathrm{D}_2] = \frac{C_g - H - [\mathrm{HD}]}{2} = \frac{(C_g - H)^2}{2C_g} \tag{7}$$

$$[\mathrm{HD}] = H\left(1 - \frac{H}{C_g}\right) \tag{8}$$

These diatomic species expressions sum to $C_g/2$, the total concentration of diatomic molecules in the gas phase. For the remainder of this report, *H* will be used to denote the eluent gas atoms, and HD to denote the mixed-isotope diatomic gas, although no assumptions are made that are specific to these isotopes. Any reference to eluate atoms as "D" will be without italics to avoid confusion with diffusivities.

In the real world, there is a small enthalpy of formation of HD, which causes K_{HD} to be slightly less than 4, and temperature-dependent.[3] This leads to the more complicated formula

$$[\mathrm{HD}] = C_g \frac{\left[1 + 4\left(\frac{4}{K_{\mathrm{HD}}} - 1\right)\frac{H}{C_g}\left(1 - \frac{H}{C_g}\right)\right]^{1/2} - 1}{\left(\frac{4}{K_{\mathrm{HD}}} - 1\right)} \tag{9}$$

which can be used to derive the other diatomic gas concentrations. The simpler expression will be used for the remainder of this work.

2.2.2. Solid phase

The total concentration of hydrogen isotopes in the solid phase is assumed to be a constant, C_s, with the eluent isotope denoted by H_s and the eluate by $\mathrm{D}_s = C_s - H_s$. In palladium hydride at room temperature under 1 atm H_2, C_s is about 70 M. Known variations with temperature, pressure, and isotopic composition are usually within about 10 percent, as long as the gas pressure is maintained above the transition to the dehydrided state. The capacity *n* of the solid is the number of moles of diatomic gas molecules that can be eluted from it:

$$n = \frac{C_s A_s L}{2} \tag{10}$$

Diffusivities D_s of hydride species within a solid phase are much lower than those of gas-phase species. 5×10^{-8} cm^2/s is a typical value at room temperature, which is about 100 times lower than that for a dye molecule in water.[18] Note that the diffusive fluxes in Ref. 18, after correcting a few errors,[19] can be written as a sum of a simple term representing the gradient of the mole fraction of a given isotope, and a term representing the gradient of the combined mole fraction of all hydrogen isotopes, which has a driving force represented by an "excess" chemical potential. In

this work, it is assumed that there is no gradient of the combined mole fraction, and only the simpler term is needed for each isotope.

2.3. Chemical reaction

The hydrogen-deuterium exchange reaction has been formulated previously by Foltz and Melius using diatomic gas-phase species,[3] but it is simpler to consider in monatomic form.[20] It can be written as

$$\mathrm{H} + \mathrm{D}_s \Leftrightarrow \mathrm{H}_s + \mathrm{D} \tag{11}$$

where the subscript indicates an atom in the solid hydride phase, and no subscript indicates an atom in the gas phase. The equilibrium constant, also known in this context as the separation factor, is

$$\alpha = \frac{H_s \cdot \mathrm{D}}{H \cdot \mathrm{D}_s} \tag{12}$$

for concentrations measured at equilibrium.[21,22,23] It reflects whether the eluent or eluate is more stable in the solid phase; it is greater than 1 in the former case, and 2 is a typical value. If the reaction is not at equilibrium, as is sometimes assumed in this report, it will approach equilibrium at a finite rate. The net reaction rate R is the forward reaction rate minus the reverse reaction rate:

$$R = \alpha k \frac{H}{C_g}\left(1 - \frac{H_s}{C_s}\right) - k \frac{H_s}{C_s}\left(1 - \frac{H}{C_g}\right) \tag{13}$$

If k is a rate constant in mol/cm^2 s, R is a flux of H from the gas into the solid. The rate law states that a reaction occurs if a gas atom collides with a solid-phase hydrogen atom at the surface with the necessary configuration to cause a displacement reaction (as reflected by k) multiplied by the probability that the pair is the right isotopic combination for a forward or reverse reaction. The reaction is at equilibrium when $R = 0$; the equilibrium constant can be derived from this case. The net reaction rate can be rewritten as

$$R = \alpha k \frac{H}{C_g} - k \frac{H_s}{C_s} + (1 - \alpha) k \frac{H \cdot H_s}{C_g \cdot C_s} \tag{14}$$

showing that the nonlinear term cancels when $\alpha = 1$. A first-order equilibrium constant K can then be written as

$$K = \frac{H_s}{H} = \alpha \frac{C_s}{C_g} \tag{15}$$

where α is retained in case a first-order approximation can be found useful when α is nearly, but not exactly, 1.

Because α is a thermodynamic property, there is an ambiguity in how α connects to the net reaction rate. As α increases, either the forward reaction gets faster, or the reverse reaction gets slower, or a combination of these. In ion-exchange chromatography, increasing α has customarily been interpreted as a slowing reverse reaction, whereas here it is interpreted as a hastening forward reaction. Foltz and Melius considered a combination of both by including $\sqrt{\alpha}$ in each term. The choice can affect how a model scales with α and k.

Determining the change per unit time of concentration in each phase caused by the reaction requires multiplication of the flux R by the surface area per unit length S to get the molecules per unit length per unit time crossing the boundary between phases, then dividing by the volume per unit length A_s or A_g to obtain concentrations. In the absence of any other transport phenomena such as advection (flow) or diffusion, this means

$$\frac{dH_s}{dt} = R \frac{S}{A_s} \tag{16}$$

$$\frac{dH}{dt} = -R \frac{S}{A_g} \tag{17}$$

A crude estimate of k can be made by constructing a flux of gas atoms that are attempting to react at the surface, and multiplying by a probability that the reaction is successful. The gas atoms move at a mean speed v_m, and the product of this and the gas concentration gives the rate of atomic impingement of a surface, if a factor of 1/4 is included to account for the fact that the atoms are moving in all directions, and not all are traveling toward the surface at a given time.[24] The mean speed is given by

$$v_m = \sqrt{\frac{8R_g T}{\pi M}} \tag{18}$$

where M is the mass of one mole of gas molecules. For H_2 at room temperature and pressure, v_m is about 1777 m/s, yielding an atomic impingement rate of about 3.6 mol H/cm^2 s. The reaction probability can be much less than 1 by various mechanisms, including an activation barrier to the reaction. At room temperature, an activation barrier E_a of 25 kJ/mol H decreases the reaction probability by more than 10^4. This motivates definition of a rate constant v_k with units of velocity:

$$v_k = \frac{k}{C_g} = \frac{v_m}{4}\exp\left(\frac{-E_a}{R_g T}\right) \tag{19}$$

In an alternative model of the reaction mechanism, the exchange reaction is mediated by surface hydride states, which can be assumed to be fully occupied.[25] The rate of hydrogen isotope transport between the surface and gas phase is taken to be faster than that between the surface and solid phase, so the gas-surface reaction is at equilibrium. The key consequence here is that k becomes independent of gas concentration and mean speed. The flux of atoms attempting reaction is instead given by the product of the concentration of surface hydrides (regardless of isotope) and an attempt frequency, a good estimate of which is the stretching vibrational frequency of the bond between the hydride and the surface. The distinction between these two models is not very important until Chapter 6, when the effect of time- and position-dependent gas concentration is considered. Until then, k is assumed to depend on a constant concentration, because this allows easier comparison to prior studies.

2.4. Gas transport

The gas velocity can be treated at several levels of detail. In some cases, the velocity can be assumed to be uniform across the cross-section of the tube. This allows for a one-dimensional model of the tube. More sophisticated versions, such as that used by Golay, include Poiseuille's parabolic velocity profile for laminar fluid flow in a pipe

$$v(r) = 2v_0\left(1 - \frac{r^2}{r_0^2}\right) \tag{20}$$

where v_0 is the radially averaged gas velocity. The symbol v_0 is also used here to describe the gas velocity in the one-dimensional case. The pressure drop associated with Poiseuille flow is given by

$$\frac{dP}{dx} = -\frac{8\pi\mu v_0}{A_g} \tag{21}$$

where μ is the gas viscosity, about 10^{-5} Pa s for H_2.[26] A hard-sphere model of viscosity[27] predicts

$$\mu = \frac{2}{3\pi}\frac{\sqrt{\pi MRT}}{a\pi d_m^{\,2}} \tag{22}$$

where M is the molecular weight of the gas in kg/mol, a is Avogadro's number, and d_m is a notional molecular diameter, obtained in practice from an empirical fit. The molecular diameter for hydrogen is approximately independent of isotope, so the viscosities of H_2, HD, and D_2 vary mainly by the square root of their molecular weight. It can be shown that the viscosity of

mixtures of such similar gases is well represented by their weighted average.[28] In this report, because the viscosities themselves are similar, a constant value is used. Measured viscosities have a slightly steeper temperature dependence than predicted by the hard-sphere model. The Chapman-Enskog models account for longer-range intermolecular forces and obtain a better fit. Temperature is assumed constant in the scenarios considered in this report, so the temperature dependence is not a major concern.

If the velocity and viscosity are constant, the pressure drop equation (21) yields

$$\frac{\Delta P}{P} = \frac{8\pi\mu v_0 L}{0.5 C_g A_g R_g T} \tag{23}$$

upon integration and incorporation of the ideal gas law. The factor of 0.5 in the denominator reflects the fact that C_g is a monatomic gas concentration, whereas pressure is determined by a diatomic gas concentration. If this pressure ratio is not much less than 1, the assumption of constant pressure and velocity is not realistic, and it is advisable to account for decreases of C_g and increases in v_0 along the length of the tube. The product $0.5 C_g A_g v_0$ is the diatomic molar flow rate $\dot{n}$ through the tube, which can be considered constant if there is no net absorption or desorption of gas by the solid, and no changes in pressure versus time within the tube. When it is desirable to account for the axial dependence of C_g and v_0, this can be achieved by integration of the Equation 21, incorporating the constant diatomic molar flow rate, and ideal gas law in the form $P = 0.5 C_g / R_g T$.

$$\frac{C_g(z)}{C_g(L)} = \frac{v_0(L)}{v_0(z)} = \left[\frac{64\pi\mu\dot{n}(L-z)}{R_g T \left(A_g C_g(L)\right)^2} + 1 \right]^{1/2} = \left[\frac{16\pi\mu(L-z)v_0^2(L)}{\dot{n} R_g T} + 1 \right]^{1/2} \tag{24}$$

Either square root expression could be used, depending on whether it is more convenient to specify the concentration or the velocity at the exit. This axial variation will be neglected until Chapter 6. The constant molar flow rate constraint can be relaxed by instead using a molar conservation equation, which can incorporate Equation 21 and the ideal gas law to eliminate gas velocity.

$$\frac{\partial C_g}{\partial t} = -\frac{\partial\left(C_g v_0\right)}{\partial x} = \frac{A_g R_g T}{16\pi\mu}\left[C_g \frac{\partial^2 C_g}{\partial x^2} + \left(\frac{\partial C_g}{\partial x} \right)^2 \right] = 0 \tag{25}$$

Equation 24 is consistent with this form.[29] Chapter 6 will consider cases where the time dependence of C_g is small enough that Equation 24 is approximately valid.

In a hard-sphere model of gas molecules, a binary diffusivity D for a mixture of gas 1 and 2 is given by[27]

$$D = \frac{2}{C_g}\frac{4}{3\pi}\frac{\sqrt{2\pi RT}}{a\pi\left(d_{m1}+d_{m2}\right)^2}\sqrt{\frac{1}{M_1}+\frac{1}{M_2}} \tag{26}$$

The measured value for the H_2-D_2 pair at room temperature and pressure is 1 cm^2/s,[30] , and values inferred from this equation for pairs including HD vary only slightly from this, so all gas-phase diffusivities are taken to be the same in this work. Gas-phase diffusivities are inversely proportional to pressure or concentration, which must be considered if concentration varies significantly along a tube. Comparison to Eq. 22 shows that, for pairs of very similar gases, the viscosity is approximately equal to the product of molecular weight, total gas concentration, and diffusivity.

3. GAS CHROMATOGRAPHY: FIRST-ORDER REACTION

In this chapter, models of open-tube gas chromatography are described, assuming a first-order chemical reaction between the gas and solid phase, with increasingly detailed descriptions of mass transport effects. These include the approach of Golay, along with some extensions, and approaches to optimization. These models will be useful for comparison to (and in some cases are applicable to) the case of the second-order reaction.

3.1. Combination of equilibrium reaction and mass transport

3.1.1. Flow plus reaction

In the simplest case considered here, the chemical reaction is assumed to be at equilibrium everywhere in the tube, and gas flows through, without diffusing axially but rapidly diffusing radially. With no radial concentration gradient, the problem can be treated in one dimension. A mass balance equation provides that the rate of increase in H at a given axial position is the sum of the difference between the amounts flowing in and out within the gas phase (given by the first term) and the amount that enters from the solid phase, which is given by the second term, assuming that the amount leaving the solid phase equals the amount entering the gas phase.

$$\frac{\partial H}{\partial t} = -v_0 \frac{\partial H}{\partial z} - \frac{A_s}{A_g} \frac{\partial H_s}{\partial t} \tag{27}$$

As boundary conditions, H and H_s are zero everywhere at $t = 0$. At all later times, $H = C_g$ at the inlet. For fast reaction kinetics, the reaction is always at equilibrium, and H_s can be eliminated by using the equilibrium constant:

$$\frac{\partial H}{\partial t} = -v_0 \frac{\partial H}{\partial z} - \alpha k' \frac{\partial H}{\partial t} \tag{28}$$

where

$$k' = \frac{C_s A_s}{C_g A_g} \tag{29}$$

which is the ratio of capacity of material in the solid phase to capacity of material in the gas phase. Golay and others lump α into k', but it will help clarify the nonlinear case if this is not done here. The mass balance equation (27) simplifies to

$$\frac{\partial H}{\partial t} = -\frac{v_0}{1+\alpha k'} \frac{\partial H}{\partial z} \tag{30}$$

With the boundary conditions given, H is a step function at $z = 0$ just after $t = 0$. The mass balance equation 30 moves the function H along the tube with the reduced velocity defined by the coefficient.

In the real world, the initial step would not be infinitely sharp. Equation 30 predicts that the sharpness is preserved. For example, if the initial distribution looks like an error function, the solution would look like

$$\frac{H}{C_g} = \frac{1}{2} - \frac{1}{2}\,\mathrm{erf}\left(\frac{x - \left(v/\left(1+\alpha k'\right)\right)t}{\sigma}\right) \tag{31}$$

where σ is a parameter that determines the width of the initial distribution. This solution has a concentration boundary that moves at the reduced velocity, but does not broaden with time. The concentration boundary is also known as the reaction front, because when σ is small, it is a localized region where R is high. Figure 2 shows the resulting diatomic gas mole fractions at the outlet as a function of time. The reaction front traverses a tube of length L in the elution time

$$t_{el} = \left(1+\alpha k'\right)\frac{L}{v_0} \tag{32}$$

This is the conventional definition of the elution time. Some eluate may elute later than the elution time, and some eluent may elute before the elution time, if the reaction front is not perfectly sharp. If the reaction front is symmetric enough, the elution time corresponds to the time when $H/C_g = 0.5$, or where the H_2 and D_2 curves cross and the HD peak is at its maximum in Figure 2.

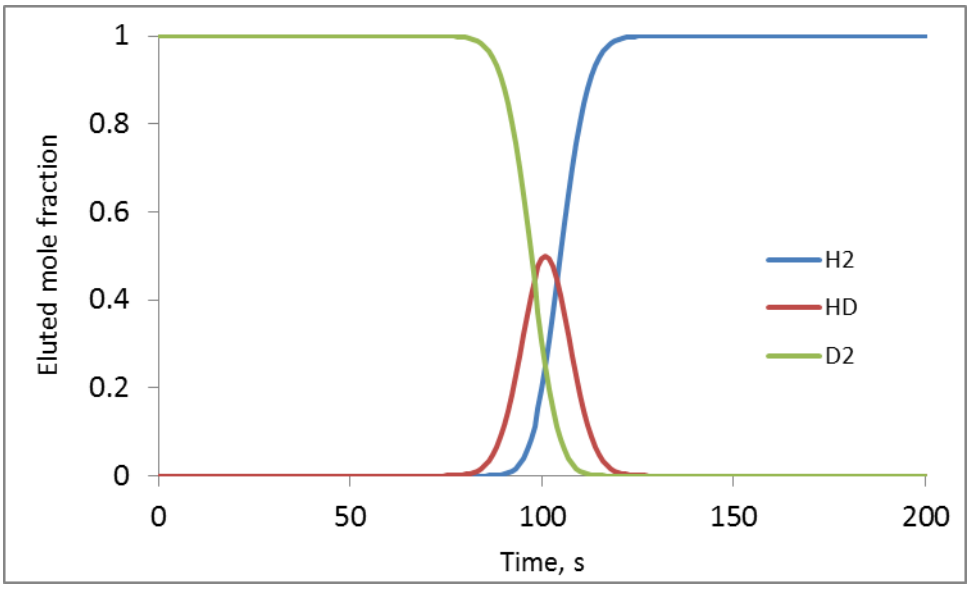

Figure 2. Eluted mole fractions versus time as predicted by error function expression for $\alpha = 1$, $k' = 100$, $L/v_0 = 1$ s, $\sigma = 0.1$.

3.1.2. Flow plus reaction plus axial diffusion

The mass balance can be modified by including a diffusion term that allows a gas species to spread along the length of the tube in the absence of flow (that is, no change in the average position of all gas molecules), and soften sharp concentration gradients.

$$\frac{\partial H}{\partial t} = D\frac{\partial^2 H}{\partial z^2} - v_0\frac{\partial H}{\partial z} - \frac{A_s}{A_g}\frac{\partial H_s}{\partial t} \tag{33}$$

At the outlet, the axial diffusion term is omitted from the equation (in other words, the spatial curvature of *H* is taken to be zero) so no information is needed from points downstream; the diffusion-free mass balance acts as the boundary condition. To determine the outlet molar flow rate for *H*, a diffusion term should be included:

$$\dot{n}_{out,H} = A_g\left(v_0 H - D\frac{\partial H}{\partial z}\right) \tag{34}$$

The diatomic species concentrations can be substituted for *H* here to determine their outlet molar flow rates. A molar flow rate could similarly be evaluated at points other than the outlet, but the outlet is usually the most interesting location. Axial diffusion provides a mechanism for more rapid transport of *H*, which can modify the elution time. An approximate correction is

$$t_{el} = \left(1+\alpha k'\right)\frac{L^2}{D + v_0 L} \tag{35}$$

which can still give a useful estimate even when one of *D* or v_0 is zero. However, the definition in Equation 32 is used in most cases throughout this report. A case where v_0 is zero is considered in Section 5.4. Incorporating reaction equilibrium leads to a simplified case of Equation 33 that can aid understanding:

$$\frac{\partial H}{\partial t} = \frac{D}{1+\alpha k'}\frac{\partial^2 H}{\partial z^2} - \frac{v_0}{1+\alpha k'}\frac{\partial H}{\partial z} \tag{36}$$

This shows that diffusion is reduced similarly to the velocity. For a sharp initial concentration step at the inlet, this has the closed-form solution

$$\frac{H}{C_g} = \frac{1}{2} - \frac{1}{2}erf\left(\frac{x - \left(v_0/\left(1+\alpha k'\right)\right)t}{\sqrt{4\left(D/\left(1+\alpha k'\right)\right)t}}\right) \tag{37}$$

This function has a reaction front that moves at the reduced velocity, and broadens according to the reduced diffusivity. Substitution of t_{el} here and assuming $v_0 L >> D$ (allowing use of Equation 32) gives the form of the function at that time:

$$\frac{H}{C_g} = \frac{1}{2} - \frac{1}{2} erf\left(\frac{x-L}{\sqrt{4DL/v_0}}\right) \tag{38}$$

This shows that the diffusive broadening in a tube of a given length is independent of *k'*, but it does depend on the gas velocity: a slower velocity gives the gas more time to diffuse and broaden as it travels down the tube.

3.1.3. Flow plus reaction plus axial and radial diffusion

Another broadening effect can be hypothesized where the gas concentration varies radially, and diffusion is the only mechanism to reduce this concentration gradient. The gas velocity could also vary radially, but that will be considered later. Including a radial diffusion term yields

$$\frac{\partial H}{\partial t} = D\frac{\partial^2 H}{\partial z^2} + D\frac{1}{r}\frac{\partial}{\partial r}\left(r\frac{\partial H}{\partial r}\right) - v_0\frac{\partial H}{\partial z} \tag{39}$$

In this case, the relationship between H and H_s is accounted for by defining a flux at the boundary $r = r_0$ that satisfies the equilibrium condition.

$$-D\frac{\partial H}{\partial r} = \frac{A_s}{S}\frac{dH_s}{dt} = \alpha k'\frac{A_g}{S}\frac{dH}{dt} = \frac{\alpha k' r_0}{2}\frac{dH}{dt} \tag{40}$$

To obtain the outlet molar flow rate for H, the flux of H is integrated over the area of the outlet. Assuming radial symmetry, this is

$$\dot{n}_{out,H} = \int_0^{r_0}\left(v_0 H - D\frac{\partial H}{\partial z}\right)2\pi r dr \tag{41}$$

A radially varying velocity could be substituted for v_0 here, and diatomic species concentrations could be substituted for H to obtain their outlet molar flow rates. This case is not known to have a closed-form solution. However, Golay chose to study a similar problem, and was able to gain a significant amount of insight.

3.1.4. Poiseuille flow, reaction, axial and radial diffusion (Golay's case)

Once the transition from the one-dimensional to the two-dimensional case has been made, it is straightforward to incorporate the radial dependence of the gas velocity, as follows.

$$\frac{\partial H}{\partial t} = D\frac{\partial^2 H}{\partial z^2} + D\frac{1}{r}\frac{\partial}{\partial r}\left(r\frac{\partial H}{\partial r}\right) - 2v_0\left(1-\frac{r^2}{r_0^2}\right)\frac{\partial H}{\partial z} \tag{42}$$

This is the case that Golay considered in detail by applying the method of moments, which postulates a peak-shaped solution (analogous to the HD peak) and derives properties of its area, position, and width. A key result of this is

$$\left(\frac{\sigma}{L}\right)^2 = \frac{1}{N} = \frac{2D}{v_0 L} + \frac{1 + 6\alpha k' + 11(\alpha k')^2}{(1+\alpha k')^2}\frac{v_0 r_0^2}{24DL} \tag{43}$$

where σ^2 is the second moment of the peak (a measure of its width), and N the number of theoretical plates, which is simply a name for this expression that invokes a connection to other theories of chemical separations such as distillation. N is a useful measure of the sharpness of the peak in comparison to the tube length. For large αk', and approximating 11/24 as 1/2, this approaches

$$\frac{1}{N} = \frac{2D}{v_0 L} + \frac{v_0 r_0^2}{2DL} \tag{44}$$

The first term captures the effect of axial diffusion, and is consistent with the observation made in the one-dimensional case. Ignoring factors of two, it is approximately the ratio of the time required for gas to blow through the tube (regardless of species identity), given by L/v_0, to a characteristic time required to diffuse the length of the tube, L^2/D. This term becomes important if the gas velocity is too slow, and is also known as the Peclet number. The second term captures the effect of radial diffusion. It is approximately the ratio of a characteristic time required for gas to diffuse radially, r_0^2/D, to the time required for gas to blow through the tube. It contributes to broadening at high gas velocities, and especially at large r_0. Golay also considered a tube with a rectangular cross section, and obtained a different polynomial coefficient on the radial diffusion term. One might expect that a method of moments analysis of the case of radially uniform gas velocity would have a similar effect on the result.

3.1.5. Optimization in Golay's case

The fact that one broadening mechanism contributes at low velocities and another at high velocities suggests that there is a gas velocity where broadening is minimized:

$$v_{opt} = \frac{2D}{r_0} \tag{45}$$

At this velocity, the number of plates is equal to the aspect ratio of the tube:

$$N_{opt} = \frac{L}{2r_0} \tag{46}$$

Figure 3 shows the number of plates as a function of gas velocity for various tube diameters. At low gas velocities, the axial diffusion term governs the number of plates. The only design parameter available to adjust this region of the curve is tube length. Radial diffusion is strongly dependent on tube radius (or diameter), affecting the optimum and the number of plates at the optimum. Note that at numbers of plates below 10, the assumption made by Golay that $\sigma << L$ breaks down, but such values are included in the plot for illustrative purposes. The plate curves are modified if the chemical reaction deviates from equilibrium, as discussed in the next section.

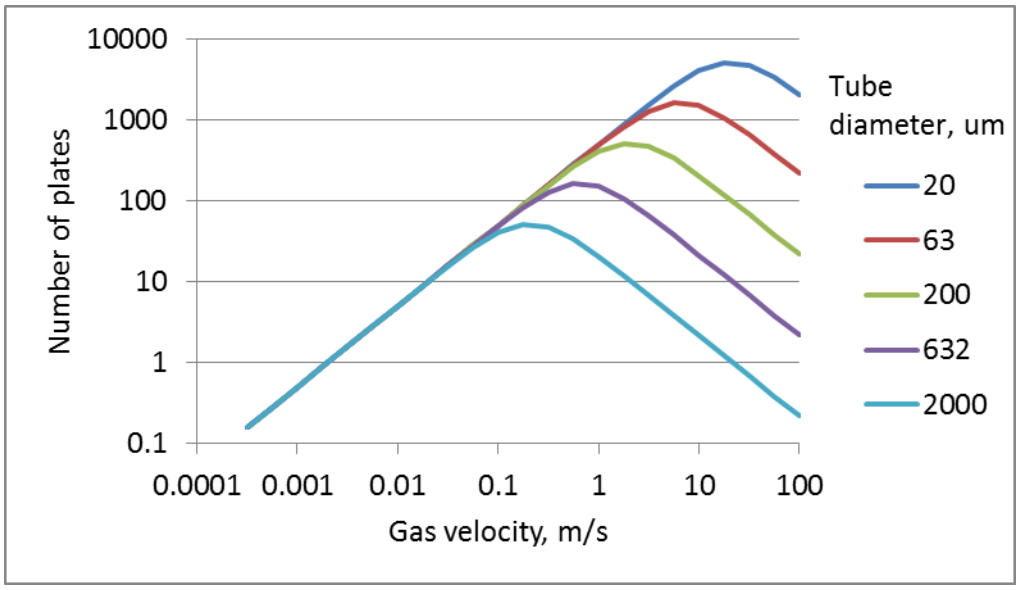

Figure 3. Number of plates versus gas velocity as predicted by Golay for several tube diameters, with D=10^{-4} m^2/s, α=1 and L=0.1 m.

For the maximum number of plates for the smallest diameter shown, the inlet pressure is about 10x the outlet pressure, so the assumption of constant velocity does not apply. That pressure difference decreases rapidly with diameter: $\Delta P/P$ is less than 50% for 63 um and less than 2% for the others.

3.2. Finite reaction rate

3.2.1. One-dimensional case

In one dimension, equations describing the kinetically limited case (neglecting all diffusion) for a first-order reaction take a relatively simple form, using the gas-phase mass balance from Equation 27, and a version of Equation 16 for a first-order reaction:

$$\frac{\partial H_s}{\partial t} = \frac{S}{A_s}\left(\alpha k \frac{H}{C_g} - k\frac{H_s}{C_s}\right) \tag{47}$$

A closed-form solution to the case of $\alpha = 1$ is known, but it is more easily introduced in the context of a second-order reaction, so it appears in the next chapter (Section 4.2). A finite reaction rate can be understood in the context of Golay's approach by focusing on the two-dimensional case.

3.2.2. Two-dimensional case

While Golay restricted his attention to the case of rapid equilibration, Clifford more recently reported a version accounting for a finite rate of reaction.[31] The version presented here is modified to account for absorption into the metal hydride, and not just adsorption to a surface. The flux at the solid-gas boundary is asserted to be equal to the rate of a finite, first-order net reaction rate. The rate law used is from the previous section (Equation 47). It has no nonlinear term, but is still relevant to that case if α is very close to 1.

$$-D\frac{\partial H}{\partial r} = R = \alpha k \frac{H}{C_g} - k\frac{H_s}{C_s} \tag{48}$$

The accumulation of H_s is also proportional to this reaction rate, with a coefficient that converts flux to a rate of concentration change in the solid phase:

$$\frac{\partial H_s}{\partial t} = \frac{S}{A_s}\left(\alpha k \frac{H}{C_g} - k\frac{H_s}{C_s}\right) \tag{49}$$

This leads to the following expression for the number of theoretical plates.[32]

$$\left(\frac{\sigma}{L}\right)^2 = \frac{1}{N} = \frac{2D}{v_0 L} + \frac{(\alpha k')^2}{(1+\alpha k')^2}\frac{v_0 r_0}{\alpha v_k L} + \frac{1+6\alpha k'+11(\alpha k')^2}{(1+\alpha k')^2}\frac{v_0 r_0^2}{24DL} \tag{50}$$

or approximately for $\alpha k' > 10$,

$$\left(\frac{\sigma}{L}\right)^2 = \frac{1}{N} = \frac{2D}{v_0 L} + \frac{v_0 r_0}{\alpha v_k L} + \frac{11 v_0 r_0^2}{24DL} \tag{51}$$

Consideration of a finite reaction rate leads to an additional term in the theoretical plate expression that measures the contribution of slow kinetics to the broadening, which can be recognized as the reciprocal of a Damköhler number. Ignoring factors of two, it is the ratio of a characteristic time required for a tube full of the gas-phase hydrogen atoms to undergo reaction, $C_g A_g L/\alpha k S L$, to the time required for gas to blow through the tube, L/v_0. This term is of increasing importance at higher gas velocities. As before, there is a gas velocity that optimizes the number of plates for a given tube geometry by balancing axial diffusion with the other broadening mechanisms. As the tube gets longer, all three terms lead to increased broadening, but the broadening increases less than the increase in length, so use of a longer tube still leads to more plates.

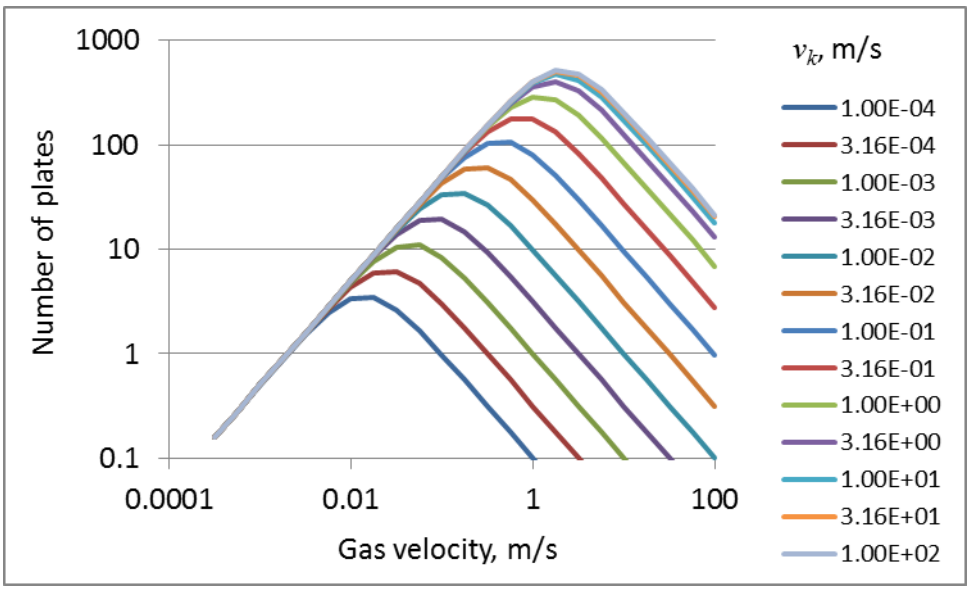

Figure 4. Number of plates versus gas velocity as predicted by Clifford for several reaction rate constants, with D=10^{-4} m^2/s, r_0=10^{-4} m, α=1 and L=0.1 m.

Figure 4 illustrates the effect of slow reaction kinetics on the optimum number of plates. For fast kinetics, the reaction rate is still limited by radial diffusion at high gas velocities, but in this example, once v_k < 3 m/s, the slow reaction limits the rate at high gas velocities, and decreases the optimum number of plates and optimum gas velocity. When kinetically limited, these values are

$$v_{opt} = \sqrt{\frac{2Dv_k}{r_0}} \tag{52}$$

At this velocity, the number of plates is:

$$N_{opt} = \frac{L}{2}\sqrt{\frac{v_k}{2Dr_0}} \tag{53}$$

3.2.3. Performance optimization

The hydride tube provides several adjustable design parameters that can be optimized toward a certain goal, given practical constraints. In an experimental context, the goal may be to maximize the contribution of kinetics to the number of theoretical plates, at the expense of the contributions from diffusion. The plate expression would suggest using higher velocities and narrower tubes.

For a practical chemical separation, maximizing the number of theoretical plates is not necessarily the most practical goal. For example, there is no need to produce an elution front

that is much sharper than the response time of a detector or valve at the outlet. More desirable would be to choose an acceptable number of theoretical plates, and maximize the number of theoretical plates obtained per unit time at the elution time. A similar approach that minimizes "plate duration" (the time required to achieve a theoretical plate) has been described.[33] Clifford provides a version of the theoretical plate expression as a function of time. Manipulation of this reveals that the rate of plate production is maximized when the following expression is minimized:[34]

$$\frac{2D}{v_0^2} + \frac{r_0}{\alpha v_k} + \frac{r_0^2}{2D} \tag{54}$$

This suggests that the velocity should be maximized, and radius minimized. However, there is a limit on how long and narrow the tube can be, because both changes in geometry cause an increase in pressure drop. If $\Delta P/P$ is limited to 0.1, the tube radius can be constrained, changing this expression to

$$\frac{2D}{v_0^2} + \frac{1}{\alpha v_k}\left(\frac{160\mu L v_0}{C_g R_g T}\right)^{1/2} + \frac{80\mu L v_0}{D C_g R_g T} \tag{55}$$

The presence of velocity in both the numerator and denominator of various terms indicates that an optimal velocity exists, given the other parameters. L can be chosen to give the desired number of theoretical plates, with the pressure drop constraint:

$$\frac{1}{N} = \frac{v_0}{L}\left[\frac{2D}{v_0^2} + \frac{1}{\alpha v_k}\left(\frac{160\mu L v_0}{C_g R_g T}\right)^{1/2} + \frac{80\mu L v_0}{D C_g R_g T}\right] \tag{56}$$

Increasing L increases N but decreases its rate of production. The required r_0 can be obtained from the pressure drop formula. Figures 2-4 show values of these criteria for the parameter values described in Table 1. There is not a single, practical optimum for both v_0 and L, but some choices are clearly better than others, and a designer retains some freedom to choose values appropriate for a specific scenario. In the example shown here, tube lengths of at least 1 m are needed to obtain 1000 theoretical plates, but unnecessary length makes the process unnecessarily slow. The gas velocity giving the optimum number of plates per unit time is about 1 m/s, although the number of plates is maximized at about half of this velocity. The radius under these conditions is in the high tens of micrometers. While the pressure drop constraint is conceptually useful here, Chapter 6 will present some more sophisticated ways to address the pressure drop.

Table 1. Parameters used in Figures 5-7.

Parameter	Value	Units
D	10^{-4}	m^2/s
μ	$9x10^{-6}$	Pa s
v_k	10^{-1}	m/s
$C_g R_g T$	$2x10^5$	Pa

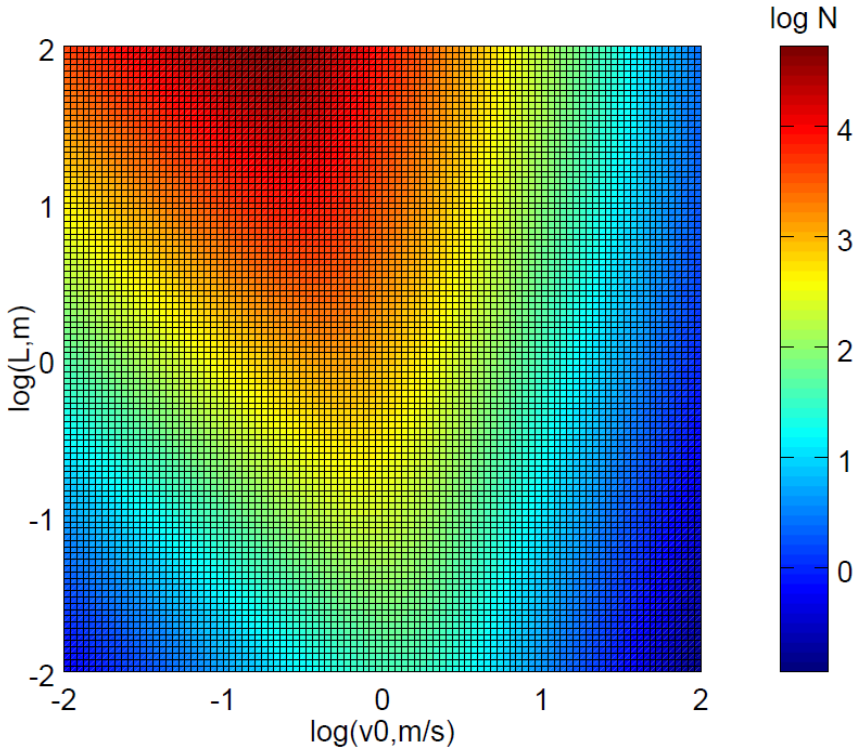

Figure 5. Number of theoretical plates as a function of gas velocity and tube length for the parameters in Table 1.

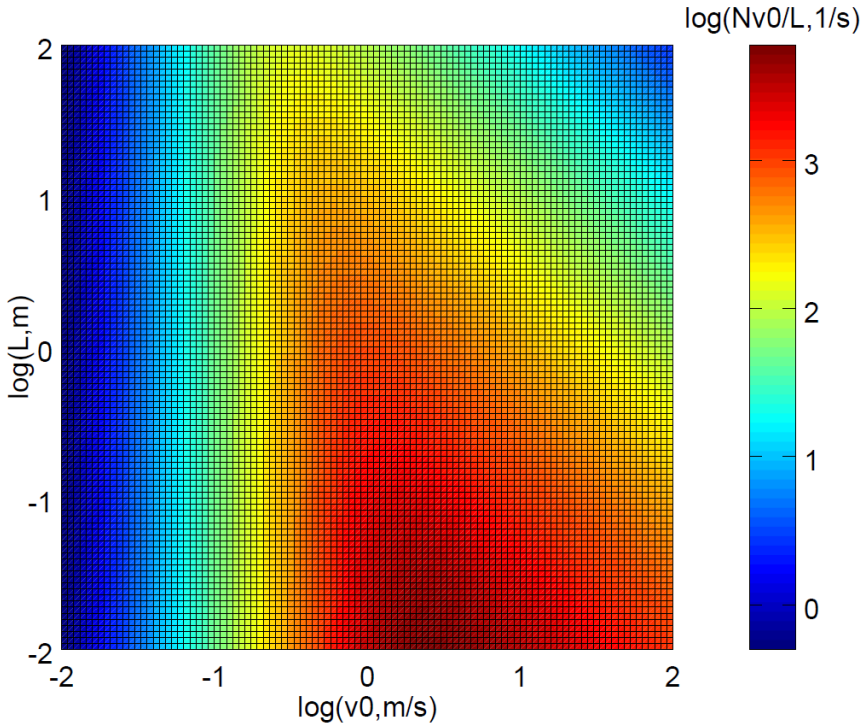

Figure 6. Nv_0/L as a function of gas velocity and tube length for the parameters in Table 1.

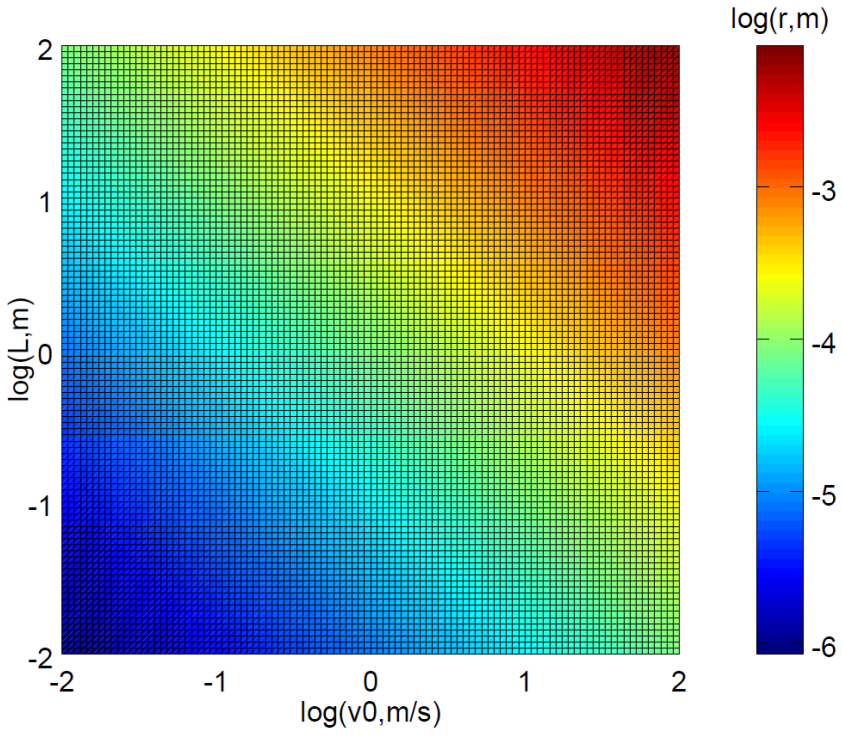

Figure 7. Tube radius as a function of gas velocity and tube length for the parameters shown in Table 1.

4. GAS CHROMATOGRAPHY: SECOND-ORDER REACTION

4.1. Properties of the solution

Walter examined the chromatography problem for the case of a second-order exchange reaction. He assumed rapid equilibrium between phases,[35] and the case of slow kinetics,[36] but did not consider diffusion. He assumed large *k'*, and treated the solid phase as a surface phase. The version presented here follows his argument, but uses a bulk solid phase, does not restrict *k'*, and uses the notation from the previous sections. Starting from the one-dimensional mass balance without diffusion:

$$\frac{\partial H}{\partial t} = -v_0 \frac{\partial H}{\partial z} - \frac{A_s}{A_g} \frac{\partial H_s}{\partial t} \tag{57}$$

H_s is eliminated using the exchange equilibrium constant expression (Equation 12) in Section 2.3, noting that D = C_g - H.

$$H_s = \frac{\alpha C_s H}{C_g + (\alpha - 1)H} \tag{58}$$

When $\alpha > 1$, this looks like a Langmuir isotherm with an initial slope equal to $\alpha C_s / C_g$, but saturating at $\alpha C_s / (\alpha - 1)$. This saturation is never reached, because H_s cannot exceed C_s, but this defines the curvature. Langmuir isotherms are considered frequently throughout the chromatography literature, and insight from that work can often be (cautiously) applied to this case. When $\alpha < 1$, this function has a positive curvature, and when $\alpha = 1$, it is a straight line. This is shown in Figure 8. The further significance of these functional forms will be discussed below. The isotherm can also be solved for H, which is sometimes a useful form:

$$H = \frac{C_g H_s}{\alpha(C_s - H_s) + H_s} \tag{59}$$

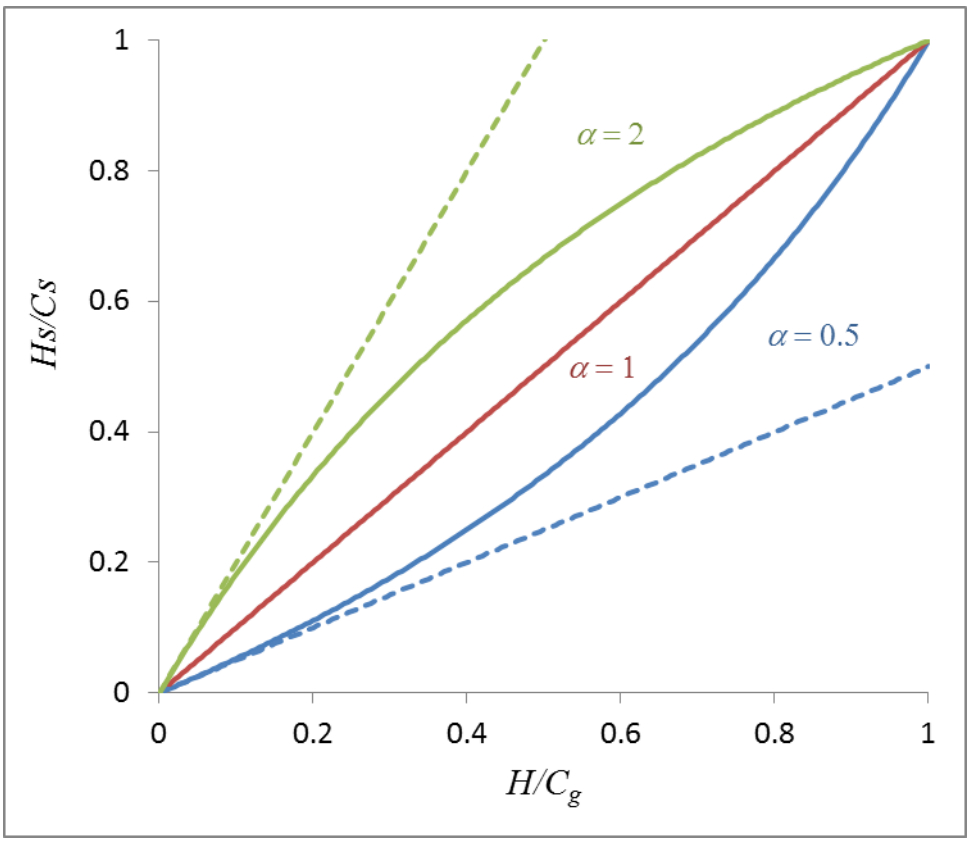

Figure 8. Relationship between H and H_s for several values of α. The dashed lines show the relationship for first-order reaction kinetics.

Proceeding with the elimination of H_s:

$$\frac{\partial H_s}{\partial t} = \frac{\alpha C_s}{C_g\left(1+(\alpha-1)(H/C_g)\right)^2}\frac{\partial H}{\partial t} \tag{60}$$

leads to

$$\left[1+\frac{\alpha k'}{\left(1+(\alpha-1)(H/C_g)\right)^2}\right]\frac{\partial H}{\partial t} = -v_0\frac{\partial H}{\partial z} \tag{61}$$

When $\alpha = 1$, this equation reduces to Equation 30. Walter invokes the method of characteristics, which provides a form for the solution

$$H = f\left(\left[1+\frac{\alpha k'}{\left(1+(\alpha-1)(H/C_g)\right)^2}\right]z - v_0 t\right) \tag{62}$$

where f is an arbitrary function. The inlet boundary condition prescribes $H = C_g$ for negative values of the argument, which is true when

$$z < \frac{v_0}{1+k'/\alpha}t \tag{63}$$

Likewise, the initial condition prescribes $H = 0$ for positive values of the argument, which is true when

$$z > \frac{v_0}{1+\alpha k'}t \tag{64}$$

Between these values of z, the argument is zero, and this can be solved for H.

$$\frac{H}{C_g} = \frac{1}{1-\alpha}\left[1-\left(\frac{1}{\alpha k'}\left(\frac{v_0 t}{z}-1\right)\right)^{-1/2}\right] \tag{65}$$

Substitution in the equilibrium constant expression yields H_s:

$$\frac{H_s}{C_s} = \frac{\alpha}{1-\alpha}\left[\left(\frac{1}{\alpha k'}\left(\frac{v_0 t}{z}-1\right)\right)^{1/2}-1\right] \tag{66}$$

The valid range of z is only finite if $\alpha < 1$, as is the case when deuterium elutes hydrogen from a tube (though in this report, the eluent is always labeled "H" and the eluate always labeled "D").

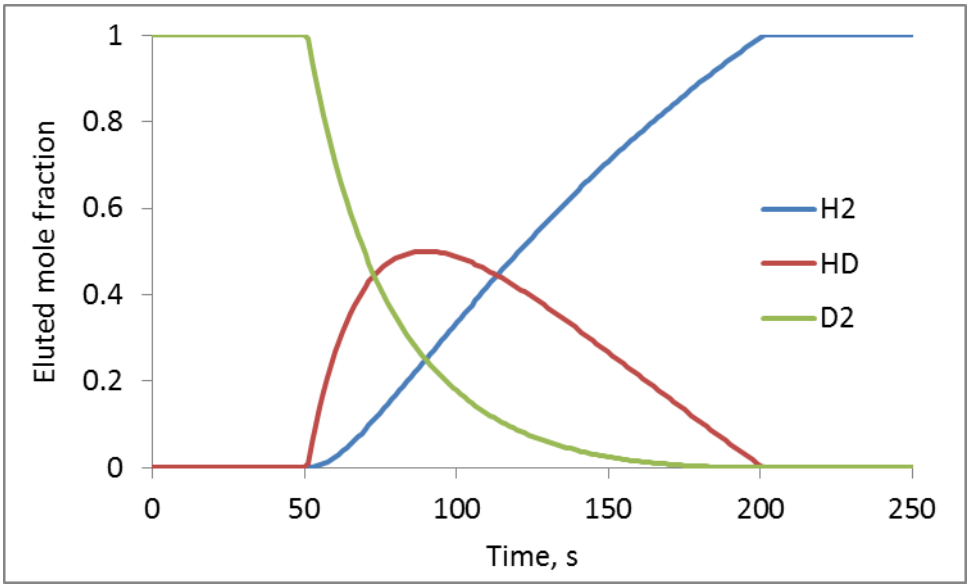

Figure 9. Eluted mole fractions versus time as predicted by Walter for α=0.5, k'=100, L/v_0=1 s.

Figure 9 shows that the HD peak is broad when $\alpha < 1$, even if the transport and reaction rates are fast. This result, and the case of larger α, can be understood by inspection of Equation 61. At high z, where H is near zero, the equation looks like the linear form from Section 3.1, Equation 30. At low z, where H is near C_g, α appears elsewhere in the reduced velocity.

$$\frac{\partial H}{\partial t} = -\frac{v_0}{1+\alpha k'}\frac{\partial H}{\partial z} \qquad \text{(high } z\text{)} \tag{67}$$

$$\frac{\partial H}{\partial t} = -\frac{v_0}{1+k'/\alpha}\frac{\partial H}{\partial z} \qquad \text{(low } z\text{)} \tag{68}$$

When $\alpha < 1$, the leading edge of the elution front moves faster than the trailing edge, causing the front to broaden. For $\alpha > 1$, assuming an elution front that starts out with a finite width, the trailing edge moves faster than the leading edge. With no other broadening mechanisms, the front gets compressed to infinite sharpness at $z = v_0 t/(1+k')$, with no dependence on α. The elution time similarly loses its α dependence:

$$t_{el} = (1+k')\frac{L}{v_0} \tag{69}$$

This time is a useful reference point for second-order kinetics with all values of α. However, for $\alpha < 1$, the elution times of the leading and trailing edges are arguably more meaningful, and are obtained by determining when the bounds in Equations 63 and 64 reach $z = L$:

$$t_{el,lead} = (1+\alpha k')\frac{L}{v_0} \tag{70}$$

$$t_{el,trail} = (1+k'/\alpha)\frac{L}{v_0} \tag{71}$$

It is notable that the leading-edge elution time matches the form of Equation 32.

For the $\alpha > 1$ case, the H has a strong thermodynamic driving force to go into the solid, but is limited by how much D is present in the solid to be displaced. The gas at the leading edge easily finds D to displace, so the gas goes into the solid rather than moving forward. The gas at the trailing edge does not easily find D to exchange with, so it keeps moving forward through the tube. However, when $\alpha < 1$, the H does not have a strong thermodynamic driving force to go into the solid, but the reaction will still proceed in the presence of an abundance of H. In this case, the D in the solid is being diluted (or soaked) out. At the leading edge, there is not much H, so not much D gets diluted into it, and the H keeps moving down the tube. At the trailing edge, more D comes out to be diluted by the larger amount of H, so there is less H to move down the tube. When $\alpha = 1$, these effects balance, and the front velocity is the same everywhere.

4.2. Solution for finite kinetics

A more complete analytical solution has been derived by Thomas for the case where exchange is kinetically limited.[37] This is the case governed by the one-dimensional flow plus reaction equation (27), and Equations 13 and 16 for the time rate of change of H_s., which combine to form

$$\frac{dH_s}{dt} = \frac{S}{A_s}\left(\alpha k \frac{H}{C_g}\left(1-\frac{H_s}{C_s}\right) - k\frac{H_s}{C_s}\left(1-\frac{H}{C_g}\right)\right) \tag{72}$$

Thomas was studying the case of ion exchange in a packed zeolite column, but the derived solution can be adopted to hydrogen isotope exchange in a tube by identifying analogous parameters. This results in a function that requires several steps to be evaluated.

$$j_1 = (1/k')\frac{v_k S}{v_0 A_g}(v_0 t - z) \tag{73}$$

$$j_2 = \frac{v_k S}{v_0 A_g} z \tag{74}$$

$$\varphi(u_1, u_2) = \int_0^1 u_1 \exp(u_1(1-u_3)) I_0\left(2\sqrt{u_1 u_2 u_3}\right) du_3 \tag{75}$$

$$\frac{H}{C_g} = \frac{I_0\left(2\sqrt{\alpha j_1 j_2}\right) + \varphi(\alpha j_1, j_2)}{I_0\left(2\sqrt{\alpha j_1 j_2}\right) + \varphi(\alpha j_1, j_2) + \varphi(\alpha j_2, j_1)} \tag{76}$$

$$\frac{H_s}{C_g} = \frac{\varphi(\alpha j_2, j_1)}{I_0\left(2\sqrt{\alpha j_1 j_2}\right) + \varphi(\alpha j_1, j_2) + \varphi(\alpha j_2, j_1)} \tag{77}$$

where I_0 is the zero-order modified Bessel function of the first kind. The u's, j's, and φ are intermediate values in the calculation. If the coefficient on j_2 is interpreted as the reciprocal of a height equivalent to a theoretical plate, then j_2 is a measure of axial position in the tube measured as a number of plates. The other intermediate parameters are of less enlightening physical significance; in the author's opinion, it is best to consider H and H_s as functions of z and t, along with parameters such as α and k'. The solution can be impractical to use for extremely large values of α, j_1, or j_2, because the Bessel function resembles an exponential function, leading to values large enough to be difficult to compute. However, it still captures a wide range of behavior for conceptually useful values of α, and includes the transient curve shapes at short times. However, the solution is undefined at times shorter than that needed for the gas to travel from the inlet to a given z. Figure 10 shows the HD peak shape predicted by Thomas under the

same conditions as Figure 9, starting with the fastest kinetics predictable by the implementation of the Bessel function found in software such as Excel and Octave; large v_k values lead to large Bessel function arguments. The other curves have decreasing v_k by factors of 3. The fastest value closely resembles Figure 9, but with rounded corners at the beginning and end of the curve. The slower values lead to increased broadening.

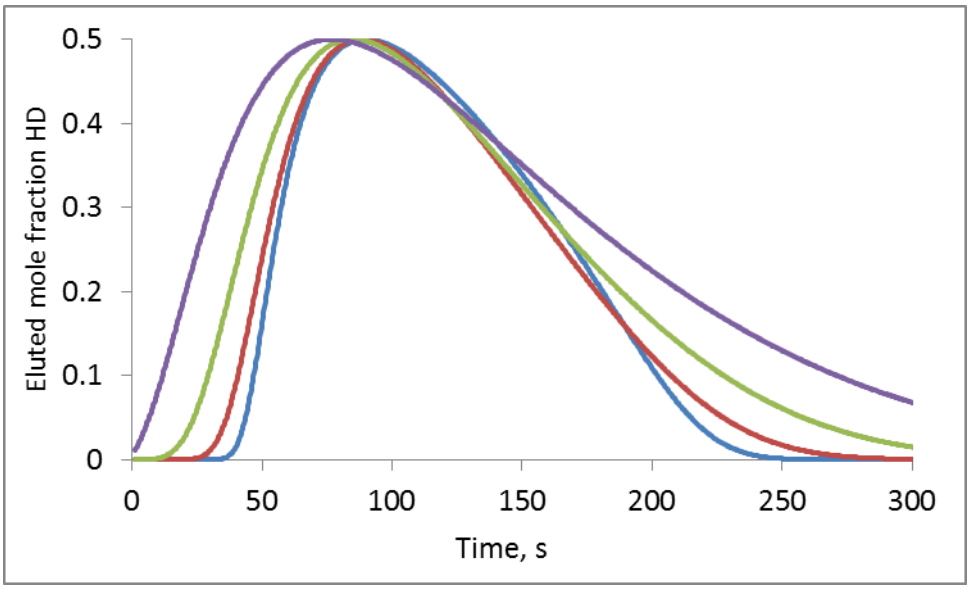

Figure 10. Eluted HD mole fractions versus time as predicted by Thomas for $\alpha = 0.5$, $k' = 100$, $L/v_0 = 1$ s, $v_k S/A_g = 280$ s^{-1} for the sharpest curve, decreasing by factors of 3.

As can also be predicted from Walter's formula, the curve broadens as the tube length increases, as shown in Figure 11. When $\alpha = 1$, the HD peak becomes more symmetric, but still broadens with time, as is expected from the theoretical plate analysis in the previous chapter (such as Equation 50). However, when $\alpha > 1$, the curve does not broaden with time, and is sharper than the cases of lower α. A faster kinetic parameter was used for $\alpha = 0.5$ in order to keep the curves on scale; a lower value leads to broader peaks.

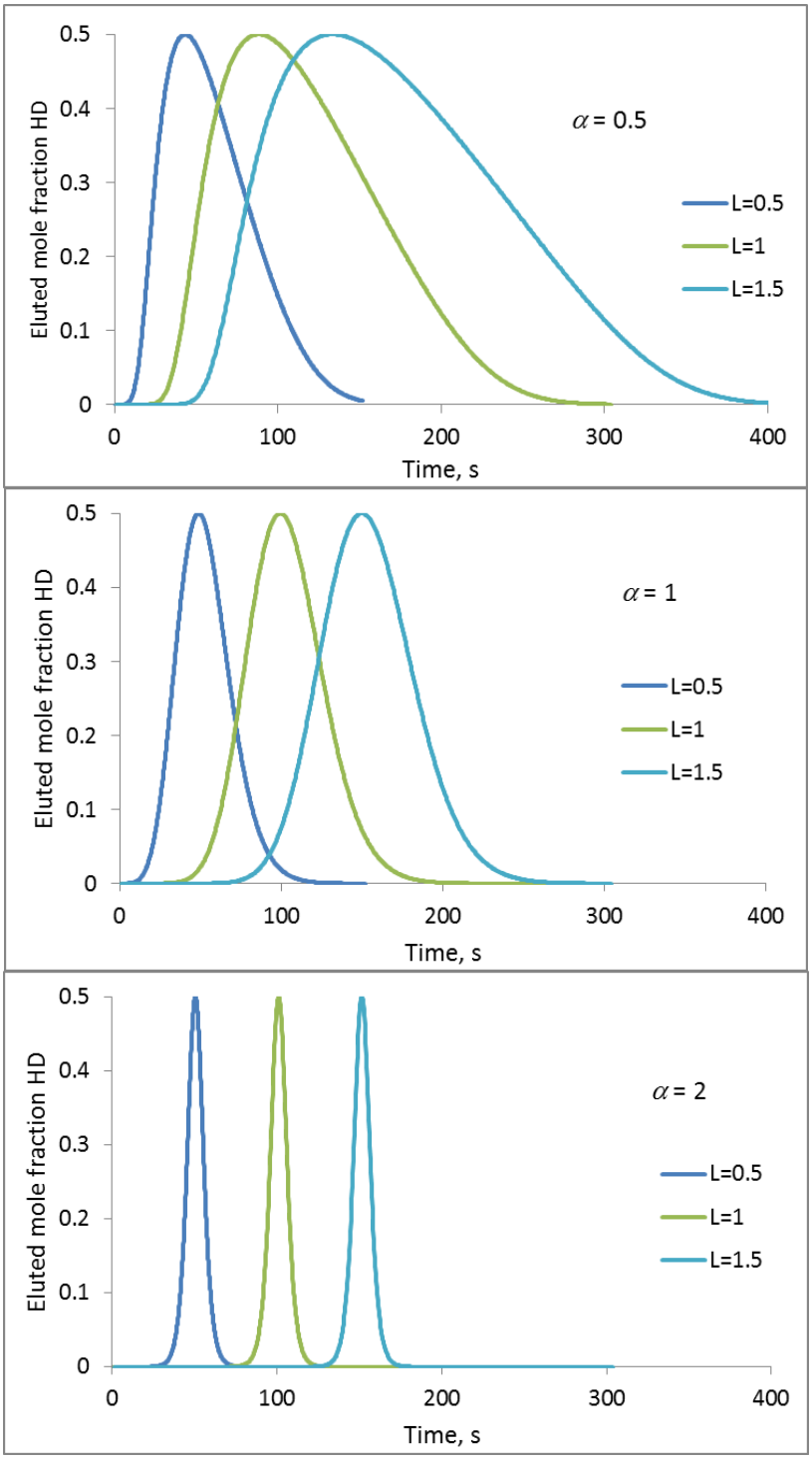

Figure 11. Eluted HD mole fractions versus time as predicted by Thomas for k' = 100, L/v_0 = 1 s, $v_k S/A_g$ = 93 s^{-1} for various tube lengths. Top: α = 0.5, $v_k S/A_g$ = 93 s^{-1}; middle: α = 1, $v_k S/A_g$ = 31 s^{-1}; bottom: α = 2, $v_k S/A_g$ = 31 s^{-1}.

When α is above 1, a balance is seen between kinetic broadening and thermodynamic narrowing of the peak. A simple limiting form can be obtained for α sufficiently above 1, and t sufficiently above zero:

$$\frac{H}{C_g} = \frac{1}{1+\exp\left[\dfrac{2v_k(\alpha-1)(1+k')}{k'v_0 r_0}\left(z-\dfrac{v_0}{(1+k')}t\right)\right]} \tag{78}$$

or equivalently

$$\frac{H}{C_g} = \frac{1}{2}+\frac{1}{2}\tanh\left(\frac{v_k(\alpha-1)(1+k')}{k'v_0 r_0}\left(z-\frac{v_0}{(1+k')}t\right)\right) \tag{79}$$

This function captures the competition between kinetic broadening, which scales with $1/v_k$, and thermodynamic sharpening, which scales with $\alpha-1$. The curve has a sigmoidal shape: that of the hyperbolic tangent, which is slightly different from the error function, as shown in Figure 12. There is apparently no simplified form of the solution derived by Thomas for the case of $\alpha = 1$, but its full form can be used. Because the nonlinear term in the rate law vanishes when $\alpha = 1$, Thomas's solution provides a connection to the first-order reaction described in the previous chapter.

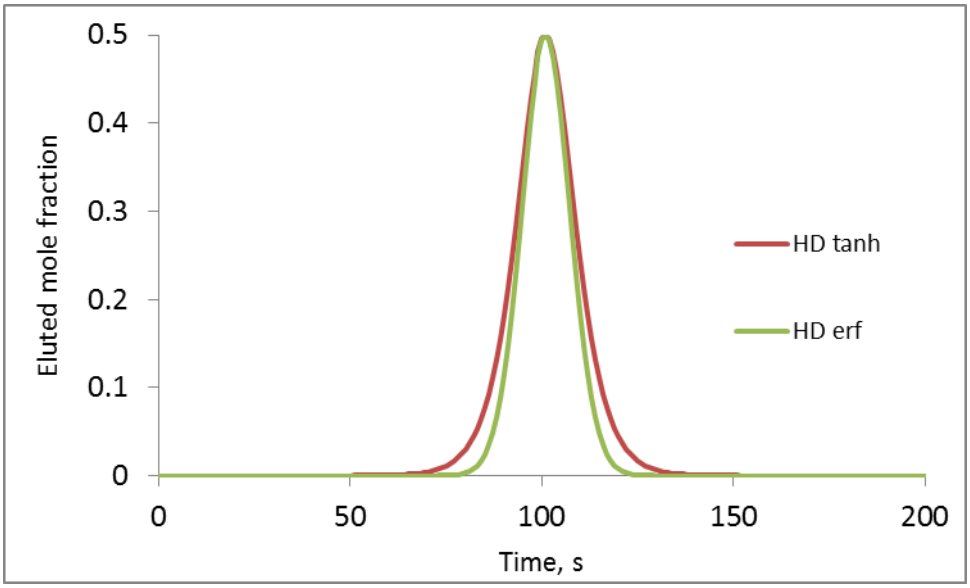

Figure 12. Eluted HD mole fractions versus time as predicted using an error function or hyperbolic tangent function to describe H/C_g under conditions equivalent to Figure 2.

The Thomas function captures the approach to this steady state limit, which occurs most slowly when α is only slightly above 1. In Figure 13, the steady-state condition is reached when the upstream tail of the HD peak is sufficiently far from the inlet of the tube.

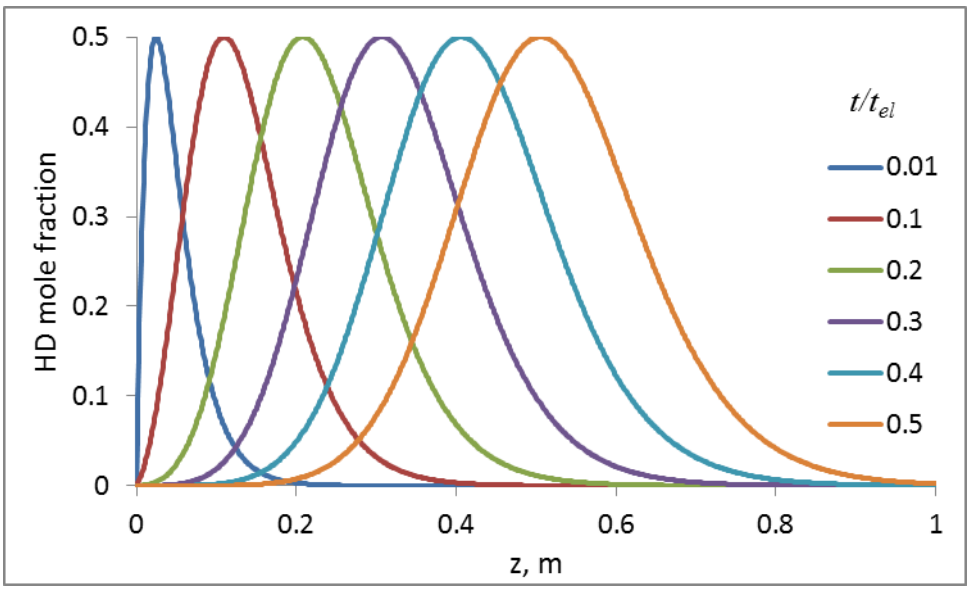

Figure 13. HD mole fractions versus position within tube at various times, expressed as a fraction of the elution time for k' = 100, L/v_0 = 1 s, α = 1.25, $v_k S/A_g$ = 31 s^{-1}.

The rate of the chemical reaction has different effects on the HD curve shape depending on the value of α. Figure 14 illustrates that the peak width grows as the -1/2 power of the rate constant when α = 1, as expected from Clifford's result. When α > 1, the peak width is inversely proportional to the rate constant.

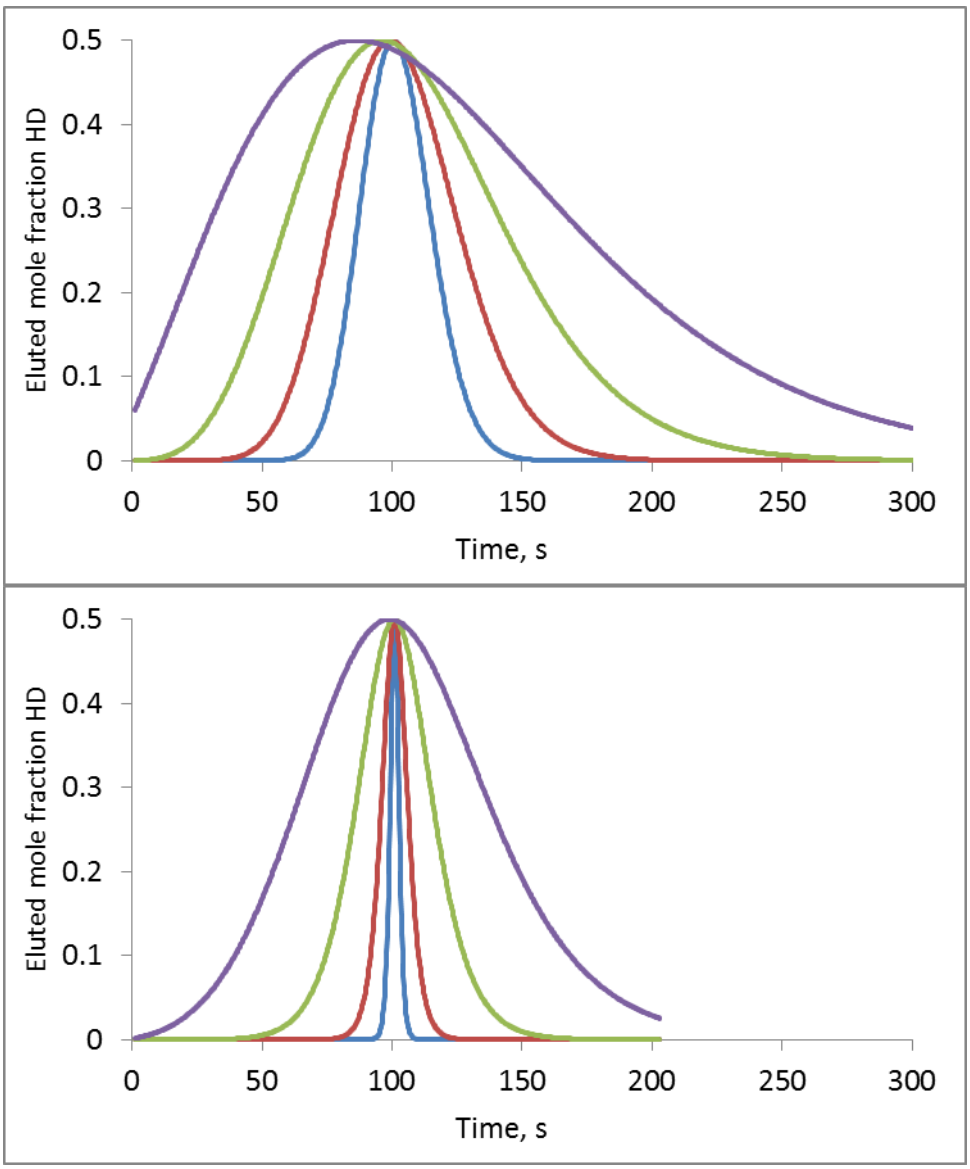

Figure 14. Eluted HD mole fractions versus time as predicted by Thomas for (top) $\alpha = 1$, (bottom) $\alpha = 2$. For both, $k' = 100$, $L/v_0 = 1$ s, $v_k S/A_g = 93$ s^{-1} for the sharpest curve, decreasing by factors of 3.

4.3. Numerical models of mass transport

In the 1940s and 50s, Thomas, Walter, Golay and others used profound mathematical methods to identify a subset of chromatography problems that can be described in detail. Currently, it is possible to substitute brains with brawn through the use of computational tools that numerically solve all varieties of the differential equations. Results presented here are obtained from the COMSOL finite element solver for both the one-dimensional case, and the two-dimensional case that includes radial diffusion. Because COMSOL is complicated and contains features that are not documented in detail, some of its solutions for the one-dimensional case were checked

against a simple finite-difference method implemented in C. The modeling results provide a clearer impression of peak shapes under the conditions described here. It is still desirable to have analytical expressions that capture the dependence of the results on experimental parameters. The models can be used to validate simple approximations of these. All of the cases described include a term for axial diffusion, because this term makes it easier for the solver to get through the very steep concentration gradient imposed by the initial conditions.

4.3.1. One-dimensional flow plus equilibrium reaction plus axial diffusion

If the chemical reaction is fast, an axial diffusion term can simply be added to the flow-plus-equilibrium reaction case considered in Section 4.1 (Equation 61). This gives

$$\left[1+\frac{\alpha k'}{\left(1+(\alpha-1)\left(H/C_g\right)\right)^2}\right]\frac{\partial H}{\partial t}=D\frac{\partial^2 H}{\partial z^2}-v_0\frac{\partial H}{\partial z} \tag{80}$$

Implementation of this equation with the usual boundary conditions yields the results shown in Figure 15, where the gas velocity is varied, which affects the timescale of the simulated experiment; slower velocities allow more time for axial diffusion of gases. Peak positions are normalized versus the elution time predicted by Equation 69. As with the rate constant dependence, the effect of diffusion is relatively small compared to the inherent broadening when $\alpha < 1$. There is an apparent dependence of peak width on gas velocity to the $-1/2$ power for $\alpha =$ 1, and -1 power for $\alpha > 1$, at least for higher gas velocities. The peak shape becomes more skewed than in the kinetic case, as diffusive transport gets to be comparable to advective transport (flow), and the maximum value of the peak leads the elution time determined by gas velocity alone. A version of Equation 35 for second-order kinetics gives an improved estimate of elution time.

$$t_{el}=\left(1+k'\right)\frac{L^2}{D+v_0 L} \tag{81}$$

At the slowest velocities shown in Figure 15, v_0L is comparable to D. For the cases where $\alpha \geq 1$, the times at which half of the HD has eluted are reduced by an amount within a few percent of the predictions of Equation 81, keeping in mind that some simulations were not run to complete elution, as can be seen in the figure. Even when the gas velocity is zero, gas transport and reaction can still be driven by diffusion on a timescale similar to $(1+k')L^2/D$, as discussed further in Section 5.4. Equation 81 does not as accurately predict the time at which half of the HD has eluted in the $\alpha < 1$ case shown in Figure 15, and similarly, Equation 35 does not accurately predict the elution time of the leading edge. However, they still qualitatively identify that elution times deviate from Equations 32 and 69 when v_0L is comparable to or less than D. Golay and Clifford restricted their analysis to the case where the width of the H front (or HD peak) are narrow compared to their position in the tube, but the numerical approach provides more detailed information about a wider range of conditions. While the oscillations observed for high values of α and v_0 in Figure 15 could have been corrected through more careful configuration of the solver, their existence illustrates the fact that cases involving reaction equilibrium (infinitely fast

kinetics) can be more difficult to compute than cases of finite kinetics, as are presented in later sections.

As Figure 16 illustrates, the peak width scales as $(\alpha - 1)^{-1}$ when $\alpha > 1$ and the peak width is much smaller than the elution time. This scaling is similar to that for the kinetically limited case described earlier. Axial diffusion is competing against the thermodynamic effect that sharpens the peak, so a strong α dependence can be expected.

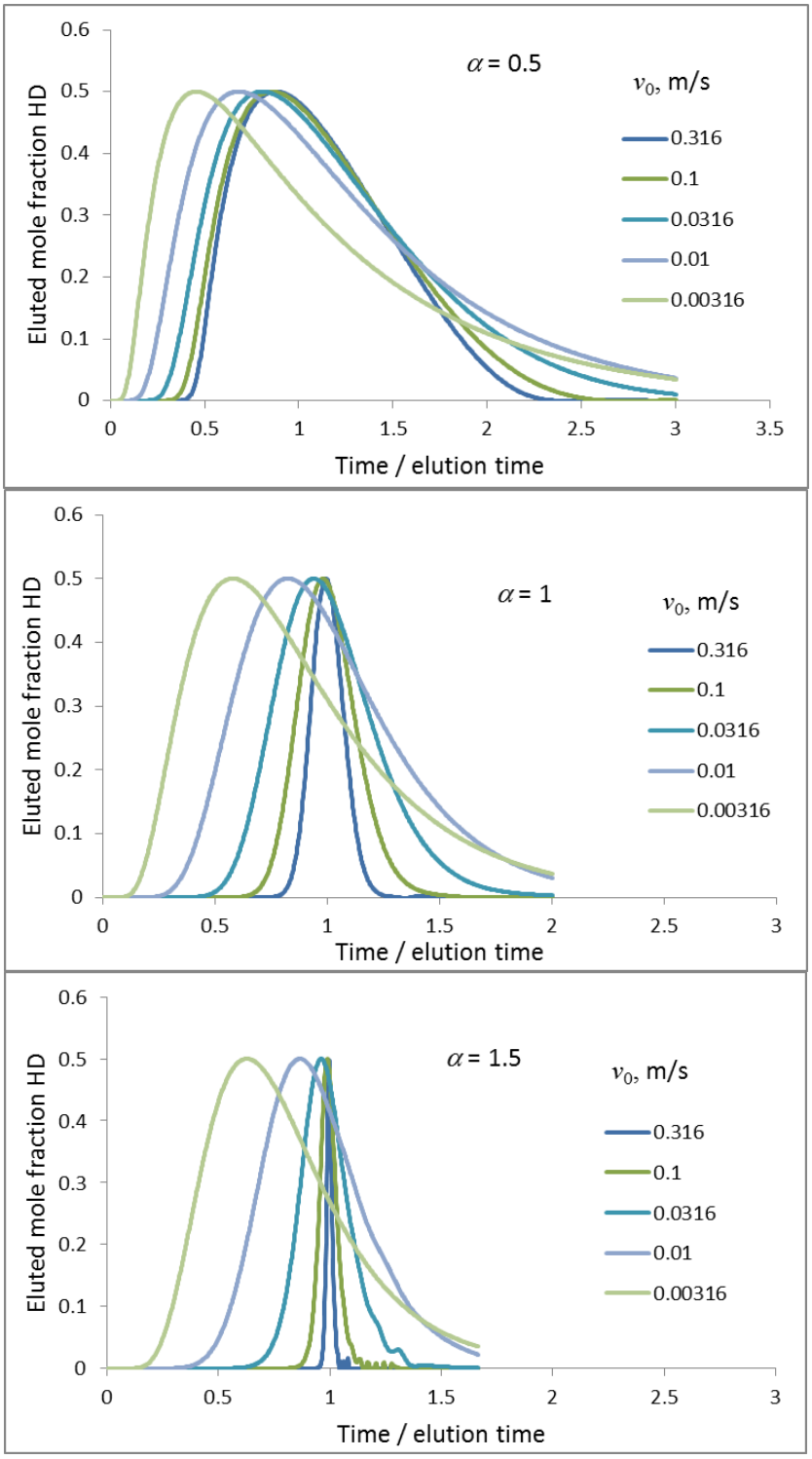

Figure 15. Eluted HD mole fractions versus time as predicted by COMSOL with chemical equilibrium for (top) $\alpha = 0.5$, (middle) $\alpha = 1$, (bottom) $\alpha = 1.5$. For each, $k' = 854$, $L = 0.1$ m, $D = 10^{-4}$ m^2/s, $v_0 = 0.316$ m/s for the sharpest curve, decreasing by factors of 3.16. Oscillations in the bottom curve are from a slightly misconfigured solver. Elution times are from Equation 69.

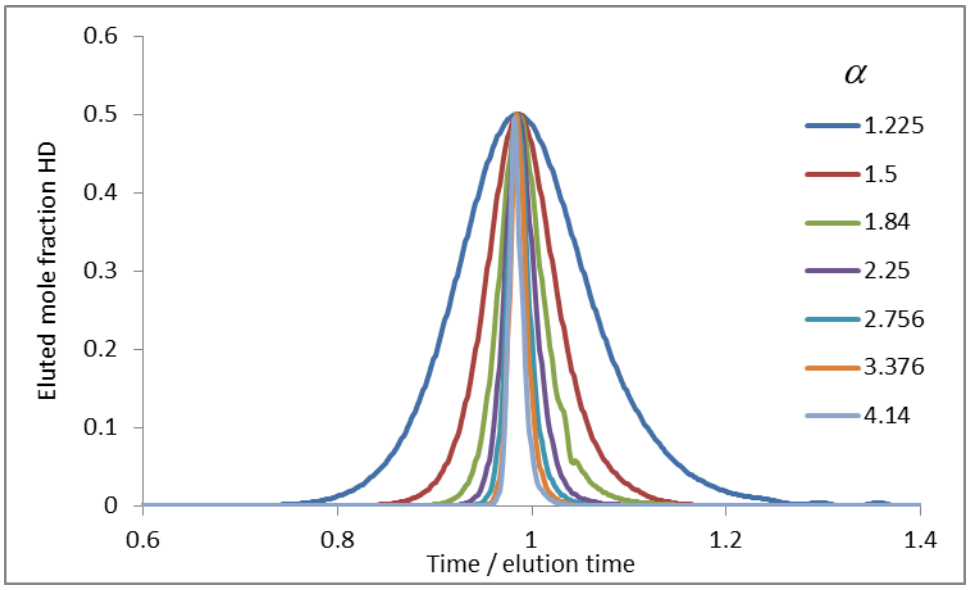

Figure 16. Eluted HD mole fractions versus time as predicted by COMSOL with fast kinetics. For each, k' = 854, L = 0.1 m, D = 10^{-4} m^2/s, v_0 = 0.1 m/s. Elution time is from Equation 69.

4.2.2. Flow plus reaction plus axial and radial diffusion

To incorporate radial diffusion, the same differential equation is used as for Golay's case (Equation 42), or a version with radially independent gas velocity:

$$\frac{\partial H}{\partial t} = D\frac{\partial^2 H}{\partial z^2} + D\frac{1}{r}\frac{\partial}{\partial r}\left(r\frac{\partial H}{\partial r}\right) - v_0\frac{\partial H}{\partial z} \tag{82}$$

along with a boundary condition modified to incorporate the nonlinear isotherm:

$$-D\frac{\partial H}{\partial r} = \frac{\alpha k' r_0}{2\left(1+(\alpha-1)\left(H/C_g\right)\right)^2}\frac{\partial H}{\partial t} \tag{83}$$

The effect of radial diffusion is illustrated in Figure 17 for both Poiseuille flow (parabolic radial dependence of gas velocity) and plug flow (no radial dependence of gas velocity) for various values of α. Poiseuille flow results in broader peaks, with a simple relationship: the plug-flow peaks are narrower by a factor of 0.75. The peaks are asymmetric, with a sharper tail on the leading side, whereas a peak limited by axial diffusion is sharper on the trailing side. The peak widths show a dependence weaker than $(\alpha-1)^{-1}$. In this case, the diffusion process is in series with the chemical reaction – that is, the gas must diffuse radially before it can react. For that reason, it makes sense that it would reduce the dependence of the peak width on chemical reaction effects, and reduce the ability of the reaction effects to sharpen the peak. Figure 17

shows that both flow types result in radial concentration variations, but confirms that the overall broadening is greater in the Poiseuille case.

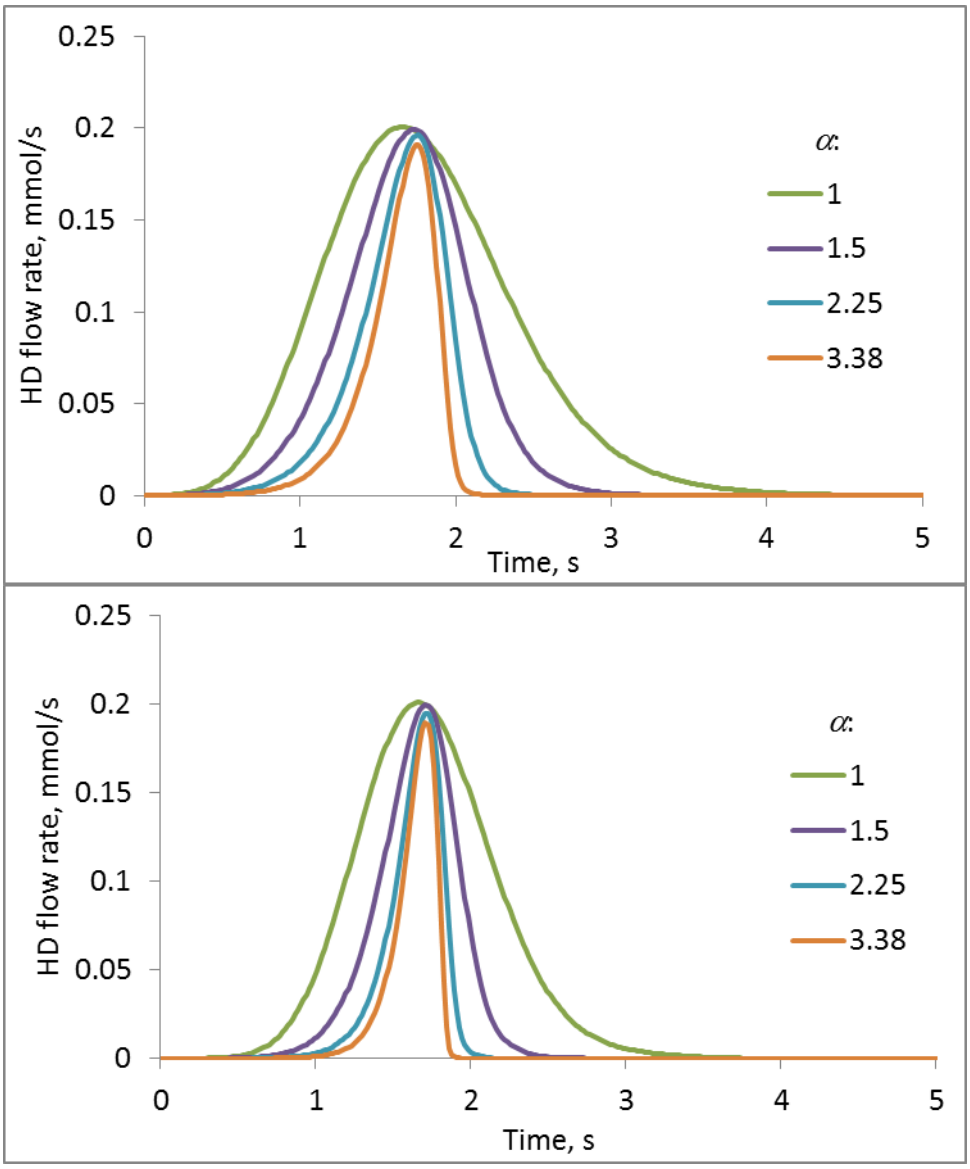

Figure 17. Eluted HD mole fractions versus time as predicted by COMSOL with fast kinetics for (top) Poiseuille flow, (bottom) plug flow. For each, k' = 854, L = 0.1 m, D = 10^{-4} m^2/s, v_0 = 50 m/s, r_0 = $5x10^{-4}$ m.

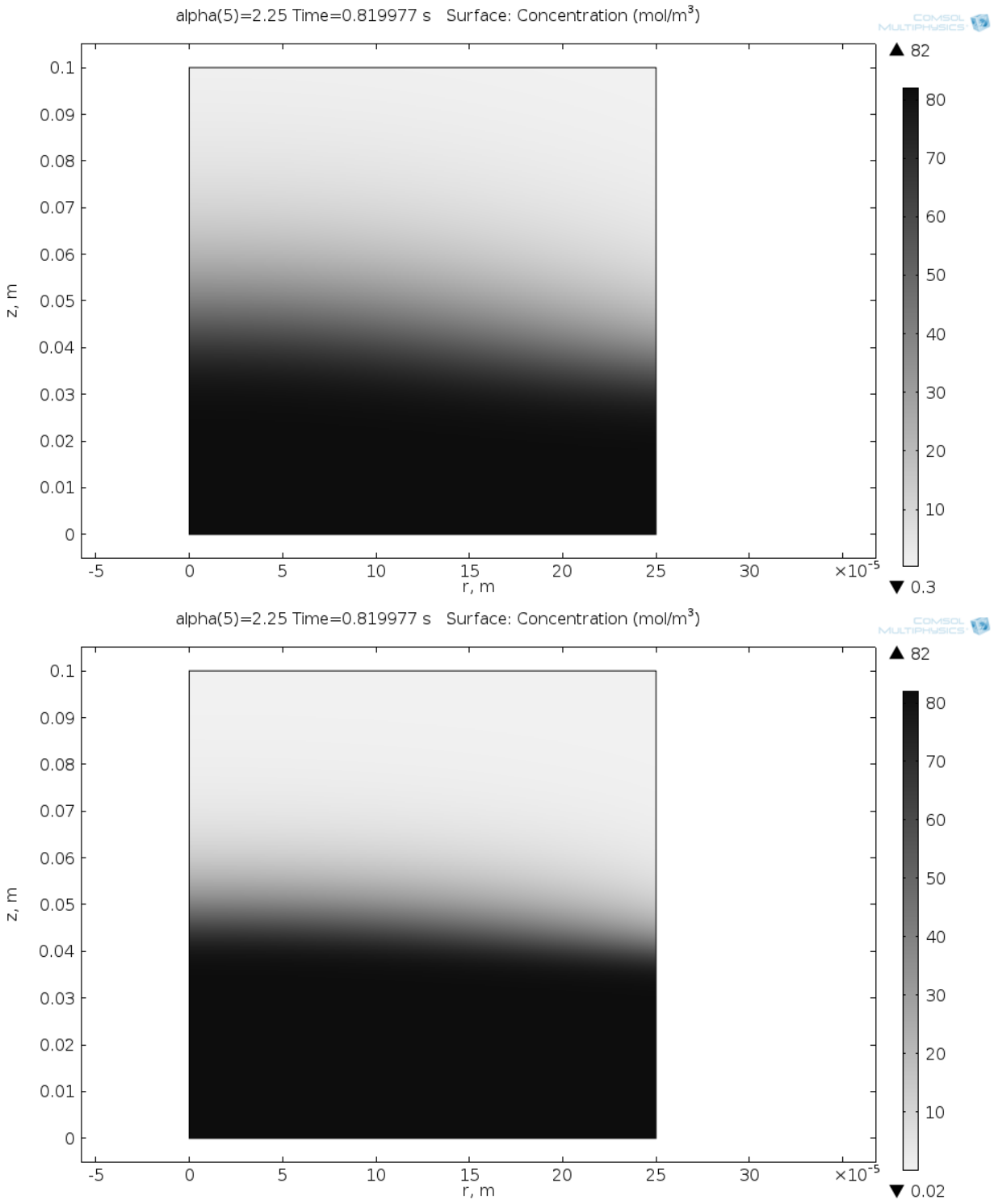

Figure 18. H concentration versus position at 0.2 s as predicted by COMSOL with fast kinetics for (top) Poiseuille flow, (bottom) plug flow. For each, α = 2.25, k' = 854, L = 0.1 m, D = 10^{-4} m^2/s, v_0 = 50 m/s, r_0 = 2.5x10^{-4} m.

4.2.1. Flow plus reaction plus diffusion with slow kinetics

Numerical methods can also be used to study the combination of the mass transport effects with a slow chemical reaction. In this case, H_s must be recorded as a separate variable. For a one-dimensional model that considers only axial diffusion, the full rate law for H_s (Equation 72) is combined with Equation 33 for mass balance of H, and initial, inlet, and outlet conditions. For a two-dimensional model that includes radial diffusion, Equation 42 or 82 provides mass balance for H, Equation 72 describes H_s, and the reaction rate defines the flux at the phase boundary:

$$-D\frac{\partial H}{\partial r} = R = \alpha k \frac{H}{C_g}\left(1-\frac{H_s}{C_s}\right) - k\frac{H_s}{C_s}\left(1-\frac{H}{C_g}\right) \tag{84}$$

Results from several of these combined models will be introduced at varying levels of detail in subsequent sections and chapters. Not every combination of assumptions of fast or slow steps is considered in detail, but the necessary concepts for a desired combination can be found in this report.

4.3. Analytical approximations to include mass transport

Hiester and Vermeulen have extended the solution obtained by Thomas to incorporate mass transport limits typical of ion exchange chromatography.[38] It has not been extended to incorporate axial or radial gas-phase diffusion, but it is still possible to compare these effects to kinetic and thermodynamic effects.

For $\alpha > 1$, if a broadening mechanism is present, such as axial diffusion or slow kinetics, a finite amount of broadening will occur that is a balance between the broadening and sharpening mechanisms. The balance is an approximately steady-state condition that can be assumed to apply at long times in long tubes, where the peak width would diverge for lower α values. There are some extreme conditions, such as near-zero gas velocity, where the steady-state approximation is less useful, as shown in Section 5.4 for purely diffusive gas transport.

The j parameters can be generalized to

$$j_2 = (z/\sigma) \tag{85}$$

$$j_1 = \frac{1}{k'\sigma}(v_0 t - z) \tag{86}$$

allowing a more general σ that combines the various broadening effects. This follows the general strategy of Vermeulen. A numerical model that incorporates axial and radial diffusion along with second-order kinetics was implemented in COMSOL as described in Section 4.2.1. Comparison of the generalized Thomas solution to solutions computed in COMSOL gives, at least in the range of $1 < \alpha < 5$,

$$\sigma = \left(\frac{1.25D}{v_0} + \frac{v_0 r_0}{2v_k} + \frac{(1+\alpha) v_0 r_0^2}{8D} \right) \tag{87}$$

If there is no radial dependence of gas velocity, a good fit to COMSOL simulations is obtained if the third term is multiplied by 0.75. A generalized version of the solution for $\alpha > 1$ incorporating these broadening terms is

$$\frac{H}{C_g} = \frac{1}{1 + \exp\left[\frac{(\alpha - 1)(1 + k')}{k'\sigma} \left(z - \frac{v_0}{(1+k')} t \right) \right]} \tag{88}$$

For $\alpha > 1.5$, COMSOL results are reasonably well described by the following expression for the width of the HD peak (defined by its area divided by its peak value):

$$\frac{\sigma_{\mathrm{HD}}}{L} = \frac{4}{\alpha - 1} \left(\frac{1.25D}{v_0 L} + \frac{v_0 r_0}{2v_k L} + \frac{(\alpha + 1) v_0 r_0^2}{8DL} \right) \tag{89}$$

This expression was obtained by performing simulations at a variety of α values in the range 1 to 5, and choices of the other parameters to ensure that they were rate-limiting in a given simulation. The resulting HD peak widths were calculated, and fit as functions of α. The tube length L is included here for comparison to similar expressions in Chapter 3 (most notably, Equations 43 and 50). As with those similar expressions, this expression is most valid when $\sigma_{\mathrm{HD}} << L$. The degree of accuracy of this generalized solution is illustrated in Figure 19 by comparison to COMSOL models. The kinetically limited case is essentially an exact match, as expected. The diffusive cases have different peak shapes. The approximate solution is far from perfect, but much better than would be obtained by neglecting the mass transport processes. It is suitable as an initial estimate that can be confirmed by a numerical solution of the equations.

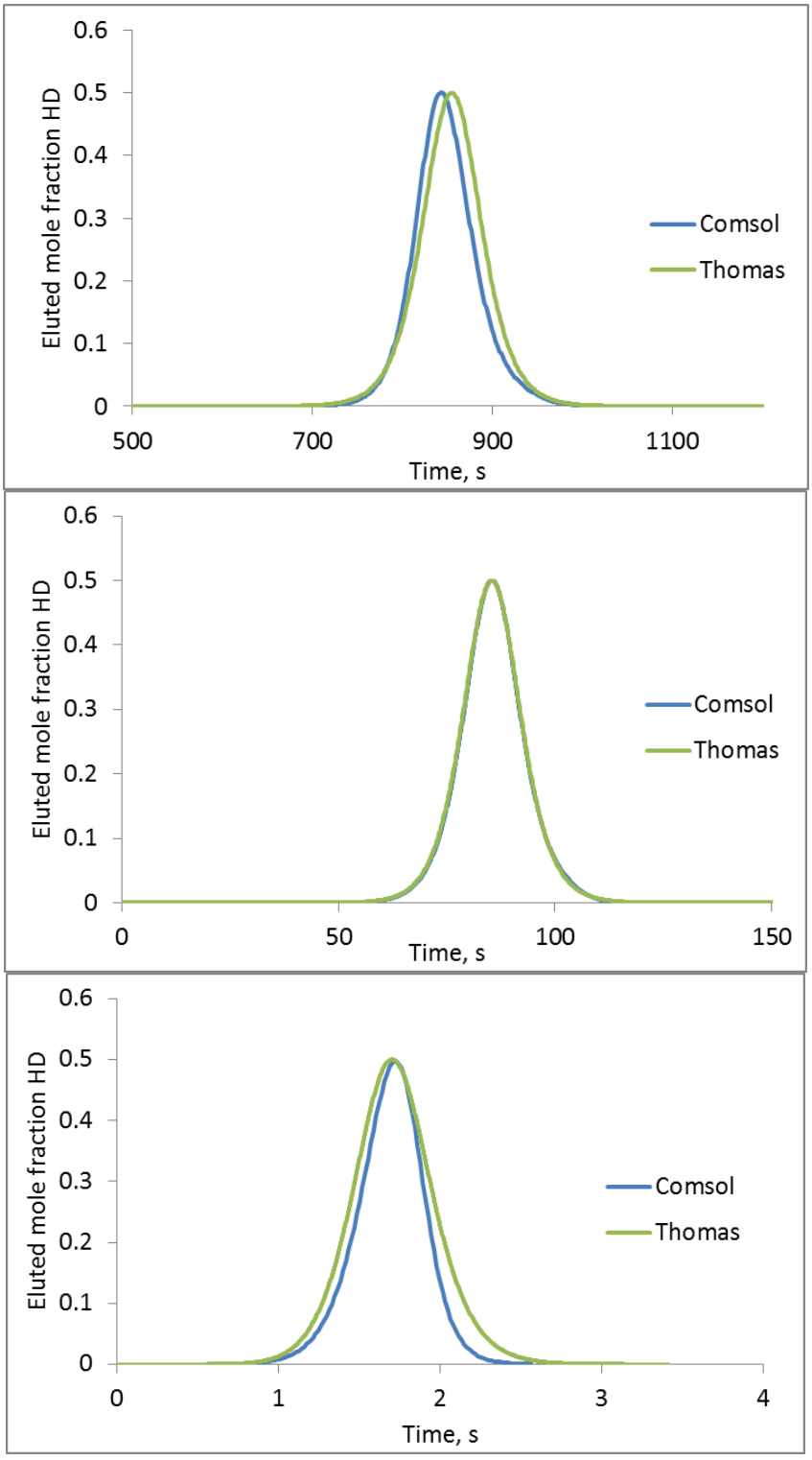

Figure 19. Eluted HD mole fractions versus time as predicted by COMSOL and the generalized Thomas equation (88) for (top, axial diffusion-limited) $D = 10^{-4}$ m^2/s, $v_0 = 0.1$ m/s, $v_k = 1$ m/s; (middle, kinetically limited) $D = 10^{-5}$ m^2/s, $v_0 = 1$ m/s, $v_k = 10^{-2}$ m/s; (bottom, radial diffusion-limited) $D = 10^{-5}$ m^2/s, $v_0 = 50$ m/s, $v_k = 1$ m/s. For each, $\alpha = 1.5$, $k' = 854$, $L = 0.1$ m.

4.4. Performance optimization

The previous section provided an expression for σ/L that resembles the theoretical plate expression derived by Clifford. These differ in their coefficients, and the fact that σ/L is squared in the case of a first-order reaction, but not in the case of the second-order reaction. Squaring σ/L in the definition of the number of plates makes sense in linear chromatography, because the peak broadens in proportion to $L^{1/2}$, but the peak does not broaden for a second-order reaction when $\alpha > 1$. The lack of broadening changes the tradeoff between number of plates and the rate of their creation, because plates are created in direct proportion to both time and length, and their rate of creation is constant. The tradeoff is instead drawn from the pressure drop constraint, which constrains r for a given L. In that case, L can be chosen, and then the optimum v_0 determined. The number of plates and elution time can be determined from these, and L adjusted as necessary. An expression to be optimized that is similar to the case of the first-order reaction is

$$\frac{1}{N} \propto \frac{\sigma_{\mathrm{HD}}}{L} = \frac{4}{\alpha - 1}\frac{v_0}{L}\left(\frac{1.25D}{v_0^2} + \frac{1}{v_k}\left(\frac{40\mu v_0 L}{C_g R_g T}\right)^{1/2} + \frac{(\alpha+1)}{D}\frac{20\mu v_0 L}{C_g R_g T}\right) \tag{90}$$

For this problem, the number of plates is defined without squaring σ/L. Plots of N and Nv_0/L as a function of v_0 and L can aid in the optimization as before, and they are very similar in form to those shown in Chapter 3, such as Equations 43 and 50.

4.5. Optimization with sharpening

An opportunity for further optimization of the plate production rate (or plate duration) exists for the case of second-order kinetics, but it is not easily addressed by the Thomas equation (76) or the theoretical plate treatments described above, such as Equation 89. The Thomas equation describes the response to a step input, and the plate treatment considers the steady-state condition where the peak width is constant. Figure 13 shows the transition from a step function to a peak of finite, constant width, as predicted by the Thomas function. As can be shown by numerical modeling, this process also occurs for the opposite case: if the initial condition is a broad smear of H and H_s across the length of the tube, the reaction front still makes a transition to the same finite, constant width. This is illustrated in Figure 20, where the initial concentrations are high over the first third of the tube. The H front achieves its steady-state sharpness by the time it is halfway through the tube.

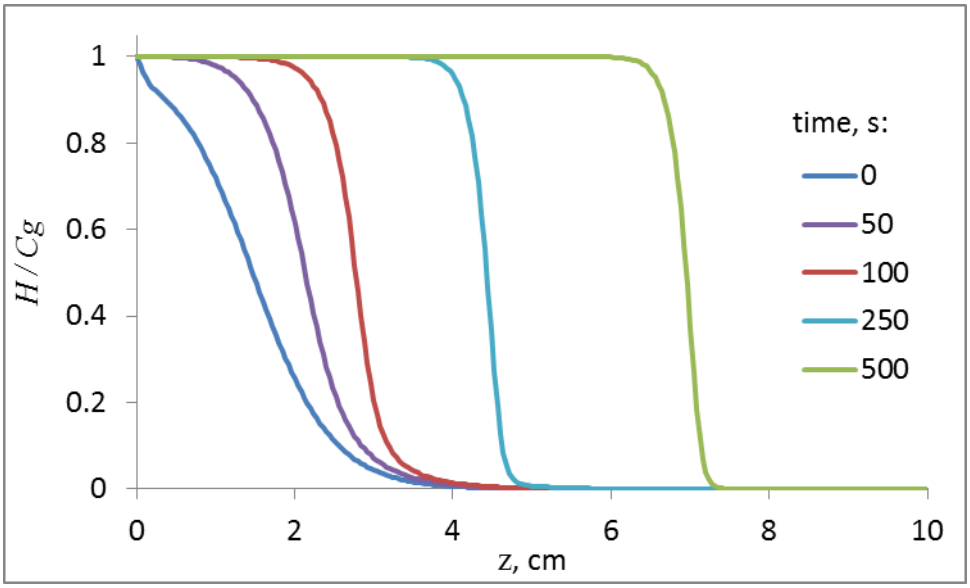

Figure 20. H concentrations inside a tube that started with a broad axial distribution of H and H_s from a one-dimensional COMSOL model with D = 10^{-4} m^2/s, v_0 = 10 cm/s, v_k = 2.75 cm/s, ID 0.01 cm, α = 3.0, k' = 854, L = 10 cm.

This self-correcting behavior could be exploited to improve the plate production rate by operating the tube at a gas velocity that is significantly faster than the optimum predicted by the previous section (Equation 89), causing a broad axial distribution of H_s, but not enough to cause a significant elution of H. Then the velocity could be reduced to the optimum, sharpening the distribution to the same shape it would be if the experiment had been performed more slowly, and allowing a sharp elution in a shorter period of time. Equations 67 and 68 describe the velocities of the leading and trailing edge of the reaction front. If the front has initially broadened so that the trailing edge is still at the inlet, it is possible to estimate how far into the tube the leading edge can be, while still allowing the trailing edge to catch up by the time the front elutes from the tube. For a large value of k', this distance is $L\left(1-1/\alpha^2\right)$. The tube would be operated at a higher-than-optimal velocity that would yield a number of plates (synonymous here with the ratio of tube length to front width) equal to about $\alpha^2/\left(\alpha^2-1\right)$. The velocity could be determined by the number of plates from a figure similar to Figure 4. When the leading edge of the front reaches $L\left(1-1/\alpha^2\right)$, the midpoint of the front has traveled about half as far. A way to measure that this condition has been reached is by determining that $0.5\left(1-1/\alpha^2\right)$ of the eluate has eluted. At that time, the velocity would be reduced to the optimal value. This assumes that the optimal number of plates is very high; reducing the eluted fraction at which the velocity transition occurs by an amount equal to the reciprocal of the optimal number of plates, with a corresponding reduction of the initial velocity, would help ensure a sharp front upon elution. Figure 21 demonstrates this concept (without precise optimization) for a case where α = 2. The high-velocity segment requires about 16 seconds to reach 37.5% elution, with a front spreading across the first three fourths of the tube at that time. After the gas velocity is reduced, elution occurs at about 535 s. The HD peak is slightly asymmetric due to a small amount of H that leaks through prior to elution. Use of a slightly lower initial velocity, such as 100 cm/s, would mitigate this. If no high initial gas velocity were used, elution would occur at about 838 s. This concept is

explored further in Chapter 6, which considers the effect of time-dependent gas velocity in greater detail.

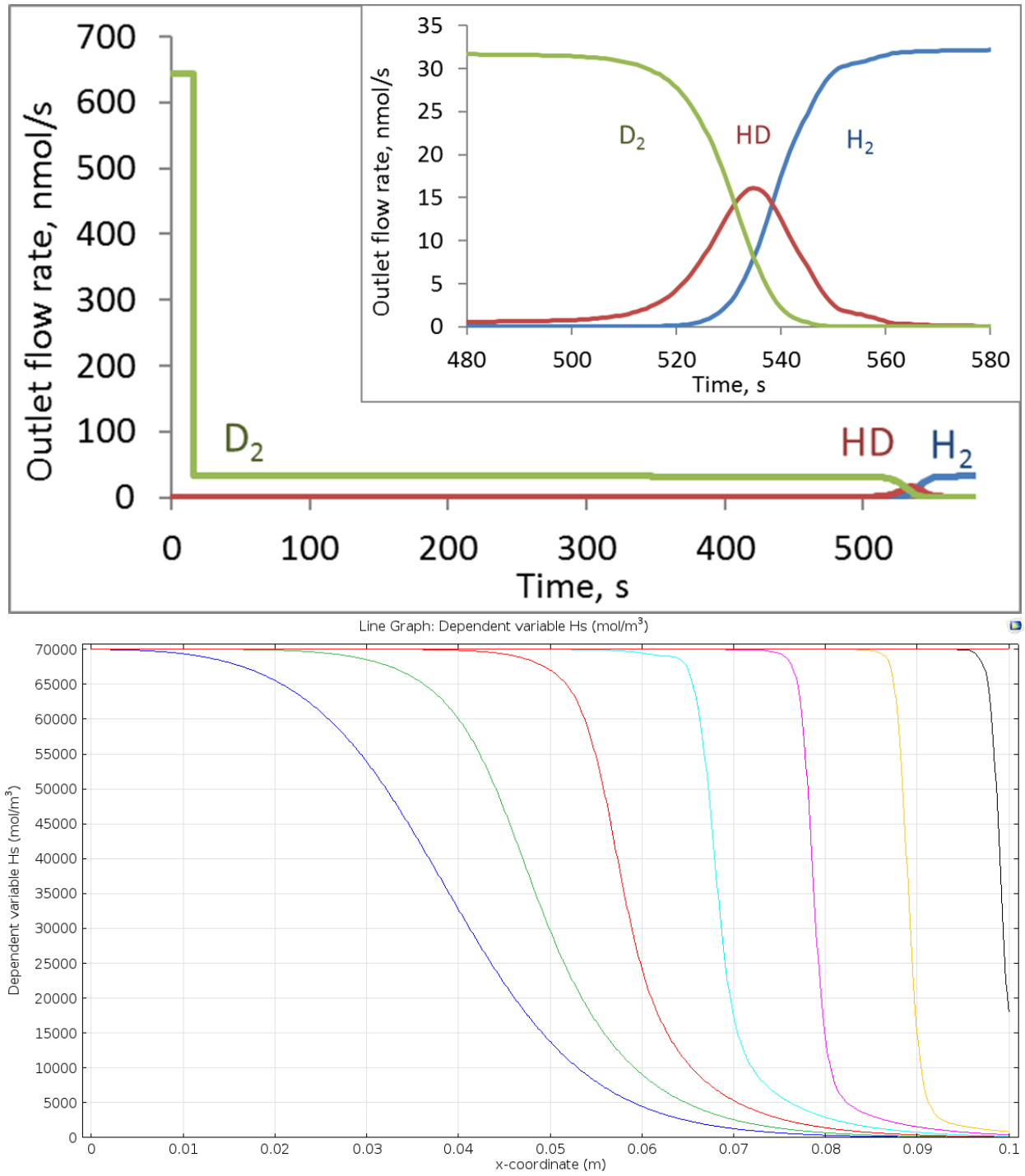

Figure 21. Top: Tube with initial v_0 = 200 cm/s, reduced to 10 cm/s at 37.5% elution. Bottom: H_s concentrations inside the tube at even time intervals starting from 37.5% elution. D = 10^{-5} m^2/s, v_k = 0.55 cm/s, ID 0.01 cm, α = 2.0, k' = 854, L = 10 cm.

5. HIERARCHICAL POROSITY

5.1. Solid-phase diffusion

The previous chapters focus on the connection between gas transport and reaction kinetics, ignoring transport in the solid phase. However, in the examples described, the fraction of the tube's cross-sectional area occupied by the solid phase is comparable to that of the gas phase. There is no flow mechanism in this phase, so diffusion is the only means of transport. Chapter 2 noted that the diffusivity in the solid is 20,000,000 times lower than in the gas phase. In the same amount of time, hydrogen can diffuse about 4,000 times farther in the gas phase. Another important aspect of this is that the concentration in the solid phase is about 1000 times higher, so to obtain a given flux, the relative concentration gradient in the solid must be about 20,000 times that in the gas. Equation 82 (axial and radial diffusion, plug flow) is used in examples here for mass balance in the gas phase. For the solid phase:

$$\frac{\partial H_s}{\partial t} = D_s \frac{\partial^2 H_s}{\partial z^2} + D_s \frac{1}{r}\frac{\partial}{\partial r}\left(r \frac{\partial H_s}{\partial r}\right) \tag{91}$$

and at the phase boundary,

$$R = -D\frac{\partial H}{\partial r} = -D_s \frac{\partial H_s}{\partial r} = \alpha k \frac{H}{C_g}\left(1 - \frac{H_s}{C_s}\right) - k\frac{H_s}{C_s}\left(1 - \frac{H}{C_g}\right) \tag{92}$$

The usual inlet, outlet, and initial conditions apply, and all other boundaries of the solid phase have zero normal slope.

Figure 22 shows two examples of COMSOL predictions of this case. Solid-phase diffusion limits transport significantly more than gas-phase radial diffusion at high gas velocities. Previous chapters (which neglect solid-phase diffusion) have shown that the optimum velocity for this geometry is around 1 m/s. Under these conditions, that value is a lower; Figure 22 shows that the phases are not far from equilibrium at about 0.1 m/s. It is reassuring that, despite the very small diffusivity for the solid phase, transport from the solid phase can still proceed at a respectable rate in this geometry. Near equilibrium, the front in the solid phase runs slightly ahead of that in the gas phase due to the nonlinear shape of the isotherm; this would not occur if $\alpha = 1$.

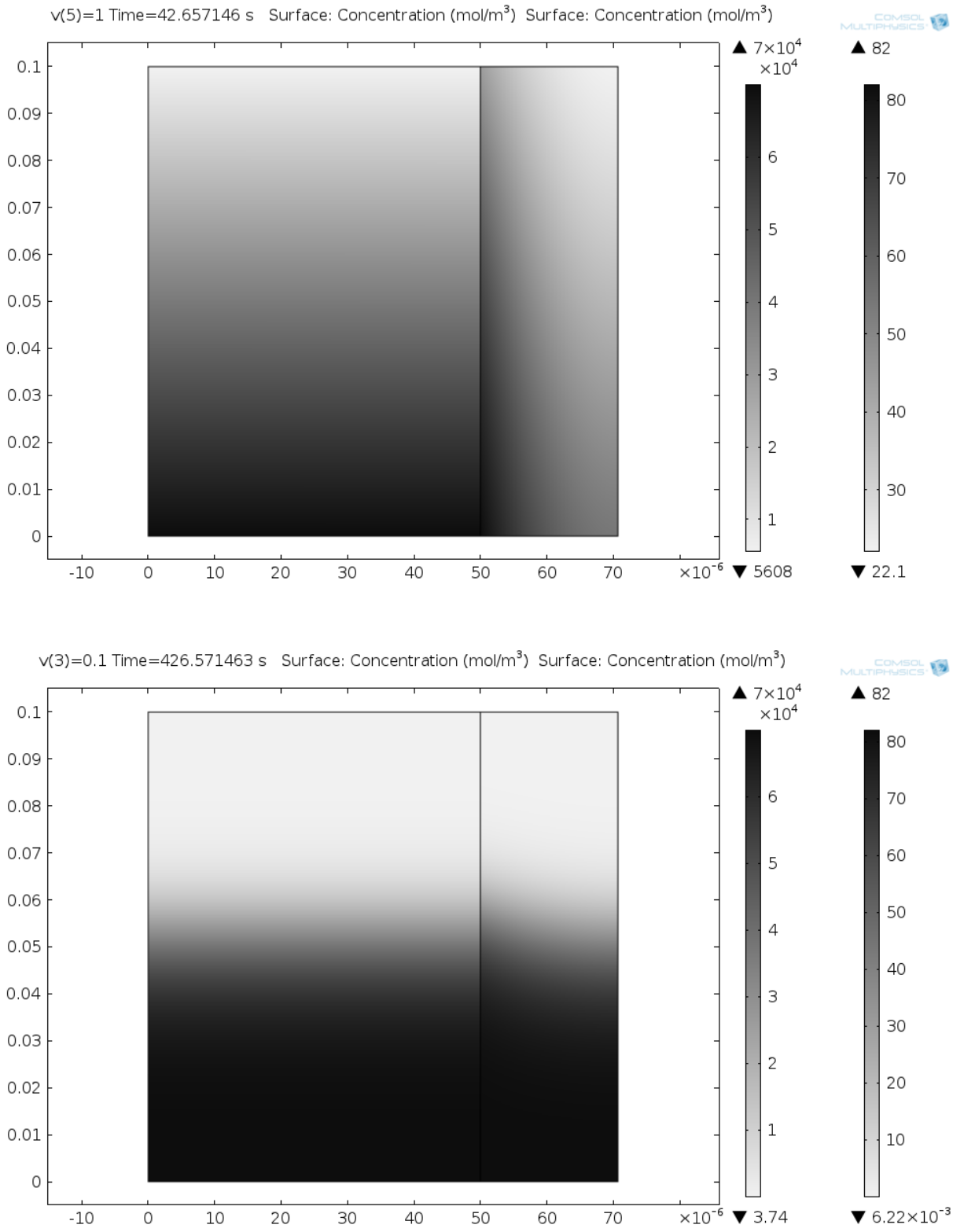

Figure 22. Maps of H (left region) and H_s (right region) in mol/m³ versus position in the tube (m) as predicted by COMSOL for gas velocities of (top) 1 m/s and (bottom) 0.1 m/s for D = 10⁻⁴ m²/s, v_k = 0.55 m/s, D_s = 5x10⁻¹² m²/s, α = 2, k' = 853, r_0 = 100 μm.

Similar COMSOL calculations were made using an anisotropic diffusivity to omit the effect of solid-phase axial diffusion. Any differences present were quite small.

Golay has provided a plate expression for solid-phase diffusion in a tubular gas chromatography column.[1] It captures the concepts described above, and provides a quantitative analytical estimate of this effect in comparison to other mechanisms that limit peak sharpness.

$$\frac{1}{N} = \frac{C_g v_0 \left(OD^2 - ID^2\right)}{24 C_s D_s L} \tag{93}$$

This predicts about 1 plate for the top plot of Figure 22, and about 10 for the bottom plot, which is approximately consistent with the ratio of front width to tube length observed there. An extension of this to $\alpha > 1.5$, which could be added to Equation 89, can be derived from fits to COMSOL model results:

$$\frac{\sigma_{\mathrm{HD}}}{L} = \frac{4}{\alpha - 1}\left(\frac{(\alpha+1) C_g v_0 \left(OD^2 - ID^2\right)}{97 C_s D_s L}\right) \tag{94}$$

It could also be added to Equation 87 if the prefactor is omitted. This has a similar form to the gas-phase radial diffusion term in Equation 89, and also closely resembles Equation 93 if the α-containing factors are neglected. It is for cases where the peak width reaches steady-state within the column, which never occurs when $\alpha = 1$, as described in Chapters 2 and 3.

5.2. Linear driving force approximation

A simplified treatment of solid-phase diffusion can be obtained using a generalization of Glueckauf's linear driving force approximation.[39,40] This reduces the dimensionality of H_s that must be accounted for, by relating the surface concentration to the average bulk concentration $\overline{H}_s$, both of which are independent of radial position. If solid-phase axial diffusion can be considered negligible, then H_s and $\overline{H}_s$ can follow ordinary differential equations. The method works for a set of simple geometries such as a sphere, cylinder, or a hollow tube, at timescales exceeding an appreciable fraction of the square of a characteristic length of the geometry (such as radius) divided by the diffusivity. That is, the approximation does not apply at very short times after an abrupt change when the concentration gradient near the phase boundary is very large. As implemented here, H_s is reinterpreted as the solid-phase hydrogen concentration near the surface.

$$\frac{\partial \overline{H}_s}{\partial t} = \frac{24}{(5\xi + 3)(\xi - 1)^2} \frac{D_s}{r_0^2} \left(H_s - \overline{H}_s\right) \tag{95}$$

Here, $\xi = OD/ID$. To incorporate this into a one-dimensional model that includes axial diffusion and flow in the gas phase, along with finite reaction kinetics,

$$\frac{\partial H}{\partial t} = D\frac{\partial^2 H}{\partial z^2} - v_0\frac{\partial H}{\partial z} - \frac{Sk}{A_g}\left[\alpha\frac{H}{C_g}\left(1-\frac{H_s}{C_s}\right) - \frac{H_s}{C_s}\left(1-\frac{H}{C_g}\right)\right] \tag{96}$$

$$\frac{\partial H_s}{\partial t} = \frac{Sk}{S\delta}\left[\alpha\frac{H}{C_g}\left(1-\frac{H_s}{C_s}\right) - \frac{H_s}{C_s}\left(1-\frac{H}{C_g}\right)\right] - \left(\frac{A_s}{S\delta}-1\right)\frac{\partial \overline{H}_s}{\partial t} \tag{97}$$

where δ is a nominal thickness of the surface layer, perhaps one percent of *OD*. The result is not expected to be sensitive to small changes in this parameter. If so, the assumptions for the given situation should be examined. For fast kinetics, the surface layer can be accounted for more simply:

$$\frac{\partial H}{\partial t} = D\frac{\partial^2 H}{\partial z^2} - v_0\frac{\partial H}{\partial z} - \frac{A_s}{A_g}\frac{\partial \overline{H}_s}{\partial t} \tag{98}$$

$$\frac{\partial \overline{H}_s}{\partial t} = \frac{24}{(5\xi+3)(\xi-1)^2}\frac{D_s}{r_0^2}\left(\frac{\alpha C_s H}{C_g + (\alpha-1)H} - \overline{H}_s\right) \tag{99}$$

However, COMSOL can often converge more quickly for cases of finite kinetics.

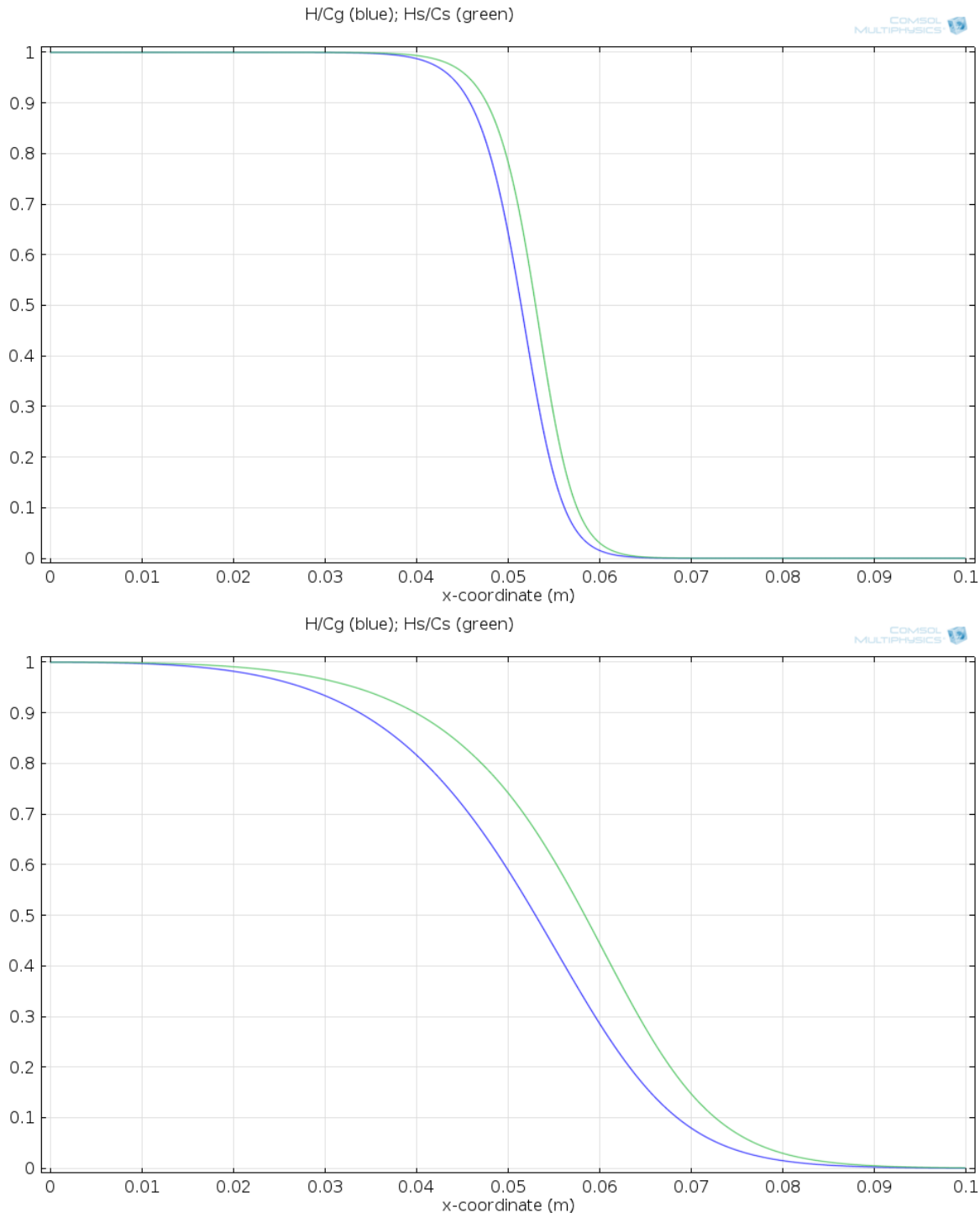

Figure 23. Plots of H (blue) and H_s (green) in mol/m^3 versus position in the tube (m) as predicted by COMSOL with a linear driving force approximation for solid-phase diffusion, using gas velocities of (top) 0.01 m/s and (bottom) 0.1 m/s, and D = 10^{-4} m^2/s, D_s = 5x10^{-12} m^2/s, α = 2, k' = 853, r_0 = 100 μm.

Figure 23 illustrates that a one-dimensional model treating solid-phase diffusion with the linear driving force approximation gives results similar to that of the full two-dimensional axisymmetric model, where the front in the solid phase leads that in the gas phase at low velocities, and at higher velocities, the front is significantly broadened in each phase, and there is a greater difference between the phases.

When generalizing the Thomas solution, Vermeulen also suggests a solid diffusion term in the theoretical plate formula based on Glueckauf's linear driving force model. It takes the form v_0/L divided by the coefficient in the linear driving force equation (95). The concentration ratio between the phases would presumably be retained, leading to

$$\frac{1}{N} = \frac{(5\xi + 3)(\xi - 1)^2 C_g v_0 r_0^2}{24 C_s D_s L} \tag{100}$$

This expression is quite similar to the expression derived by Golay, who did not make thorough considerations of the annular geometry of the solid phase, effectively using $\xi^2 - 1$ as the function of ξ. The Glueckauf version increases more steeply, reflecting that the volume increases more than linearly with *OD*, so it is likely a better model of thick solid layers.

5.3. Concept of hierarchical porosity

A useful strategy to reduce any mass transport limitations caused by long-distance diffusion in the solid phase, and also to increase surface area to improve the molar throughput of the chemical reaction, is to include pores in the solid phase. An example geometry is an array of cylindrical pores of diameter much smaller than *ID* that extend radially from the gas-solid boundary to the outer diameter, packed so that the pore volume fraction equals the solid volume fraction (a 50% porous solid phase). Hydrogen can diffuse through the gas phase more quickly than through the solid phase, and the pore surface area is much higher than that of the macroscopic gas-solid boundary. This scenario is easily modeled in COMSOL by combining several concepts introduced in this report. More elaborate arrangements could be envisioned in which flow occurs in the pore channels, but that will not be considered here. Porous solid phases are widely used in analytical (first-order) gas chromatography, even though the solid phase is usually thinner than described here. In that context, this geometry is known as "porous-layer open tube" (PLOT).

5.4. Purely diffusive channel

To understand the hierarchical arrangement, it is helpful to first understand the behavior of an individual pore in the solid phase, where there is no flow, and the pore has only one entrance. Hydrogen transport in a diffusion channel could be described by

$$\frac{\partial H}{\partial t} = D\frac{\partial^2 H}{\partial z^2} - \frac{A_s}{A_g}\frac{\partial H_s}{\partial t} \tag{101}$$

where H is fixed at the inlet and there is a zero-slope boundary condition at the end.

Incorporating first-order reaction equilibrium leads to

$$\frac{\partial H}{\partial t} = \frac{D}{1+\alpha k'}\frac{\partial^2 H}{\partial z^2} \tag{102}$$

This is basically the diffusion equation with a reduced diffusivity. H_s obeys the same differential equation, and differs from H only by the scaling factor

$$H_s = \alpha k' H \tag{103}$$

For the second-order reaction, it is

$$\left[1+\frac{\alpha k'}{\left(1+(\alpha-1)(H/C_g)\right)^2}\right]\frac{\partial H}{\partial t} = D\frac{\partial^2 H}{\partial z^2} \tag{104}$$

which is more complicated, but is easily modeled in COMSOL. Figure 24 shows the molar flow rate of H from a diffusive channel after a concentration step at the inlet. Higher values of α result only in small changes in flow rate, mostly at longer times. Figure 25 shows the HD concentration within the channel at various times. An HD peak is present at short times, but it is quite broad, and only slightly sharpened by increased α. It soon transforms into a monotonic gradient along the channel length, and decreases to zero as the reaction completes.

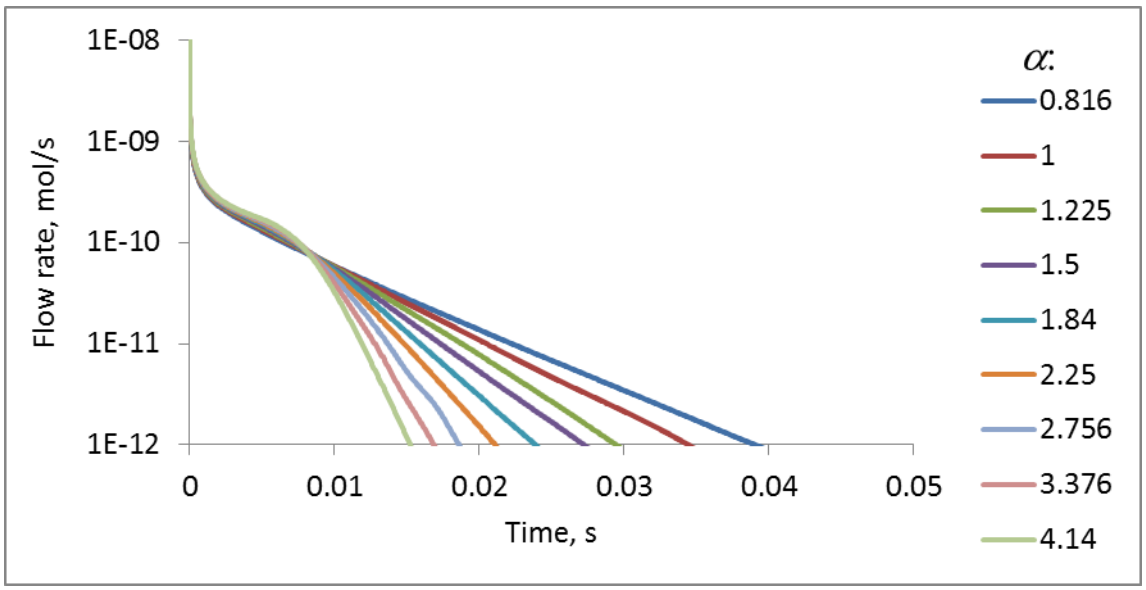

Figure 24. Molar flow rate of H from diffusive channel when the inlet H is stepped from zero to C_g with ID 1 μm, OD 1.41 μm, D 1 cm^2/s, and L 41.4 μm.

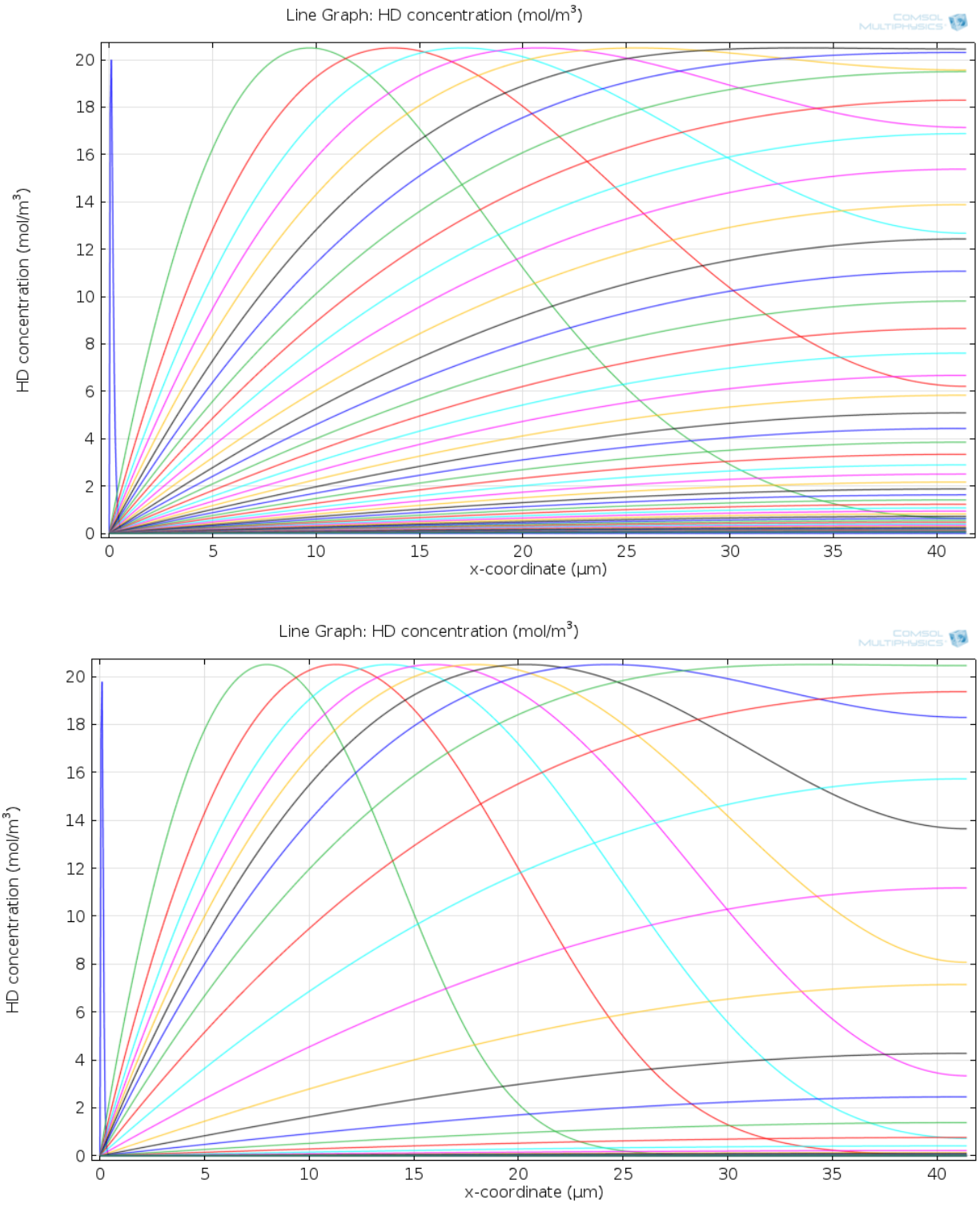

Figure 25. HD concentration in single-ended diffusion channel at various times when (top) a = 1, (bottom) a = 4.14. At increasing times, the peaks move from left to right. After the peaks have flattened, the curves move down with time. Colors match at equal times for the two plots.

5.5. Porous stationary phase

A one-dimensional model of transport in a pore is a convenient simplification, but the problem is still complicated when there is a very large number of such pores, and the state of each depends on their axial position. This problem has been addressed by Newman *et al*. for the case of porous battery electrodes,[41] as well as by common treatments of packed-powder columns. Both H and H_s are treated as continuous functions throughout the porous solid, regardless of whether a given microscopic point is within the solid volume or pore volume. However, the concentrations in the porous region are those in their respective phases: moles per pore volume, or moles per solid volume. The porosity ϕ is the ratio of pore volume to total volume, and can be used to convert between pore, solid, and total volumes. The term "stationary phase" is a generalization of what previous sections have called the solid phase. It is a region consisting of the solid along with gas that is not flowing. The region where the gas is flowing is the mobile phase.

For a two-dimensional axisymmetric model of a tube with a porous stationary phase, the mobile phase can be described by Equation 42, Golay's case from Section 3.1.4. To describe H in the stationary phase, an equation analogous to Equation 101 in Section 5.4 can be used, noting that the pores are now taken to extend radially rather than axially.

$$\frac{\partial H}{\partial t} = \frac{D}{r}\frac{\partial}{\partial r}\left(r\frac{\partial H}{\partial r}\right) - \frac{A_s^*}{A_g^*}\frac{\partial H_s}{\partial t} \tag{105}$$

Here, the asterisks are meant to indicate pore geometry rather than tube geometry. That area ratio is

$$\frac{A_s^*}{A_g^*} = \frac{1-\phi}{\phi} \tag{106}$$

The assumption of straight, uniform radial pores and walls is not very realistic if the porous layer is thick, but the current treatment will ignore this. Especially if the pores have axial interconnections, an axial diffusion term can be included. Considerations of the effect of three-dimensional porosity on the diffusivity can get complicated, but often do not significantly improve accuracy. Including the axial diffusion term may allow a simulation to proceed with larger timesteps without significantly changing the result, so it can be practical to include it. The results shown in this section include axial diffusion in the stationary phase for COMSOL calculations.

H can be considered continuous across the boundary between mobile and stationary phases. However, the concentrations have different interpretations in each region: moles per total volume in the mobile phase, and moles per pore volume in the stationary phase. This can be accounted for by a flux discontinuity at the boundary. The outward flux at the boundary just inside the mobile phase is $-D\partial H/\partial r$, whereas just inside the stationary phase it is $-D\partial(\phi H)/\partial r$, measuring flux in terms of moles per total boundary area per unit time. The net flux created at the boundary must be equal to the difference of these: $-D(1-\phi)\partial H/\partial r$.[42] This assumes that

$\partial H/\partial r$ is continuous across the boundary, which is true if there is rapid equilibration with the solid phase right at the boundary, and thus no flux into the solid. Essentially, this boundary condition destroys the flux resulting from the fictitious presence of *H* in the solid. This condition is necessary to obtain mass balance. Further elaborations, which are not implemented here, can impose mass transport limitations, such as the entropic barrier at the pore entrance.[43]

The model geometry does not capture microscopic transport along the pore radius, but that is still of interest, because a key goal is to determine how big or small the pores must be. That effect can still be captured using the linear driving force model, which is only considered here for transport in the solid, and not for gas transport along the pore radius. $\overline{H}_s$ can be described as in Section 5.2 (Equation 95), with the tube radius replaced by the pore radius r_p, and noting that, in the context of a pore, $\xi = \phi^{-1/2}$.

$$\frac{\partial \overline{H}_s}{\partial t} = \frac{24\phi^{3/2}}{\left(5+3\sqrt{\phi}\right)\left(1-\sqrt{\phi}\right)^2}\frac{D_s}{r_p^2}\left(H_s - \overline{H}_s\right) \tag{107}$$

Transport from *H* to $\overline{H}_s$ must be broken into two steps, with H_s as an intermediate.

$$\frac{\partial H}{\partial t} = \frac{D}{r}\frac{\partial}{\partial r}\left(r\frac{\partial H}{\partial r}\right) - \frac{S^* k}{A_g^*}\left[\alpha\frac{H}{C_g}\left(1-\frac{H_s}{C_s}\right) - \frac{H_s}{C_s}\left(1-\frac{H}{C_g}\right)\right] \tag{108}$$

$$\frac{\partial H_s}{\partial t} = \frac{S^* k}{S^*\delta}\left[\alpha\frac{H}{C_g}\left(1-\frac{H_s}{C_s}\right) - \frac{H_s}{C_s}\left(1-\frac{H}{C_g}\right)\right] - \left(\frac{A_s^*}{A_g^*}\frac{A_g^*}{S^*\delta} - 1\right)\frac{\partial \overline{H}_s}{\partial t} \tag{109}$$

$$\frac{A_g^*}{S^*} = \frac{r_p}{2} \tag{110}$$

The capacity of the stationary phase is such that

$$k' = \frac{\left((1-\phi)C_s + \phi C_g\right)A_s}{C_g A_g} \tag{111}$$

Figure 26 illustrates that the incorporation of 5 µm diameter pores into the stationary phase effectively cures the solid-phase mass transport limitation described for a nonporous solid phase as described in Section 5.1. This justifies the use of simpler models that neglect solid-phase transport, as used in the previous chapters. However, it is important to have this more complex model to verify that the stationary-phase porosity achieves its goal.

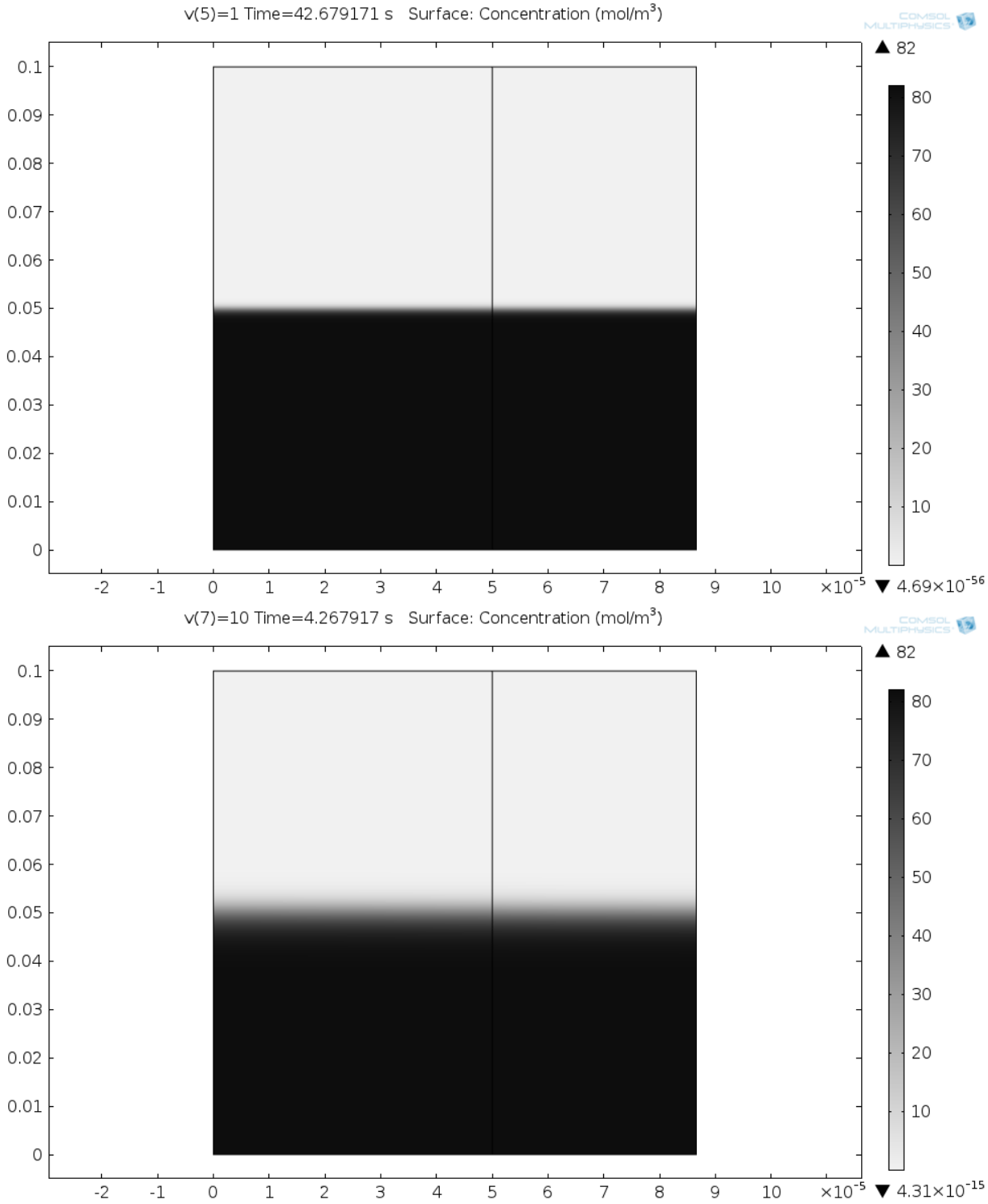

Figure 26. Maps of H in the mobile phase (left) and stationary phase (right) in mol/m^3 versus position in the tube (m) as predicted by COMSOL for gas velocities of (top) 1 m/s and (bottom) 10 m/s for D = 10^{-4} m^2/s, v_k = 0.55 m/s, D_s = 5x10^{-12} m^2/s, α = 2, k' = 853, r_0 = 100 µm, r_p = 5 µm.

Further understanding of the effect of stationary phase pore size can be obtained by simulating a variety of values of r_p while holding other conditions constant. Figure 27 shows that pores of 10 µm radius result in a broad HD peak, whereas any value 1 µm or below results in a sharp peak under these conditions.

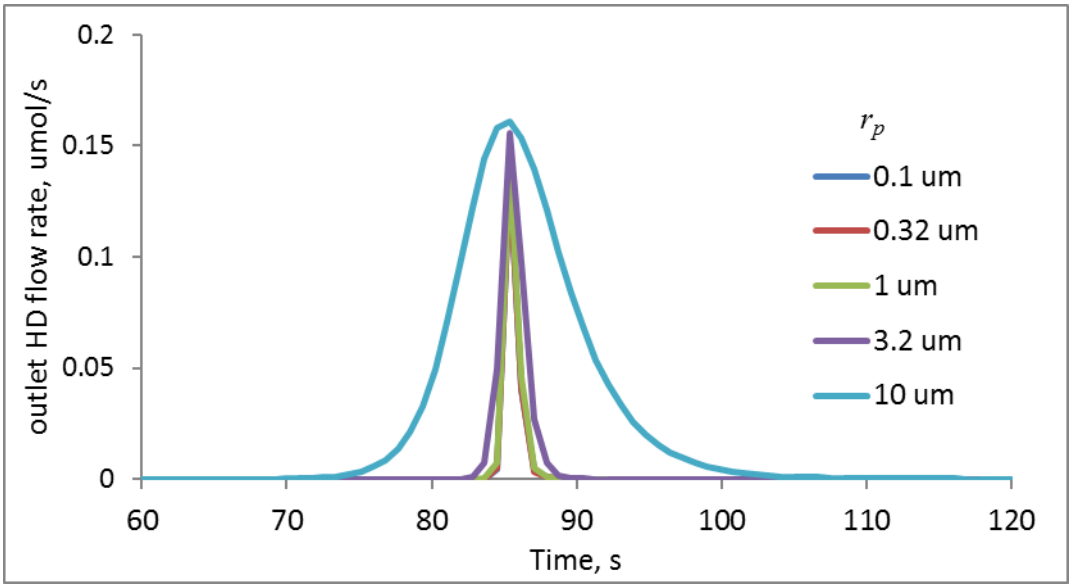

Figure 27. Outlet molar flow rate of HD for several values of r_p and v_0 = 1 m/s, D = 10^{-4} m^2/s, v_k = 0.55 m/s, D_s = $5x10^{-12}$ m^2/s, α = 2, k' = 853, ID = 0.01 cm. Values of r_p of 1 um or less are overlapping.

5.5. Plate expression

From these considerations, a more complete plate expression can be proposed for the case of hierarchical pores:

$$\frac{1}{N} \propto \frac{\sigma_{\mathrm{HD}}}{L} = \frac{4}{\alpha - 1}\left(\frac{1.25D}{v_0 L} + \frac{v_0 r_p}{4(\xi - 1)\phi v_k L} + \frac{(\alpha+1)\xi v_0 r_0^2}{8DL} + \frac{(\alpha+1)\left(1-\sqrt{\phi}\right)^2 C_g v_0 r_p^2}{16\phi^{3/2} C_s D_s L} \right) \quad (112)$$

where ξ refers to the tube geometry, and not the pore geometry. The first term is the same axial diffusion term as in Equation 89 in Section 4.3. The second term is the same kinetic term, but divided by the ratio of the surface area of a pore wall to the corresponding area of the boundary between the mobile and stationary phases. The third term is the same radial gas-phase diffusion term, but multiplied by ξ to reflect that the gas must diffuse across both the flow channel radius and much of the pore length. Because the gas is absorbed along the length of the pore, this term is likely a more complicated function of ξ; a linear relationship is proposed as a simple estimate. The fourth term accounts for solid-phase diffusion by transforming Equation 100 in analogy to the transformation from Equation 93 to 94, with the porosity substitution as described in the

previous section for Equation 107, and approximating $5+3\sqrt{\phi}\approx 6$. Some effort would be required to validate the dependence of each parameter through COMSOL modeling, but this plate expression may be a useful starting point for estimation of the performance of a hydride tube with a porous stationary phase.

6. PRESSURE DROP

6.1. Steady-state pressure drop

In the previous chapters, the effect of a finite pressure drop was neglected for simplicity. This assumption is especially questionable for large values of v_0 and small values of *ID*. Optimizations were constrained to ensure a low pressure drop in previous chapters, but if this constraint can be relaxed, improved optimization methods are possible.

Though a tube is expected to have a lower pressure drop than a similarly performing packed powder column, and previous chapters have focused on cases of low $\Delta P/P$, it is still useful to consider the consequences of a larger pressure drop, because this can affect choices of tube radius and gas velocity. The key aspects have been pointed out by Golay,[1,44] and important concepts are presented in Chapter 2. Because both the diffusivity and velocity are inversely proportional to pressure, the ratio v_0/D does not change, even if the pressure (or concentration) varies axially. This means that the plate expressions for axial and radial diffusion, which contain this ratio, do not vary axially. Similarly, the ratio v_0/k' does not change, so if $k' >> 1$, the front velocity does not vary axially. So the neglect of pressure drop in the previous sections has some justification, and the low-pressure drop constraint described earlier may be more useful as a conceptual simplification than a practical necessity. However, the kinetic and solid-phase diffusion terms lead to broadening with increasing gas velocity, and velocity increases along the tube as pressure decreases.

To examine a simple one-dimensional model that includes a finite pressure drop, axial diffusion, and finite kinetics, the spatial variation of total concentration and velocity are obtained from Equation 24, and Equation 72 is used to describe the rate of reaction. Mass balance equation 33 is modified by incorporating spatially varying terms within the appropriate derivatives, and arranging that the equation is a function of the mole fraction H/C_g. (Equation 13 is already in this form.) Spatially invariant products C_gD and C_gv_0 are then pulled out of the derivatives. Dividing by C_g then yields an equation closely resembling Equation 33, but a function of gas-phase mole fraction instead of absolute concentration H, and with each right-side term proportional to velocity (or equivalently, $1/C_g$). This results in a form similar to one described in Ref. 27.

$$\frac{\partial\left(H/C_g\right)}{\partial t} = D\frac{\partial^2\left(H/C_g\right)}{\partial z^2} - v_0\frac{\partial\left(H/C_g\right)}{\partial z} - \frac{A_s}{C_g A_g}\frac{\partial H_s}{\partial t} \tag{113}$$

The outlet molar flow rate of H atoms can be found from the outlet mole fraction and total molar flow rate by

$$\dot{n}_{out,H} = C_g A_g\left[v_0\left(H/C_g\right) - D\frac{\partial\left(H/C_g\right)}{\partial z}\right] \tag{114}$$

Diatomic mole fractions can be obtained by dividing Equations 6-8 by $C_g/2$, yielding

$$x_{HH} = \left(\frac{H}{C_g} \right)^2 \tag{115}$$

$$x_{DD} = \left(1 - \frac{H}{C_g} \right)^2 \tag{116}$$

$$x_{HD} = 2\left(\frac{H}{C_g} \right)\left(1 - \frac{H}{C_g} \right) \tag{117}$$

where x_{HH}, x_{DD}, and x_{HD} are the mole fractions of the corresponding diatomic species. These can be substituted for H/C_g in Equation 114 to obtain outlet molar flow rates for diatomic species, but the right-hand side of the expression must also be divided by 2 to convert the total concentration in the prefactor from atomic to molecular.

Similar models to this one-dimensional model can be obtained using different assumptions, such as fast kinetics, or slow radial or solid-phase diffusion. It could be argued that the gas-phase diffusion terms are uninteresting in this context, because axial diffusion is most important when velocities are low, and radial diffusion is most important when *ID* is large, which are both cases where the pressure drop is relatively low. Most interesting, then, are cases with high velocities and slow kinetics or solid-phase diffusion. When examining the effect of pressure drop at fixed outlet concentration, the chemical reaction has a greater ability to keep up with the flow at points upstream, because the velocity is slower there, and if the chemical reaction rate is proportional to gas concentration (as assumed here) that concentration is also higher.

Figure 28 shows results for a one-dimensional model with fast gas flow and slow kinetics for two different gas viscosities, but the same total molar flow rate. There is only a small change in the HD peak width for a factor of 10 change in viscosity, which changes the pressure drop across the tube proportionally. The higher pressure drop actually yields a slightly narrower peak, as expected due to the slower velocity near the inlet. This example illustrates that the approximations of constant velocity and constant total gas concentration throughout a tube can often be useful.

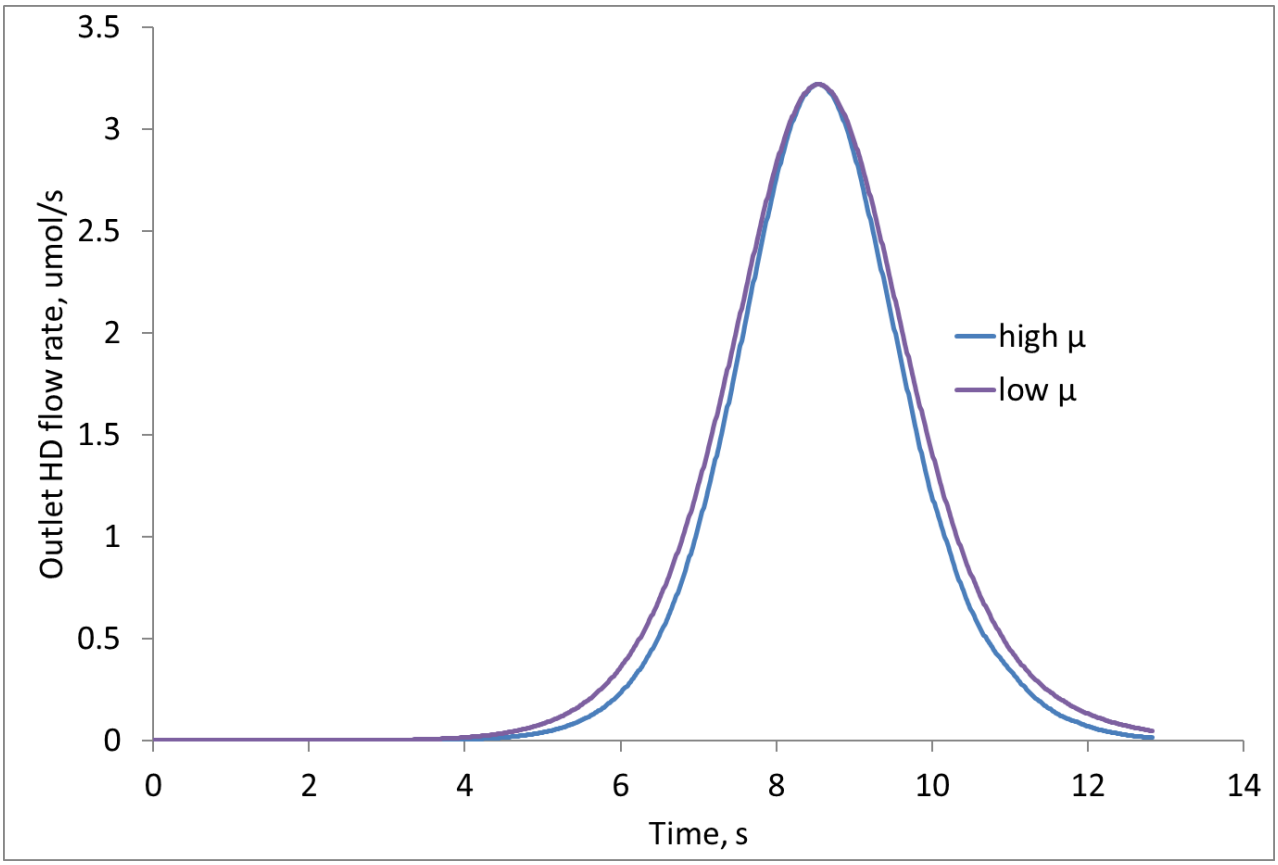

Figure 28. Outlet molar flow rate of HD for μ = 9x10^{-6} (the usual value) and 9x10^{-7} Pa s, v_0 = 10 m/s, D = 10^{-4} m^2/s, v_k = 0.028 m/s, α = 2, k' = 853, ID = 0.0071 cm, L = 10 cm.

The effect of pressure drop can affect optimization scenarios such as that presented in Section 4.5, which involves a high velocity followed by a low velocity; the optimal applied pressure would not be simply proportional to the desired velocities if the pressure drop is large enough. In another scenario, it may be desired to maintain the sharpest possible spatial front width for the full duration of an experiment, such as in a neutron radiography experiment in which the front can be measured at all times.[45] This could be obtained by keeping the gas velocity in the vicinity of the front near the optimal value. If the pressure drop is significant, this would require gradually reducing the applied pressure to maintain a near-constant velocity near the reaction front.

6.2. Time-dependent pressure drop

The optimization scenarios described above involve controlling flow as a function of time, and would be aided by a greater understanding of the behavior of the tube when the inlet or outlet concentration or velocity is changed. That behavior is relatively complicated when abrupt changes cause a departure from the steady-state concentration profile. An approximate time to reach steady state is described in Ref. 29, which in the current context is

$$t_{ss} = \frac{8\pi\mu L^2}{A_g P_{in}} \tag{118}$$

where P_{in} is the inlet pressure. When concentration and velocity changes are small on this timescale, the model described in Section 6.1 may still be valid. In this case, the axial dependence of concentration and velocity are closely approximated by Equation 24, using time-dependent values for the molar flow rate and for gas velocity and total concentration at the inlet and outlet. In this approximation, the molar flow rate still has no spatial variation. One change to Equation 113 is worth consideration. When modifying Equation 33 to allow C_g to vary with both space and time, and arranging to account for H by mole fraction, a product-rule term results that includes the time derivative of C_g. When it has already been assumed that C_g is slowly varying with time, this term can be expected to be small, and perhaps negligible, but in some cases, this time dependence is already known, and easy to include as a step toward improved accuracy. The mass balance equation is then

$$\frac{\partial\left(H/C_g\right)}{\partial t} = D\frac{\partial^2\left(H/C_g\right)}{\partial z^2} - v_0\frac{\partial\left(H/C_g\right)}{\partial z} - \frac{A_s}{C_g A_g}\frac{\partial H_s}{\partial t} - \frac{\left(H/C_g\right)}{C_g}\frac{\partial C_g}{\partial t} \tag{119}$$

Here, H/C_g, C_g, D, and v_0 all vary in time and space, although the greatest variation is in H/C_g, near the reaction front.

A simple example of this is where the outlet is open to the atmosphere, and the inlet is connected to a vessel of fixed volume V and known initial pressure P_0. This configuration leads to high initial velocities that then decrease, approximating the profile needed for the optimization scenarios described above, and provides adjustable design parameters. As shown in Ref. 29, the inlet pressure varies as

$$P_{in}(t) = P_{out}\frac{(P_0 + P_{out}) + (P_0 - P_{out})e^{-k_V t}}{(P_0 + P_{out}) - (P_0 - P_{out})e^{-k_V t}} \tag{120}$$

where

$$k_V = \frac{A_g^2 P_{out}}{8\pi\mu L V}. \tag{121}$$

The near-steady-state approximation is expected to be valid when

$$k_V t_{ss} = \frac{P_{out}}{P_0}\frac{A_g L}{V} << 1 \tag{122}$$

If a valve between the vessel and tube is closed at and before $t = 0$, this product is the initial ratio of moles of gas in the tube to moles of gas in the vessel. To obtain the velocity, the diatomic molar flow rate is needed:

$$\dot{n}(t) = \frac{A_g^2\left(P_{in}^2 - P_{out}^2\right)}{16\pi\mu R_g T L} = -\frac{V}{R_g T}\frac{dP_{in}}{dt} = \frac{2P_{out}V}{R_g T}\frac{(P_0 + P_{out})(P_0 - P_{out})ke^{-k_V t}}{\left[(P_0 + P_{out}) - (P_0 - P_{out})e^{-k_V t}\right]^2} \tag{123}$$

where the first form is a general steady-flow form from Ref. 29, the second is from a mole balance on the vessel, and the third is the form most specific to this case, obtained by combining Equation 120 with either of the more general forms. For given time-dependent inlet and outlet pressures (not specific to Equation 120), the atomic gas concentration and gas velocity are

$$C_g(z) = 2\left[\left(1 - \frac{z}{L}\right)\left(\frac{P_{in}}{R_g T}\right)^2 + \frac{z}{L}\left(\frac{P_{out}}{R_g T}\right)^2\right]^{1/2} \tag{124}$$

$$v_0(z) = \frac{2\dot{n}}{A_g C_g(z)} \tag{125}$$

and the time derivative of the gas concentration is

$$\frac{C_g(z)}{2}\frac{dC_g(z)}{dt} = \left(1 - \frac{z}{L}\right)\frac{2P_{in}}{R_g T}\frac{d}{dt}\left(\frac{P_{in}}{R_g T}\right) + \frac{z}{L}\frac{2P_{out}}{R_g T}\frac{d}{dt}\left(\frac{P_{out}}{R_g T}\right) \tag{126}$$

which for constant outlet pressure yields

$$\frac{dC_g(z)}{dt} = \frac{-32\pi\mu(L - z)}{A_g R_g T}\frac{P_{in}(t)}{P_{out}}k_V v_0(z,t) \tag{127}$$

The equations in this section, along with the concentration form of Equation 24 and the ideal gas law, allow for modeling of a tube with a time-varying pressure source that can be tuned by selection of P_0 and V. Useful formulas for selection of these include the time and outlet velocity v_{el} upon elution, recalling from Equation 10 in Section 2.2.2 that n is the molar capacity of the solid or stationary phase in the tube to absorb diatomic gas:

$$t_{el} = -\frac{1}{k_V}\ln\left[\frac{(P_0 + P_{out})(P_0 - P_{out} - nR_g T/V)}{(P_0 - P_{out})(P_0 + P_{out} - nR_g T/V)}\right] \tag{128}$$

This is obtained by determining the pressure in the vessel after n moles have been removed, $P_{in} = P_0 - nR_g T/V$, and solving Equation 120 for t under that condition. It neglects the contribution of the molar capacity of the gas phase, which is consistent with the assumption described by Equation 122. It also neglects the effect of diffusive transport on the elution time. The outlet velocity upon elution is (showing some intermediate calculations):

$$v_0(L) = \frac{2\dot{n}}{A_g C_g(L)} = \frac{R_g T}{A_g P_{out}} \dot{n} = \frac{A_g \left(P_{in}^2 - P_{out}^2\right)}{16\pi\mu L P_{out}} = \frac{A_g \left(P_{in} + P_{out}\right)\left(P_{in} - P_{out}\right)}{16\pi\mu L P_{out}} \tag{129}$$

$$v_{el} = \frac{A_g}{16\pi\mu L P_{out}} (P_0 + P_{out} - nR_g T/V)(P_0 - P_{out} - nR_g T/V) \tag{130}$$

To examine the effect of varying the initial pressure, values of P_0 and V can be chosen that hold t_{el} or v_{el} at a fixed value.[46] The top four plots in Figure 29 show results for a series of source vessel volumes with t_{el} held constant. For large vessel volumes, the results approximate cases of time-independent pressure. For smaller vessel volumes, there are increasingly significant decays of pressure during elution. In these cases, the flow rates of pure eluate are initially high, and the flow rates are relatively low upon elution, where the gas is less pure. The front width is approximately independent of volume until it begins to broaden for volumes below 0.544 mL. This suggests that, for a given elution time, there is an optimal volume that achieves the highest yield of eluate of a given purity, balancing the flow rate reduction at smaller volumes with the front broadening. This is confirmed in the bottom plot in Figure 29, which more clearly illustrates the tradeoff between yield and purity for a given elution time. The 0.544 mL volume yields more gas with greater than 99% purity than either the higher or lower volumes shown. The smaller volumes produce higher purity at extremely high yields, but this occurs at times exceeding the elution time, when the purity is degrading rapidly due to depletion of the eluate and continued flow of the eluent. A possibly useful criterion is the fill factor, by analogy to the similar measure of a photovoltaic panel's current-voltage relationship, where it is most desirable to operate in the upper right corner of the plot. In this case, it is simply the area under the curve in the plot, which is highest (0.9982) for the 0.544 mL case.

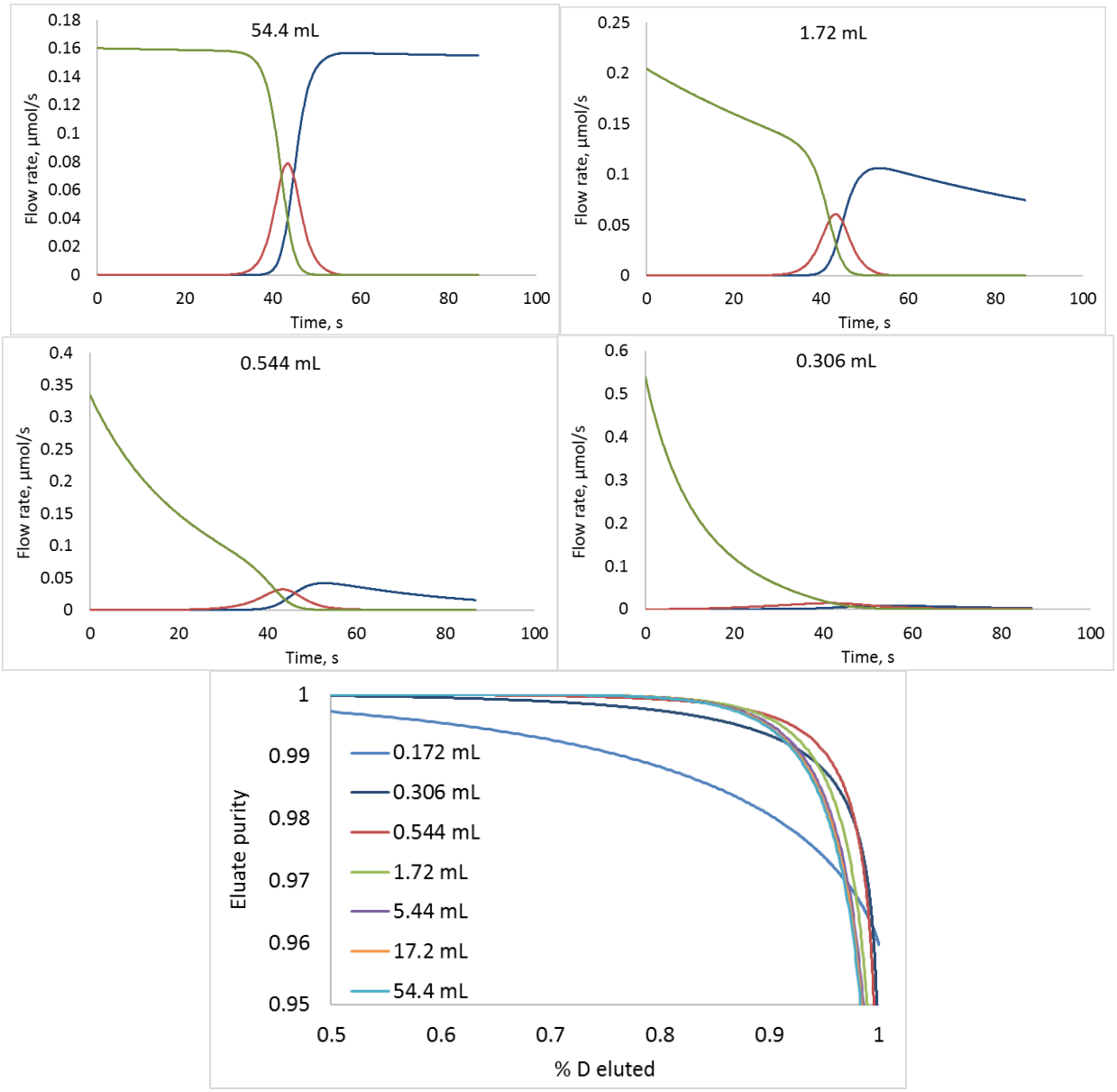

Figure 29. Top four plots: Outlet molar flow rate of H_2 (blue), HD (red), and D_2 (green) for a fixed outlet pressure of 0.1 MPa and a fixed elution time of 43.35 s, with varying source vessel volumes and initial pressures. Flow rate scales vary between plots. Bottom: Yield (fraction D eluted) versus eluate purity for varying source vessel volumes. $D = 10^{-4}$ m^2/s, $v_k = 0.55$ cm/s, ID 0.005 cm, $\alpha = 2.0$, $k' = 867$, $L = 10$ cm.

Front sharpening occurs to a significant extent for the smaller volumes considered here. Figure 30 plots H_s as a function of position in the tube, a convenient representation of front width, at several time points for the 0.306 mL case shown in Figure 29. The tube is about halfway to elution at 8.67 s, the second curve from the left. At 4.3 s, the first curve on the left, the front is about 2.5 cm wide, as measured from 10 to 60 mol/L. By the elution time, as shown by the red curve that is at 35 mol/L at the outlet, the front width has reduced to 1.0 cm, measuring front width there as twice the distance between 35 and 60 mol/L.

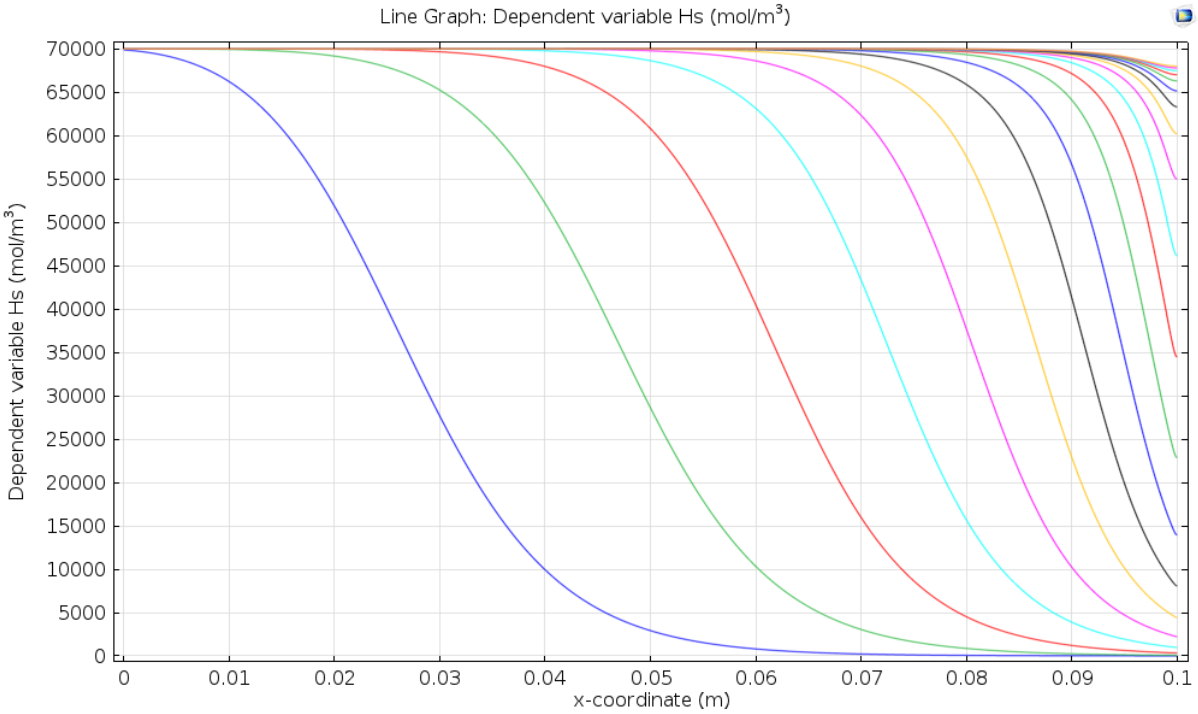

Figure 30. H_s as a function of axial position in the tube for the 0.306 mL case in Figure 29 at intervals of 4.335 s.

A series with varying vessel volumes but v_{el} held constant is shown in the top four plots of Figure 31. At volumes above 1.72 mL, the results approximate a case of constant pressure and velocity, with an elution time of about 43 s and total gas flow rate of 160 nmol/s. Smaller volumes lead to faster elution times and higher initial flow rates, but also broader fronts. The lower plot showing purity versus yield shows a monotonic decrease in fill factor as volume decreases. The decrease is most significant when the elution time is decreasing significantly. However, there are finite volumes, such as 1.72 mL among these examples, where there is a modest reduction in elution time, about 20% versus the 54.4 mL case, with only a 9% increase in front width, and without significantly changing the purity-versus-yield tradeoff. This case does not exhibit a significant amount of front sharpening, but simply strikes a better balance between high initial flow rates where pure D_2 is eluted, and front broadening effects, while maintaining modest flow rates until elution, which contributes to a shorter elution time.

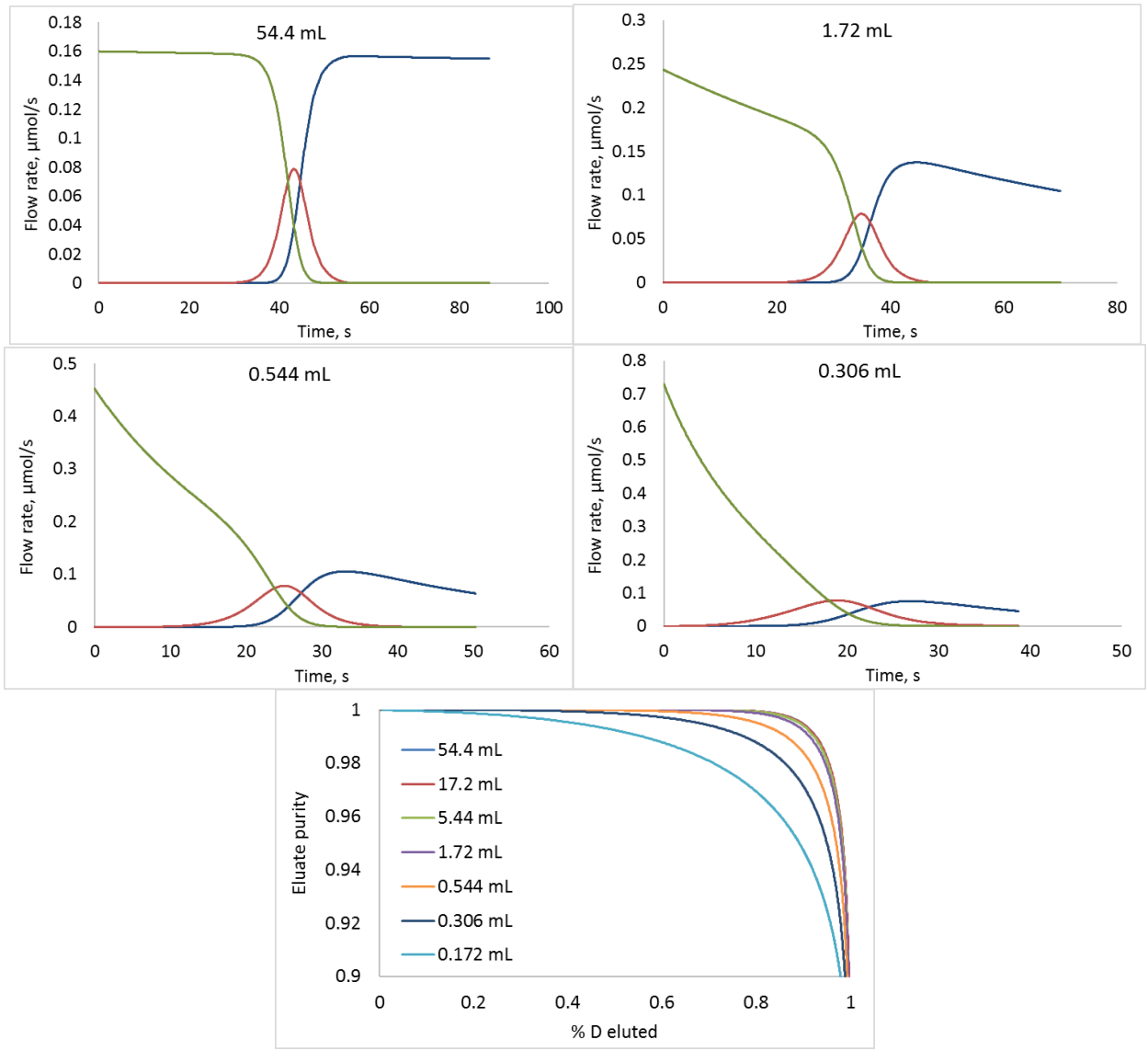

Figure 31. Top four plots: Outlet molar flow rate of H_2 (blue), HD (red), and D_2 (green) for a fixed outlet pressure of 0.1 MPa and a fixed gas velocity of 1.986 m/s at elution time, with varying source vessel volumes and initial pressures. Bottom: Yield (fraction D eluted) versus eluate purity for varying source vessel volumes. D = 10^{-4} m^2/s, v_k = 0.55 cm/s, ID 0.005 cm, α = 2.0, k' = 867, L = 10 cm.

Previous chapters emphasized optimization of the number of theoretical plates through choice of the gas velocity. Section 4.5 showed an elaboration using two different gas velocities that allowed for a faster elution time without much broadening at the outlet. This section shows that a time-dependent inlet pressure allows for additional dimensions of inputs and outputs that can be optimized. It may be possible to more arbitrarily define an inlet pressure function (perhaps more closely matching the conditions described in Section 4.5) that allows both purity and yield to be closer to 100% for a given elution time. However, the example shown here is simple to

implement either as a model or an experiment, offers an additional degree of freedom that results in decreasing inlet pressures qualitatively similar to those prescribed in Sections 4.5 and 6.1, enables taking advantage of front sharpening, and allows significant improvements in the yield of high-purity eluate.

6.3. Feedback control

The previous section illustrates that, at early times, it may be desirable to speed up elution by increasing the inlet pressure. This could be done to the extent that the desired peak sharpness can still be obtained, which could be aided by the front-sharpening phenomenon described in Section 4.5. The inlet pressure and velocity profiles versus time described in Sections 6.2 and 4.5 may not be optimal, or easily implemented. Furthermore, those profiles must be designed using a set of assumptions or prior measurements of tube behavior, which may not adequately represent future behavior. One way to address these concerns is to consider a feedback loop in which the inlet pressure is adjusted to maintain a tolerable molar flow rate of eluent at the outlet. This feedback loop could correct for inaccurate assumptions in the design of a pressure profile, or for changes in tube properties since a prior calibration. If a feedback loop is difficult to implement in practice, a model of it can still be useful to propose and evaluate an open-loop pressure profile.

A feedback loop can be implemented in an experiment or a one-dimensional COMSOL model through several steps. In the scenario considered here, there is a maximum practical inlet pressure P_{max}, and the inlet pressure must be greater than the outlet pressure, which is held constant. Within these constraints, the inlet pressure is a function of recent values of the molar flow rate of H at the outlet. The function can be designed to balance various desirable attributes of a feedback control system, such as fast response time, well damped oscillations about the desired output value, low noise sensitivity, low steady-state error, and low system complexity. In this case, it is desirable to minimize digression on this topic, so a simple method is used that works reasonably well. It damps changes that occur on a timescale faster than a chosen time τ_d, which reduces the effect of numerical errors produced by the solver, reduces the effect of changes that occur on a timescale that is not much slower than t_{ss}, and reduces overshoot due to the time lag between pressure changes at the inlet and compositional changes at the outlet.

The COMSOL solver must be configured to compute the outlet molar flow rate of H atoms from the previous timestep for use in a feedback loop. To obtain a unitless feedback signal, a reference molar flow rate of H atoms is defined (differing from the diatomic molar flow rate expression in Equation 123 by a factor of 2):

$$\dot{n}_{ref,H} = \frac{2A_g^2\left(P_{max}^2 - P_{out}^2\right)}{16\pi\mu R_g T L} \tag{131}$$

An error signal E is defined as the difference between the measured ("out") and desired ("set") molar flow rate of H atoms. "H" is used in the subscript to reduce confusion with the diatomic molar flow rate.

$$E = \frac{\dot{n}_{set,H} - \dot{n}_{out,H}}{\dot{n}_{ref,H}} \tag{132}$$

The damped signal E_d can be expressed as several forms:

$$\begin{aligned} E_d &= \int_0^t E(t') \exp\left(-\frac{(t-t')}{\tau_d} \right) dt' \\ \tau_d \frac{\partial E_d}{\partial t} &= E - E_d \\ E_d &= \frac{E}{\tau_d s + 1} \end{aligned} \tag{133}$$

The first form shows that the damped signal is a weighted average of the history of the error signal, with values in the more distant past having exponentially decreasing weight. It is the solution to the second form (with E_d = 0 at t = 0) which is the differential equation actually solved by COMSOL. The third form is the Laplace transform of the second, which the reader may recognize as defining a pole at $s = -1/\tau_d$. The inlet pressure is then defined as

$$P_{in} = P_{out} + k_{gain}(P_{\max} - P_{out})E_d \tag{134}$$

subject to the maximum and minimum constraints described above, where k_{gain} is a unitless proportionality constant. Higher values of this constant can provide fast response time (the error signal rapidly approaches zero) and steady-state accuracy (the error signal is close to zero at long times). However, values that are too high can result in overshoot or oscillation. For scenarios considered in this section, except where specified, k_{gain} is 1000, P_{max} is 2 MPa, P_{out} is 0.1 MPa, α = 2, and τ_d is 0.3% of the elution time that would be obtained if P_{in} were always equal to P_{max}. The set (target) point for the control system is an outlet molar flow rate of H atoms that is 0.3% of the total molar flow rate that would be obtained if P_{in} were always equal to P_{max}.

Figure 32 compares cases where P_{in} is always at P_{max} with cases that use feedback control to maintain a low molar flow rate of H atoms at the outlet. The feedback control is inoperative until the control signal reduces the pressure below P_{max}. After that, P_{in} is reduced, allowing more D_2 to elute while mostly suppressing elution of H_2 and HD. The resulting pressure profiles cannot be accurately described by a simple function, such as a power law or exponential function.

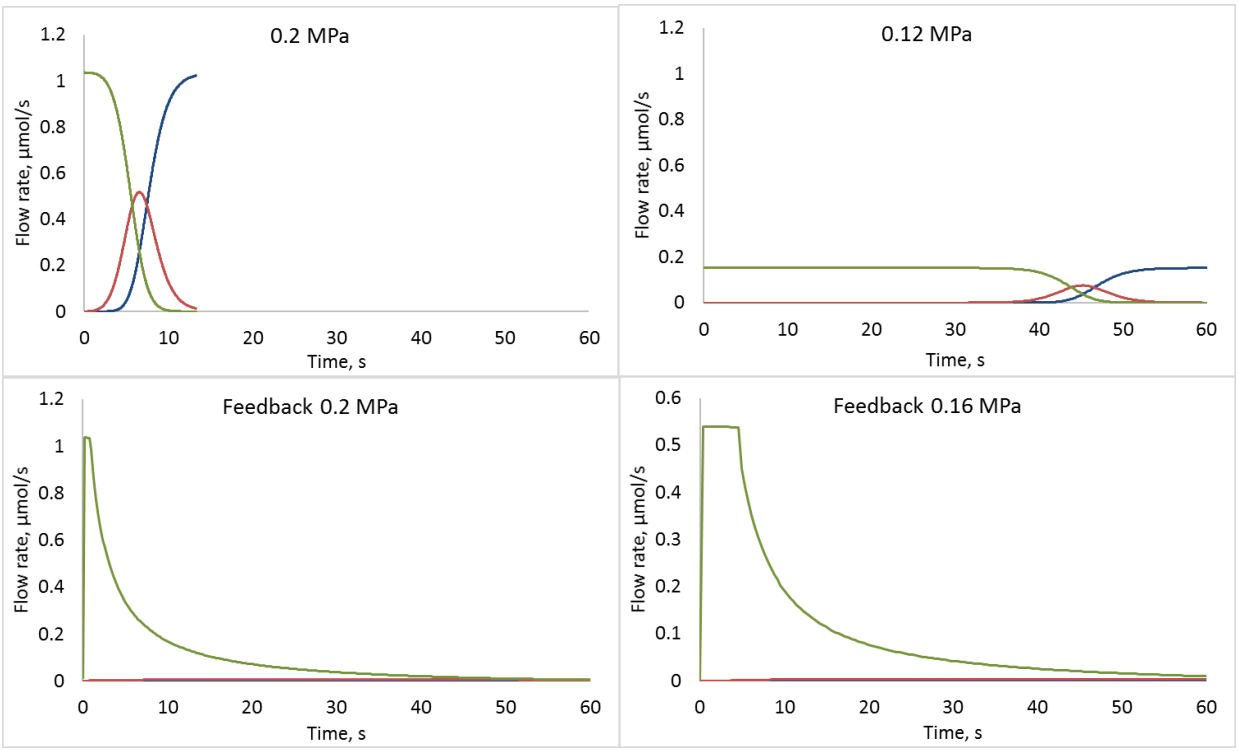

Figure 32. Outlet molar flow rate of H_2 (blue), HD (red), and D_2 (green) for (top left) P_{in} always equal to P_{max}, where t_{el} is 6.53 s, (top right) a lower constant value of P_{in} with t_{el} 45.2 s, and (bottom) feedback loops designed to adjust P_{in} between P_{out} and P_{max} to obtain a constant, low value of the molar flow rate of H atoms at the outlet, with P_{max} 0.2 MPa (left) and 0.16 MPa (right).

The tradeoff between purity and yield is examined in Figure 33, which compares the cases of feedback control with several cases that use a constant inlet pressure. For constant inlet pressures, fill factor steadily increases as the pressure decreases. The feedback-controlled cases cross through these curves. The fill factor for the case of feedback with P_{max} = 0.16 MPa has about the same fill factor (0.997) as the case of constant 0.12 MPa inlet pressure, although there are combinations of purity and yield that each can uniquely achieve among the examples considered here. Evidently, constant pressures less than P_{max} can be chosen that achieve a purity and yield in a given time that are close to that of the feedback-controlled case, but with feedback, it is not necessary to determine that pressure in advance, and only the elution time must be chosen or predicted. Compared to a constant-pressure case that achieves the same total purity and yield in the same time (as when the curves in Figure 33 cross), the feedback-controlled case yields more D earlier in the process, and the purity is less sensitive to the time at which the flow is stopped.

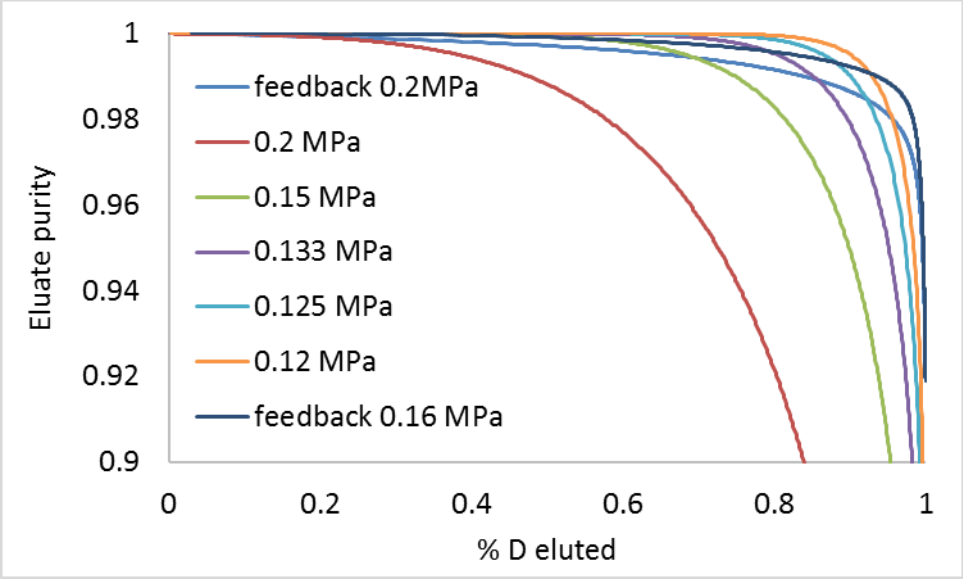

Figure 33. Comparison of tradeoff between yield and purity for several cases of constant inlet pressure and for two cases of feedback-controlled inlet pressure with different maximum pressure constraints.

Front sharpening occurs in the cases of feedback control, as is shown in Figure 34. The case of P_{max} = 0.2 MPa, the upper plot in the figure, shows a large amount of initial broadening, similar to the conditions described in Section 4.5, where for α = 2 and 37.5% elution the leading edge of the front is 75% eluted. The cyan fourth curve from the left, at about 4 s, is close to this condition; the width between the 10 and 60 mol/L concentrations is about 3.6 cm. By the elution time, as represented by the curves that are near 35 mol/L at the end of the tube, the full width is about 1.1 cm. The sharpening effect also occurs for the P_{max} = 0.16 MPa case, sharpening from about 3.0 to 1.0 cm. There is probably room for further optimization of the control system to yield pressure-versus-time profiles that maximize the amount of front sharpening. However, the simple control loop presented here is at least able to take advantage of the phenomenon.

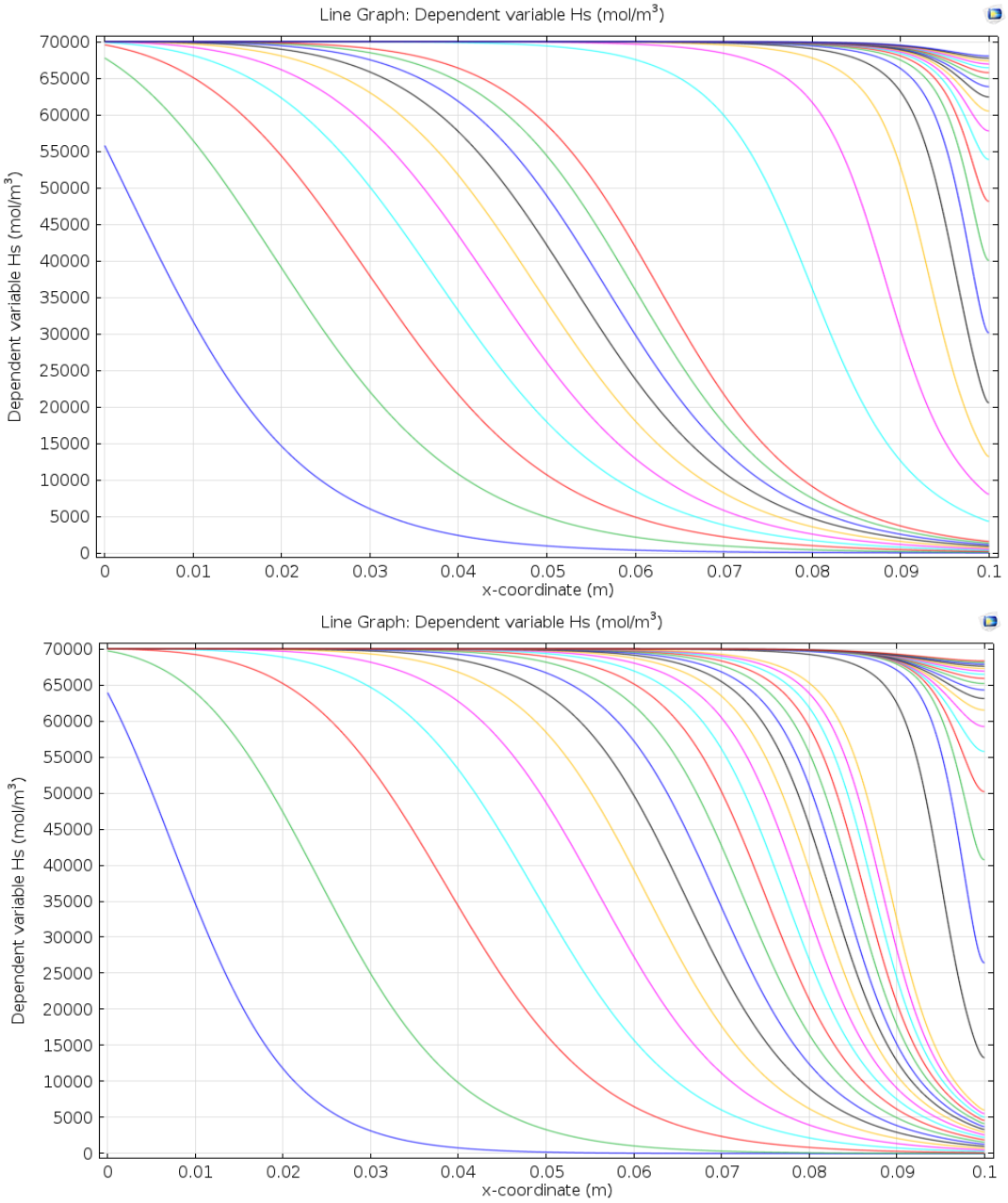

Figure 34. H_s versus position and time for feedback cases. Top: P_{max} = 0.2 MPa, with curves every 0.996 s until 9.96 s, then every 9.96 s. Bottom: P_{max} = 0.16 MPa, with curves every 1.915 s until 38.3 s, then every 19.15 s.

6.4. Equal vessel volumes

Section 6.2 considered a relatively simple case in which the outlet pressure is held constant. Another simple case is where there are inlet and outlet vessels with finite, equal volumes. The pressures have a simple exponential time dependence, which can be easy to compare to experimental data.

$$P_{in}(t) = P_{eq} + (P_0 - P_{eq})e^{-k_V t} \tag{135}$$

$$P_{out}(t) = P_{eq} - (P_0 - P_{eq})e^{-k_V t} \tag{136}$$

Where P_{eq} is the average of the initial pressures in the vessels and

$$k_V = \frac{A_g^2 P_{eq}}{4\pi\mu LV}. \tag{137}$$

The near-steady-state approximation is expected to be valid when

$$k_V t_{ss} = \frac{2P_{eq}}{P_0}\frac{A_g L}{V} << 1 \tag{138}$$

which is similar to Equation 122. To obtain the velocity, the diatomic molar flow rate is needed:

$$\dot{n}(t) = \frac{A_g^2\left(P_{in}^2 - P_{out}^2\right)}{16\pi\mu R_g TL} = -\frac{V}{R_g T}\frac{dP_{in}}{dt} = \frac{V}{R_g T}\frac{dP_{out}}{dt} = \frac{k_V V}{R_g T}(P_0 - P_{eq})e^{-k_V t} \tag{139}$$

where the first form is a general steady-flow form from Ref. 29, the second and third are from mole balances on the vessels, and the fourth is the form most specific to this case, obtained by combining Equations 135 and 136 with one of the appropriate general forms. The spatial dependence of the gas concentration does not get much simpler than Equation 124, but the time derivative of the gas concentration simplifies to

$$\frac{dC_g(z)}{dt} = \frac{2A_g}{V}\left[\frac{z}{L}\frac{P_{out}}{R_g T} - \left(1 - \frac{z}{L}\right)\frac{P_{in}}{R_g T}\right]v_0(z) \tag{140}$$

The elution time is

$$t_{el} = -\frac{1}{k_V}\ln\left[\frac{(P_0 - P_{eq} - nR_g T/V)}{(P_0 - P_{eq})}\right] \tag{141}$$

And the outlet velocity upon elution is

$$v_{el} = \frac{A_g P_{eq}(P_0 - P_{eq} - nR_g T/V)}{4\pi\mu L(2P_{eq} - P_0 + nR_g T/V)} \tag{142}$$

The results in this case are qualitatively similar to those obtained in Section 6.2.

7. OTHER NOTABLE CASES

7.1. Studies of chemical reaction kinetics

An open-tube reactor that operates at well defined values of v_0 and r would be ideal for the study of the isotope exchange reaction. In this case, and at values of those parameters where diffusive transport does not contribute to HD peak width, v_k can be reliably extracted from that peak width. The proper conditions can be identified by eluting at different velocities (N should decrease with increasing velocity) and by consideration of peak shape; asymmetric peaks usually indicate a significant amount of some form of diffusion, whereas kinetically limited peaks have a symmetric shape derived from Equation 79. The kinetic measurements would apply to a given hydride material in a given form. Using an ample amount of hydride material increases k', slowing the elution process and allowing HD concentrations to be measured on a convenient timescale. However, the material form must be one that ensures that any solid-phase transport processes are fast, and the geometry well defined so the surface area is known.

7.2. Preparative scale

The total number of moles of diatomic hydrogen gas that can be absorbed by the solid portion of the tube, n, can be increased by making the tube longer or wider (with a thicker stationary phase), but this changes the transport properties of the tube. Hypothetically, more moles can be held in a column if many tubes in are placed parallel. Prior studies caution against this, due to sensitivity to slight variations in tube diameter.[47] Distribution of eluent to the inlet of each tube, and collection of eluate from each outlet, will be increasingly challenging if a tube array becomes extremely thin and wide. One solution to the diameter variation is to occasionally shuffle flow between tubes, such as by stacking short segments of tube arrays.[48] An inert material of similar geometry at the entrance and exit could help distribute flow. These are expected to be fruitful topics for future study.

7.3. Packed columns

For comparison of the open tube model to columns made of packed powder, only a few variable substitutions are needed. Two key parameters of the packed column are its cross-sectional area A_c and its porosity (void fraction) ϕ_c.

$$\phi_c = 1 - \frac{\rho}{\rho_{bulk}} \tag{143}$$

where the densities ρ are of the packed column and of a nonporous (bulk) slab of the hydride. Table 2 describes most of the necessary changes.

Table 2. Transformations between open-tube geometry and packed column geometry.

Open Tube	Packed Column
A_g in species concentration or mole fraction equations	$\phi_c A_c$
A_s	$(1-\phi_c)A_c$
Axial D	D/q, q = tortuosity factor
S	Empirical surface area (m^2/g) multiplied by ρA_c
$8\pi/A_g$ in pressure drop equations	Empirical permeability B

The areas in Table 2 do not correspond in an absolute sense, but the substitutions apply to ratios of areas. For uniformly sized spherical particles of diameter d_p, S can be estimated as

$$S = \frac{6A_c}{d_p}\left(1-\phi_c\right) \tag{144}$$

This is the sphere surface-to-volume ratio multiplied by the ratio of sphere volume to total volume, and by A_c to obtain surface area per unit length. The tortuosity is a dimensionless number representing the increased path length for diffusion imposed by the irregular flow paths through the column. It is not expected that an open-tube model can predict the results of a packed column experiment, but it may aid understanding of how a packed column experiment might behave if it had a more regular geometry, and lower pressure drop. For example, a comparable tube geometry to the Foltz and Melius experiment[3] would be an array of about 17,000 tubes with 47 μm inside diameter and 76 μm outside diameter, and a gas velocity of about 60 cm/s, requiring about 3x lower pressure drop (130 as opposed to 440 Torr). Modeling of one such tube by the approaches described here could add insight into the interpretation of this experiment.

8. SUMMARY

This report combines the theories of mass transport in open-tube gas chromatography with that of chemical reaction kinetics in ion exchange chromatography. This combination is applicable to hydrogen isotopic displacement chromatography in an open tube. The report describes how a tube is expected to behave under a wide range of operating conditions and geometries, and shows how to obtain performance where the system is either robustly limited by chemical reaction kinetics, or optimized to obtain elution fronts with optimal sharpness, or an optimal amount of sharpness generated per unit time. Computational analysis and design tools could easily be implemented with the information provided here.

The model includes many simplifications, with the goals of making the process easy to understand, and allowing rapid computations that provide good estimates of performance. The simplifications include treating the tube as a one-dimensional model, assuming that radial transport is fast; as well as assuming a small pressure drop across the length of the tube. Some simplifications are relaxed in later chapters to aid their justification, and clarify when they apply. There is no attempt here to account for the isotopic dependence of gas transport parameters like diffusivity and viscosity, parameters that can vary by approximately 50% between isotopes. Real metal hydrides can have pressure- and isotope-dependent capacities, so C_s is not necessarily a constant. For some hydrides, especially in the context of preparative-scale chromatography, the isothermal approximation may not be realistic. Despite these limitations, the simple model presented here can still be a useful first pass in a design that can be validated using more sophisticated models.[25,49] The neglect of solid-phase diffusion is shown to be unrealistic for thick tube walls, but porosity in that wall can eliminate this mass transport limitation.

8. REFERENCES AND NOTES

[1] M.J.E. Golay. Theory of Chromatography in Open and Coated Tubular Columns with Round and Rectangular Cross Sections, in Gas Chromatography 1958: Proceedings of the Second Symposium, D.H. Desty, ed., p. 36-55.

[2] E. Glueckauf, G. P. Kitt. Gas Chromatographic Separation of Hydrogen Isotopes, Proceedings of the Symposium on Isotope Separation, Amsterdam, 1957, Chapter 15, pages 210-225, published 1958. J. Kistemaker, J. Bigeleisen, A. O. C. Nier, eds.

[3] B.M. Andreev, A.S. Polevoi, O. V. Petrenik. Separation of isotopic mixtures of hydrogen in the hydrogen-palladium system. Soviet Atomic Energy 40 (5) 431-433, 1976.

[4] G.W. Foltz, C.F. Melius. Studies of Isotopic Exchange Between Gaseous Hydrogen and Palladium Hydride Powder, J. Catalysis 108 409-425, 1987.

[5] M. Li, W.F. Yang. Highly porous palladium bulk: Preparation and properties as active metal material for displacement chromatographic process. Int. J. Hydrogen Energy 34 1585-1589, 2009.

[6] S. Fukada, K. Fuchinoue, M. Nishikawa. Isotope separation factor and isotopic exchange rate between hydrogen and deuterium of palladium. J. Nuc. Mater. 226 311-318, 1995.

[7] F. Strzelczyk, D. Leterq, A.M. Wilhelm, A. Steinbrunn. Gas-solid chromatographic separation of hydrogen isotopes: a comparison between two palladium-bearing materials – alumina and kieselguhr. J. Chromatography A 822 326-331, 1998.

[8] S. Fukada, Numerical simulation of elution chromatography for separation of H_2-HD-D_2 mixtures using a palladium particle bed. Separation Sci. Tech. 34 (14) 2699-2721, 1999.

[9] S. Charton, J.P. Corriou, D. Schweich. Modeling of hydrogen isotopes separation in a metal hydride bed. Chem. Eng. Sci. 54 (1) 103-113, 1999.

[10] M. Matsuyama, H. Sugiyama, M. Hara, K. Watanabe. Applicability of Pd-Cu alloy to self-developing gas chromatography of hydrogen isotopes. J. Nuc. Mater. 367-370, part B, 1096-1101, 2007.

[11] K. Watanabe, M. Matsuyama, T. Kobayashi, S. Taguchi. Gas chromatographic separation of H_2-D_2 mixtures by Pd-Pt alloy near room temperature. J. Alloys Compounds 257 (1-2) 278-284, 1997.

[12] S. Fukada, H. Matsuo, T. Okunaga, N. Mitsushi. A study of isotopic exchange of hydrogen and deuterium in a $LaNi_3Al_2$ hydride bed. J. Nuc. Mater. 195 (1-2) 191-197, 1992.

[13] A.D. Shugard, G.M. Buffleben, T.A. Johnson, D.B. Robinson. Isotope Exchange between Gaseous Hydrogen and Uranium Hydride Powder. Journal of Nuclear Materials 447 (1–3) 304–313, 2014.

[14] G. Guiochon, A. Felinger, D.G. Shirazi, A. M. Katti. Fundamentals of Preparative and Nonlinear Chromatography, 2nd ed. Academic Press, 2006.

[15] T. Vermeulen, Separation by adsorption methods, in Advances in Chemical Engineering, T. B. Drew and J.W. Hoopes, Jr., eds., vol. II, 147-208, 1958.

[16] D. Robinson. Hydrogen Isotope Exchange in a Metal Hydride Tube. Sandia National Laboratories, SAND2014-17174, 2014, available upon request from ntis.gov.

[17] R. Javaid, U.Y. Qazi, S.-I. Kawasaki. Efficient and Continuous Decomposition of Hydrogen Peroxide Using a Silica Capillary Coated with a Thin Palladium or Platinum Layer. Bull. Chem. Soc. Japan 88 976-980, 2015.

[18] S.C. James, J. Hamilton, W.G. Wolfer. Diffusional exchange of isotopes in a metal hydride sphere. Chem. Eng. Sci. 68 (1) 250-257, 2012.

[19] In Ref. 18, Eqs. 21 and 22 should be functions of total mole fraction of all isotopes, not mole fraction of individual isotopes. Indices in Eqs. 12 and 27 have errors. The equation referenced at the end of section 5 should be to Eq. 21. Though Table 1 states that it should only be used with Eq. 25, the authors use the parameters elsewhere, and presumably readers may also do this.

[20] In Ref. 3, the proposed mechanism requires the existence of an HD intermediate, so that both atoms of a molecule of H_2 or D_2 cannot be directly absorbed. This leads to some complications that are avoided in this work.

[21] B.M. Andreev, E.P. Magomedbekov. Separation of Hydrogen Isotopes by Chemical isotope Exchange in Systems Involving Metal and Intermetallic Compound Hydrides. Separation Science and Technology 36 (8-9) 2027-2086, 2001.

[22] W.F. Luo, D.F. Cowgill, T.B. Flanagan. Separation Factors for Hydrogen Isotopes in Palladium Hydride. J. Phys. Chem. C 117 13861-13871, 2013.

[23] T. B. Flanagan, W.A. Oates. The Palladium-Hydrogen System. Ann. Rev. Mater. Sci. 21 269-304, 1991.

[24] http://www.chem.arizona.edu/~salzmanr/480a/480ants/collsurf/collsurf.html

[25] M. Salloum, S. C. James, D. B. Robinson. Effects of Surface Thermodynamics on Hydrogen Isotope Exchange Kinetics in Palladium: Particle and Flow Models. Chem. Eng. Sci. 122, 474-490, 2015.

[26] F.M. White. Viscous Fluid Flow. McGraw-Hill, New York, 3rd ed., 2006.

[27] R. B. Bird, W. E. Stewart, E. N. Lightfoot. Transport Phenomena, 2nd ed., Wiley, 2002.

[28] C. R. Wilke. A viscosity equation for gas mixtures. J. Chem. Phys. 18 (4) 517-519, 1950.

[29] A. D. Shugard, D. B. Robinson. A Simple Model of Gas Flow in a Porous Powder Compact. Sandia National Laboratories, SAND2014-2858, 2014, available at osti.gov.

[30] T. R. Marrero, E. A. Mason. Gaseous Diffusion Coefficients, J. Phys. Chem. Ref. Data 1 (1) 3-87, 1972.

[31] A.A. Clifford. Theory of open-tube chromatography: an exact proof of Golay's equations. J. Chrom. 471 61-69, 1989.

[32] This requires substitution for Clifford's $k_d = kS/C_s A_s$ where the rate constant on the right-hand side is derived from the linear form of the rate law, and the dimensional terms convert Clifford's surface concentration to the concentration in the solid.

[33] C.A. Cramers, H.-G. Janssen, M.M. van Deursen, P.A. Leclercq. High-speed gas chromatography: an overview of various concepts. J. Chromatography A 856, 315-329, 1999.

[34] In this section, the fraction 11/24 is approximated as 1/2, and $\alpha k'$ is assumed large.

[35] J.E. Walter. Multiple Adsorption from Solutions, J. Chem. Phys. 13 (6) 229-234, 1945.

[36] J.E. Walter. Rate-dependent chromatographic adsorption, J. Chem. Phys. 13 (6) 332-336, 1945.

[37] H.C. Thomas. Heterogeneous Ion Exchange in a Flowing System. J. Am. Chem. Soc. 66 1664-1666, 1944.

[38] N. K. Hiester and T. Vermeulen. Saturation performance of ion-exchange and adsorption columns. Chem. Eng. Prog. 48 (10) 505-516, 1952.

[39] E. Glueckauf. Theory of Chromatography. Part 10: Formulae for diffusion into spheres and their application to chromatography. Trans. Faraday Soc. 51 1540-1551, 1955.

[40] A. Patton, B. D. Crittenden, S. P. Perera. Use of the Linear Driving Force Approximation to Guide the Design of Monolithic Adsorbents. Chem. Eng. Res. Des. 82 (A8) 999-1009, 2004.

[41] J. Newman, K. E. Thomas-Alyea. Electrochemical Systems. 3rd ed. Wiley, 2004.

[42] The flux discontinuity can be implemented in COMSOL using the internal variable *Hr*, which is the average of $\partial H/\partial r$ in the mobile phase and $\partial(\phi H)/\partial r$ in the stationary phase. Assuming no discontinuity in $\partial H/\partial r$ (which requires assuming rapid equilibration with the solid at the surface) this can be rearranged so the net flux into the mobile phase is specified as $-2[(1-\phi)/(1+\phi)]D\ Hr$.

[43] A. M. Berezhovskii, A. V. Barzykin, V. Yu. Zitserman. One-dimensional description of diffusion in a tube of abruptly changing diameter: Boundary homogenization based approach. J. Chem. Phys. 131, 224110, 2009.

[44] M.J.E. Golay. A problem of optimization in capillary gas chromatography. J. Chromatography 348 416-420, 1985.

[45] B. M. Wood, K. Ham, D. S. Hussey, D. L. Jacobson, A. Faridani, A. Kaestner, J. J. Vajo, P. Liu, T. A. Dobbins, L. G. Butler. Real-time observation of hydrogen absorption by $LaNi_5$ with quasi-dynamic neutron tomography. Nucl. Inst. Meth. Phys. Res. B 324 95-101, 2014.

[46] The term including the time derivative of the concentration in Equation 119 was confirmed to be negligible even for the highest pressure drops described in this section.

[47] D. K. Schisla, H.B. Ding, P.W. Carr, E.L. Cussler. Polydisperse Tube Diameters Compromise Multiple Open Tubular Chromatography. AIChE J., 39 (6) 946-953, 1993.

[48] J. Billen, G. Desmet. Understanding design of existing and future chromatographic support formats. J. Chromatography A 1168 73-99, 2007.

[49] R.S. Larson, S.C. James, R.H. Nilson. Isotope Exchange Kinetics in Metal Hydrides I: TPLUG Model. Sandia report 2011-3243, May 2011. DOI: 10.2172/1030413

Distribution

7	MS9161	David B. Robinson	8651
1	MS9158	Maher Salloum	8961
1	MS9035	Steve Rice	8254
1	MS9035	Andrew Shugard	8254
1	MS0899	Technical Library	9536 (electronic copy)


Sandia National Laboratories